Improving Safety and Efficacy of Protein Therapeutics by Chemical Modifications

Peng Zhang

A dissertation

submitted in partial fulfillment of the

requirements for the degree of

Doctor of Philosophy

University of Washington
2018

Reading Committee:

Shaoyi Jiang, Ph.D., Chair
Cole A. DeForest, Ph.D.
Suzie H. Pun, Ph.D.

Program Authorized to Offer Degree:
Chemical Engineering

University of Washington

Abstract

Improving Safety and Efficacy of Protein Therapeutics by Chemical Modifications
Peng Zhang

Chair of the Supervisory Committee:
Professor Shaoyi Jiang
Chemical Engineering

Protein therapeutics offer the advantages of high specificity and potency. However, their applications are greatly limited due to undesired immune responses, which not only reduce their therapeutic efficacy, but also cause many adverse effects including anaphylaxis and infusion reactions. Although several PEGylated protein drugs were brought into clinic, they are still vulnerable to anti-PEG antibodies. In this dissertation, tactics to improve the efficacy and safety of protein therapeutics are discussed. Learning lessons from PEGylation, a zwitterionic gel encapsulation technology is developed to protect protein drugs from body clearance and immune recognition. This strategy is proved to be effective in increasing protein stability, prolonging *in vivo* circulation half-life and reducing immunogenicity, and is successfully applied to uricase, butyrylcholinesterase (BChE) and organophosphate hydrolase (OPH) for both therapeutic and protective applications. In addition, several new capabilities have also been developed in the course of this work. First, to reduce current PEG related clinical risks, a surface plasmon resonance biosensor is applied to detect anti-PEG antibodies quantitatively with better sensitivity than direct ELISA. Second, to solve potential organ accumulation and associated toxicity problems, a carboxybetaine group functionalized polypeptide is synthesized to introduce biodegradability to the protein modification material. Third, to handle highly immunogenic therapeutics, an immunomodulatory bioconjugation is developed to proactively suppress anti-drug antibodies. These new technologies have the potential to improve the pharmacokinetics and immunogenicity of currently marketed biopharmaceutics, and unlock the possibility of adopting highly immunogenic proteins to improve human health.

Acknowledgements

For all the works presented here, the author would like to thank his advisor, Dr. Shaoyi Jiang for support, monetary, inspiration and funding. The author also thanks all committee members, Dr. Suzie Pun, Dr. Cole DeForest, and Dr. Karl F. Böhringer, for their support and insights into the project. The author would also thank Dr. Priyesh Jain, Dr. Fang Sun and all members in Prof. Jiang's research group for their kind help and discussion. The author would especially thank his family for the continuous support along this long journey.

Table of Contents

List of Tables

List of Figures

Chapter 1 Introduction

Biopharmaceutical drugs, including peptides, proteins, monoclonal antibodies, drug-antibody conjugates and aptamers, offer significant advantages over small molecule therapeutics due to their specific bioactivity and high potency. More than 200 biotech products were marketed during the last three decades, with over 900 new products currently in the pipeline.[1] Despite the huge success of biopharmaceutics, these structurally complex biomacromolecules usually face great challenges including instability, inadequate circulation half-life and immunogenicity.[2, 3] A short half-life limits therapeutic efficacy and requires a frequent administration regimen. Immune responses against many biological drugs not only result in accelerated blood clearance during chronic use, but also threaten patients' lives with adverse effects including anaphylaxis and infusion reactions.[4]

The most successful strategy thus far to overcome these shortcomings is the conjugation of polyethylene glycol (PEG) to these biomacromolecules, a process known as PEGylation.[5] PEG is a water-soluble synthetic polymer consisted of ethylene glycol ($-CH_2-CH_2-O-$) repeating units. It has been recognized as a classic "non-fouling" material that resists non-specific protein adsorption, and is used to coat various surfaces from biomedical devices to drug delivery nanoparticles. In an aqueous solution, PEG holds a stable hydration layer through hydrogen bonding to water molecules; this hydration layer in tandem with PEG's flexible chains can resist nonspecific protein adsorption to the underlying surfaces.[6-8] Similar to this adsorption-resistance mechanism, covalently conjugating PEG to biomacromolecules significantly increases their hydrodynamic size through the strong hydration effect, helping them avoid rapid renal clearance and prolong

circulation half-life. In addition, it is believed that hydrated PEG brushes can shield antigenic epitopes from immune system recognition, helping the underlying biomacromolecule escape from clearance by the reticuloendothelial system and thus mitigate immunogenicity.[9] Since the launch of the first commercial PEGylated protein pegademase bovine used to treat severe combined immunodeficiency disease (SCID) in 1990, at least 10 PEGylated drugs have been approved by the United States Food and Drug Administration (US FDA) and more than 20 are currently in clinical trials. Several review articles have summarized the progress and future prospects of this technology.[5, 10-12]

PEG has been considered as a biologically inert material with no immunogenicity and antigenicity in early studies.[9, 13] For example, the first publication utilizing PEG to alter protein immunogenicity tested PEGylated bovine serum albumin (BSA) in rabbits, in which neither anti-BSA nor anti-PEG Abs were found in the study.[9] However, animal studies in the ensuing decade have found anti-PEG Abs after immunization with PEGylated proteins, although whether it was clinically relevant remained unclear at that time.[14] Until recently, with more PEGylated products entering the clinic, several reports correlated the generation of anti-PEG Abs with loss of therapeutic efficacy and there has been an increase of reported adverse effects after repeated administrations.[15-19] In addition to PEGylated proteins, PEG-modified nanoparticles, e.g., liposomes and micelles, have also been reported to stimulate anti-PEG Ab generation in animal models.[20-26] Ishida et al. did extensive studies on PEG-liposome stimulated immune responses and summarized their findings in a recent review.[27] Altogether, these findings raise obvious concerns regarding the safety and efficacy of

PEGylated drugs. An alternative to this ‘gold standard’ strategy is urgently needed to supplement or replace PEGylation.

In this dissertation, alternative protein modification technologies are developed aiming to improve the safety and efficacy of biological therapeutics. In Chapter 2, the key factors affecting the immunological properties of PEGylated protein drugs from both material and methodology points of view are analyzed. The material immunogenicity determines polymer-specific immune responses while protein surface coverage density affects the immunogenicity of the conjugate. Based on these findings, a zwitterionic encapsulation technology is proposed to increase protein stability, prolong circulation half-life and reduce immunogenicity. To protect the protein cargo from the body clearance and immune system, a poly(carboxybetaine) (PCB) hydrogel thin layer is coated on a protein surface. PCB is a superhydrophilic polymer, which possesses lower immunogenicity than PEG while the crosslinked hydrogel coating maximizes protein surface coverage. The coated PCB hydrogel shields protein epitopes by strong hydration effect, rendering the whole protein invisible to the body immune system. Highly immunogenic uricase is used as the model therapeutic for technology development.

In Chapter 3, we apply this new technology to protective applications. Organophosphate (OP) compounds pose great challenges to public health, since they are widely used as pesticides and chemical weapons. Their acute toxicity makes rescue extremely difficult, and post-exposure effects are serious. Enzyme based bioscavenger is a potential strategy to countermeasure these challenges. Butyrylcholinesterase (BChE) is a candidate that can scavenge OP molecules stoichiometrically in bloodstream before these toxic molecules reach their targets. Human blood derived BChE is considered as a

safe and effective bioscavenger for human use. However, the blood source for its production is quite limited. Animal blood derived BChE is also able to scavenge OP molecules effectively, but its strong immunogenicity hinders its further applications. By adopting the zwitterionic encapsulation technology, the immunogenicity of equine serum derived BChE can be significantly reduced, making it possible to be used for human protection.

Compared with stoichiometric bioscavengers, catalytic bioscavenger offers much higher potency in scavenging OP compounds. Although numerous efforts have been devoted, long-lasting catalytic bioscavengers have seldom been reported. In Chapter 4, we construct a nanoparticle-based bioscavenger that offers long-term protection against OP intoxication. The nanoscavenger is designed by encapsulating an organophosphate hydrolase (OPH) enzyme within a stealth zwitterionic PCB polymer hydrogel layer. Native OPH is a highly immunogenic bacterial membrane protein with extremely short *in vivo* circulation half-life. The stealth gel surface aims to protect the nanoscavenger from blood clearance, while OPH core catalytically breaks down toxic OP compounds. Combining the high catalytic scavenging capability with long blood residence time, the nanoscavenger prophylactic strategy aims to provide a promising solution to fill the needs for both civilian and military applications.

Besides developing PEGylation alternative technologies, efforts are devoted to reducing current PEG related clinical risks. As more PEGylated therapeutics entering market, and high prevalence of pre-existing anti-PEG antibody existing in general population[28, 29], screening blood anti-PEG antibody is becoming necessary in clinical settings. However, the existing technologies are usually laborious, time-consuming and

lack of comparability. In Chapter 5, a surface plasmon resonance (SPR) biosensor is developed for the rapid detection of anti-PEG antibodies in blood samples. By tailoring the surface chemistry, mPEG is selected as the coating material for sensor chips. The coated mPEG layer serves dual roles – as the non-fouling coating to reduce background noise and as the anchored antigen to catch analytes. The SPR sensor is able to detect anti-PEG antibodies quantitatively with better sensitivity than direct ELISA. By using secondary antibodies, different anti-PEG antibody isotypes can also be differentiated and measured. The clinical application of the SPR sensor is also demonstrated using one patient blood sample.

Chapters 2-4 demonstrate the effectiveness of zwitterionic gel encapsulation as an alternative tactic to PEGylation for protein modification. Although pharmacokinetics and immunological properties are greatly improved, the material is still non-biodegradable. To endow biodegradability to protein modification materials, zwitterionic polypeptide are designed and synthesized in Chapter 6. A carboxybetaine group functionalized polypeptide (PepCB) is synthesized via N-Carboxyanhydrides (NCA) ring-opening polymerization and "click" type thiol-yne chemistry. Superhydrophilicity is maximized by integration of two CB groups in one repeating unit and the backbone endgroup is sophisticatedly tailored to facilitate protein conjugation. The polypeptide backbone endows the biodegradability, while high density zwitterionic CB groups ensure long circulation half-life and low immunogenicity. PepCB is aiming to serve as a biodegradable non-immunogenic modifier material for biologic therapeutic modifications.

Besides all of these passive strategies to simply hide proteins from the immune system, it is also of particular interest to prevent the undesired immune responses proactively. An immunomodulatory bioconjugation compatible to current PEGylation is described in Chapter 7. To suppress anti-drug antibodies, PEGylated uricase was conjugated with an immunomodulator, rapamycin, through a cleavable disulfide bond. When circulating in blood, the bioconjugate will play its therapeutic role as normal PEGylated drugs while the conjugated rapamycin can be released and prevent immune responses once the bioconjugate is uptaken by antigen presenting cells. The conjugation chemistry ensures the co-delivery of the immunomodulator and the protein, avoiding potential systemic immune suppression and related complications.

The goals of new protein drug modifications are: 1) increasing *in vivo* circulation half-life; 2) reducing undesired immune responses; and 3) avoiding material-related side effects. The strategies described in this dissertation have the potential to be translated, not only to improve the performance of existing protein therapeutics, but also enable new drugs into clinics.

Chapter 2 Zwitterionic Gel Encapsulation Promotes Protein Stability, Enhances Pharmacokinetics and Eliminates Immunogenicity

Advances in protein therapy are hindered by the poor stability, inadequate pharmacokinetic (PK) profiles, and immunogenicity of many therapeutic proteins. Polyethylene glycol conjugation (PEGylation) is the most successful strategy to date to overcome these shortcomings, and more than ten PEGylated proteins have been brought to market. However, anti-PEG antibodies induced by treatment raise serious concerns about the future of PEGylated therapeutics. Here, we demonstrate a zwitterionic polymer network encapsulation (ZPNE) technology that effectively enhances protein stability and pharmacokinetics while mitigating immune response. Uricase modified with a comprehensive zwitterionic polycarboxybetaine (PCB) network exhibited exceptional stability and a greatly prolonged circulation half-life. More importantly, the PK behavior was unchanged and neither anti-uricase nor anti-PCB antibodies were detected after three weekly injections in a rat model. This technology is applicable to a variety of proteins and unlocks the possibility to adopt highly immunogenic proteins for therapeutic or protective applications.

2.1 Introduction

As an emerging class of therapeutics, protein drugs offer the advantages of higher specificity and potency than small molecules due to their structural complexity [1]. However, this complexity increases their vulnerability to environmental changes and immune system recognition, and thus hinders their formulation and delivery. Additionally, the immunogenicity of many protein drugs not only limits their therapeutic efficacy, but also threatens patients' lives with adverse effects including anaphylaxis and infusion

reactions [4]. As a result, only minimally immunogenic proteins can be developed into human therapeutics, which greatly restricts the possibilities and diversity of protein therapies. Numerous efforts have been made to humanize non-human sourced proteins, but limited successes have been achieved compared with the bright initial prospects.

Conjugating polyethylene glycol (PEG) to proteins, known as PEGylation, is thus far the most successful tactic used to mitigate an immune response to therapeutic proteins [5, 11, 15]. When it was first introduced to alter protein immunogenicity in the 1970s, PEG was thought to be non-immunogenic and non-antigenic [9]. However, several studies in the subsequent decades have found anti-PEG antibodies after treatment with PEGylated therapies, with titers strongly related to modification density and the immunogenicity of the anchoring protein [14, 15]. The haptenic character of PEG is considered the main culprit in the therapeutic efficacy loss of PEGylated products. Recent clinical studies of Pegloticase (PEGylated uricase) in refractory chronic gout patients unequivocally demonstrated that anti-PEG antibodies correlate with a reduction in drug effectiveness—Pegloticase loses efficacy in more than 40% of patients, and the presence of anti-PEG antibodies doubles the risk of infusion reactions [17, 19]. Similar results have also been observed for other PEGylated proteins in clinical use, including PEG-asparaginase [16] and Peginterferon alfa [30]. PEGylated nanoparticles such as liposomes also stimulate a strong anti-PEG response, and these antibodies were found to cross-react with different PEGylated products [22, 23]. Even more concerning, the prevalence of anti-PEG was found to be 22-25% in a sample of 350 healthy blood donors, attributed to daily exposure of PEG-containing consumer products [31]. Altogether, these findings raise obvious concerns regarding the current and future efficacy of PEGylated

drugs. An alternative to this ‘gold standard’ strategy is urgently needed to supplement or replace PEGylation.

Based on extensive studies of PEGylation, we believe that two issues are responsible for its immune response: the immunogenicity/antigenicity of PEG itself, and limited PEG coverage on the protein surfaces. Systematic studies have shown that PEG immunogenicity strongly correlates with the hydrophobic characteristics of this amphiphilic polymer [32-34]; we thus hypothesize that a truly hydrophilic polymer should do a better job. Zwitterionic materials have emerged as an important class of extremely hydrophilic biomaterials, demonstrating particularly high hydration and ultra-low protein adsorption [35-37]. Carboxybetaine is unique among these zwitterionic materials due to its structural similarity to glycine betaine, a naturally occurring compound in the human body [35]. Surfaces modified with polycarboxybetaine (PCB) have exhibited protein adsorption below 0.3 ng/cm^2 from 100% blood plasma or serum [38]. In a more recent study, zwitterionic hydrogels comprising carboxybetaine monomer and crosslinker were shown to resist the foreign-body reaction when implanted in mice for 3 months, due to the ultra-hydrophilic and biocompatible nature of the gel [39]. Moreover, PCB-coated gold nanoparticles were shown not to induce a measurable antibody response in rats after repeated intravenous (IV) injections [40]. These findings motivated us to test polymer-protein constructs utilizing PCB as an alternative with no or less immunogenic to PEGylation. In terms of methodology, PEGylation processes conjugate multiple linear polymers to a protein surface to camouflage surface epitopes. Due to the limited number of conjugation sites available, or as a tradeoff to preserve protein activity, conjugated polymers may be insufficient to conceal all “danger signals”.

The anchoring protein may in turn amplify the immunogenicity of conjugated polymers, causing the inverse correlation reported between the graft density and immune response [14]. To overcome this limitation, we adopted bifunctional CB monomers to crosslink conjugated polymers into a "mesh" network, designed to possibly mask protein surfaces completely and maximize surface hydration. We evaluated the *in vitro* and *in vivo* performance of this zwitterionic polymer network encapsulation (ZPNE) technology by choosing highly immunogenic fungal-derived uricase as a model therapy, and compared the stability, pharmacokinetics and immunogenicity to its PEGylated counterpart.

2.2 Experimental Section

2.2.1 Materials

Recombinant uricase from *Candida* sp. and all chemicals were purchased from Sigma-Aldrich unless otherwise noted, and were used as received. Methoxy polyethylene glycol succinimidyl carbonate, MW 10kD (mPEG-NHS, 95%) was obtained from Nanocs Inc., USA. Carboxybetaine acrylamide (CBAA) monomer was synthesized following a previously published method[41].

2.2.2 Synthesis of carboxybetaine acrylamide crosslinker (CBAAX)

The synthetic route of CBAAX is shown in **Figure 2.1**. A solution of acryloyl chloride (5.3 mL, 65.1 mmol) in 20 mL DCM was added dropwise to a solution of N-methyl-2,2'-Diaminodiethylamine (4 mL, 31.0 mmol) and DIPEA (11.9 mL, 68.3 mmol) in 50 mL DCM at 0 ^{o}C for a period of 30 min. The reaction mixture was allowed to warm to room temperature and stirred for two hours. The reaction mixture was then washed with (2 x 25 mL) water. The aqueous layer was re-extracted with DCM (3 x 75 mL). The combined organic layers were dried using sodium sulfate, filtered and

concentrated in vacuo to leave a residue which was further purified by column chromatography to give compound **2** (5.2 g) in 75.3% yield. ^{1}H NMR (300 MHz, D_2O) δ 6.02 – 5.97 (m, 4H), 5.56 – 5.51 (m, 2H), 3.14 (t, *J* = 6.7 Hz, 4H), 2.37 (t, *J* = 6.7 Hz, 4H), 2.07 (s, 3H).

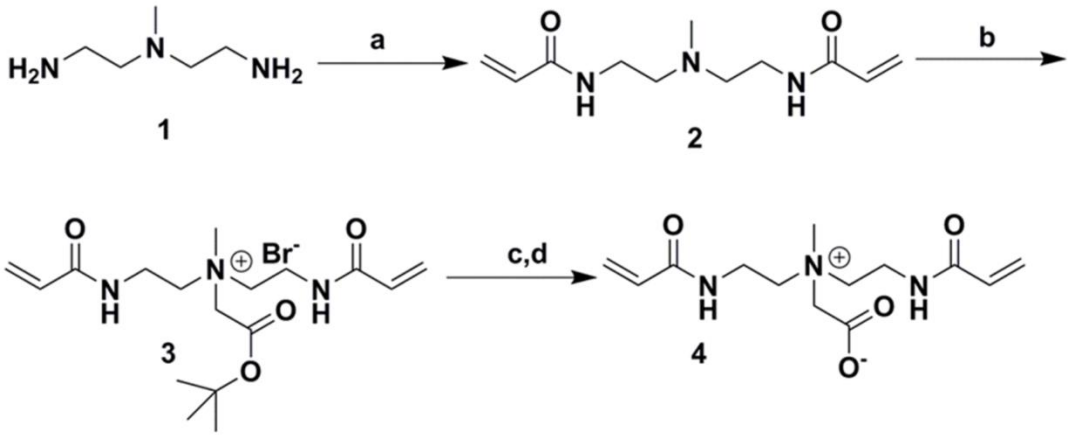

Figure 2.1 Synthesis of CBAAX. (a) DIEA, Acryloyl Chloride, DCM, 75%; (b) $BrCH_2CO_2tBu$, CH_3CN, 60 ^oC, 73%; (c) TFA:DCM 1:1; (d) MeOH, IRN-78 resin hydrolysis, 84%.

Compound **2** (3.2 g, 10.5 mmol) was dissolved in 20 mL acetonitrile and tert-butyl bromoacetate (4.2 mL, 31.6 mmol) was added to it. The reaction contents were stirred for 18 hours at 65 ^oC until the TLC showed complete consumption of starting material. The reaction mixture was concentrated to dryness in vacuo and further purified by column chromatography to give compound **3** (4.3 g) in 72.6% yield. ^{1}H NMR (300 MHz, DMSO-d_6) δ 6.31 – 6.08 (m, 4H), 5.67 (dd, $J_1 = J_2 =$ 2.4 Hz, 2H), 4.48 (s, 2H), 3.75 – 3.54 (m, 8H), 3.29 (s, 3H), 1.45 (s, 9H).

Compound **3** (2.0 g, 4.7 mmol) was dissolved in 15 mL DCM and 15 mL TFA was added to it. The reaction contents were stirred overnight at room temperature. After complete hydrolysis, the reaction mixture was concentrated in vacuo and co-evaporated with DCM (3 x 15 mL). The resulting residual mixture was further dissolved in 15

methanol and 4 g IRN-78 resin was added to it for complete neutralization. The reaction mixture was then filtered over celite and concentrated to dryness in vacuo. The residue was dissolved in water and lyophilized on freeze dryer to give compound **4** in 84.1% yield. ^{1}H NMR (300 MHz, DMSO-d_6) δ 6.31 – 6.05 (m, 4H), 5.63 (dd, $J_1 = J_2 = 2.4$ Hz, 2H), 3.70 (s, 2H), 3.69 – 3.50 (m, 8H), 3.21 (s, 3H).

2.2.3 Protein encapsulation and polymer conjugation

For zwitterionic polymer network encapsulation, uricase was first modified to introduce acryloyl group onto its surface. The reaction was performed by dissolving 20 mg uricase into 10 ml 50-mM HEPES buffer (pH 8.5), followed by adding 75 μl N-acryloxysuccinimide (NAS) DMSO solution (20 mg/ml) dropwise. The reaction was stirred at 4 ℃ for two hours. The polymer encapsulation was done via *in situ* radical polymerization by adding 400 mg CBAA monomer, 80 mg CBAAX crosslinker, 10 ml HEPES buffer, 15 mg APS and 60 μl TEMED into the former reaction solution. After stirring for another 2 hours, the reaction mixture was concentrated and washed extensively by PBS 7.4 using 300 kDa molecular weight cutoff centrifugal filters.

Uricase-PEG conjugates were prepared in 50-mM HEPES buffer (pH 8.5), with uricase concentration at 1 mg/ml and mPEG-NHS concentration at 10 mg/ml. The reaction was stirred at 4 ℃ overnight. Then the conjugates were concentrated and washed extensively by PBS 7.4 using a 300 kDa molecular weight cutoff centrifugal filter. The protein residue activity was measured by a commercially available uricase activity kit (Life technologies, USA).

2.2.4 Pharmacokinetics and biodistribution study

The pharmacokinetics of native and modified uricase is studied using Spraque Dawley rats (male, body weight 74~100 g) as the animal model. Each sample has three duplicates to generate statistical significance. All animal experiments adhered to federal guidelines and were approved by the University of Washington Institutional Animal Care and Use Committee. For pharmacokinetic studies, each protein sample was administered into the rat via tail vein injection at the dose of 25 U/kg body weight. Blood samples were collected from the tail vein at 5 min, 6 h, 24 h, 48 h and 72 h after the injection. The blood samples were put in heparinized vials, centrifuged and the enzyme content in plasma was estimated by enzyme activity. The IV injections and bleeding procedure were repeated three times with one week as time interval between each injection. Five weeks after the first injection, 5 mL of blood were drawn by using cardiac punch and serum was prepared for antibody detections. All pharmacokinetical parameters were calculated using PKSolver following instructions.

For biodistribution study, all rats were given unlabeled samples for the first and second dose, followed by fluorescein isothiocyanate (FITC) labeled samples for the third dose. At 72 h postinjection, all rats were sacrificed and the heart, liver, spleen, lung, kidney and blood were collected for further analysis. The collected organ tissues were homogenized using a tissue ruptor, followed by centrifugation at 4200 rpm for 30 min at room temperature. The fluorescence of particles in the tissues was measured using a microplate reader and compared to a standard curve generated using FITC labeled samples added to untreated homogenized tissues.

2.2.5 Measurement of thermal stability

Modified protein samples (protein concentration 40 ug/mL in 0.1 M Tris buffer, pH 8.0) were incubated at 65℃ in water bath. At different time points, each sample was

taken out and quenched in ice bath until measurement. After the final samples taken out at 2 h, activities of all samples were measured using the uricase activity kit following the manufacturer's protocol. Values were recorded as percentage of each sample activity before heating.

2.2.6 Enzyme-linked immunosorbent assay (ELISA)

The antigens used in direct ELISAs consisted of native uricase (for detection of anti-uricase antibody), BSA-PEG conjugates (for detection of anti-PEG antibody) and BSA-PCB conjugates (for detection of anti-PCB antibody). BSA-PEG conjugates were made following the same procedure as uricase-PEG samples. BSA-PCB conjugates were made following similar procedure as making uricase-PCBX but with no crosslinkers during polymerization. For ELISA experiments, 100 μL antigen solution (10 μg/mL of protein concentration) prepared in 0.1 M sodium carbonate buffer, pH 10.5, was used to coat each well of the 96-well plates. During coating procedure, plates were incubated at 4 ℃ overnight. After removing antigen solutions, the plates were washed five times using phosphate-buffered saline (PBS 7.4) and then filled with blocking buffer (1% BSA solution in 0.1 M Tris buffer, pH 8.0). It is important to avoid using any buffer that contains PEG-like detergents, e.g. Tween 20 and Tween 80. After incubation at room temperature for 1 hour, blocking buffer was removed and all wells were washed by PBS for another five times. Serial dilutions of rat sera in PBS containing 1% BSA were added to the plates (100 μL/well), which were incubated for 1 h at 37 °C. The plates were then washed five times with PBS. Goat anti-rat IgM or IgG conjugated to horseradish peroxidase (HRP) (Bethyl labs, USA) was used as the secondary antibody for detection of IgM and IgG. After adding the secondary antibody, plates were incubated at room

temperature for 1 hour, and then washed five times using PBS before the addition of 100 μL/well HRP substrate 3,3',5,5'-Tetramethylbenzidine (TMB, Bethyl labs). The plates were shaken for 15 min and 100 μL stop solution (0.2 M H_2SO_4) was added to each well. Absorbance at 450 nm (signal) and 570 nm (background) was recorded by a microplate reader. Pre-bleeding sera were used as negative control for all ELISA detections. Commercially available rat anti-PEG antibodies were used as positive control for anti-PEG detections. The positive signal was defined as absorbance significantly larger than corresponding negative control.

2.2.7 SPR detection of anti-polymer antibodies

Both PCB and PEGMA polymer brushes were grafted onto gold-coated SPR sensor chips following previously published methods[41]. Brush thickness was measured by a spectroscopic ellipsometer (Sentech SE-850, GmbH). SPR detection of anti-polymer antibodies was optimized at different polymer brush thickness and ~10 nm film thickness was found to have the best signal/noise ratio. A custom-built SPR sensor was used in this study. All experiments were done following the sequence of flowing PBS 10 min, 1:20 diluted serum in PBS 15 min, PBS 15 min at flow rate of 30 μL/min. For the SPR sensor used in the study, a 1 nm SPR wavelength shift represents a surface coverage of ~17 ng/cm^2 for proteins. Detection limit for the SPR sensor used in this work is 0.3 ng/cm^2.

2.2.8 Statistics

Student's t test was chosen to compare two small sets of quantitative data when data in each sample set were related, with $P < 0.05$ being considered as statistically significant.

2.3 Results and Discussion

2.3.1 Zwitterionic encapsulation of uricase

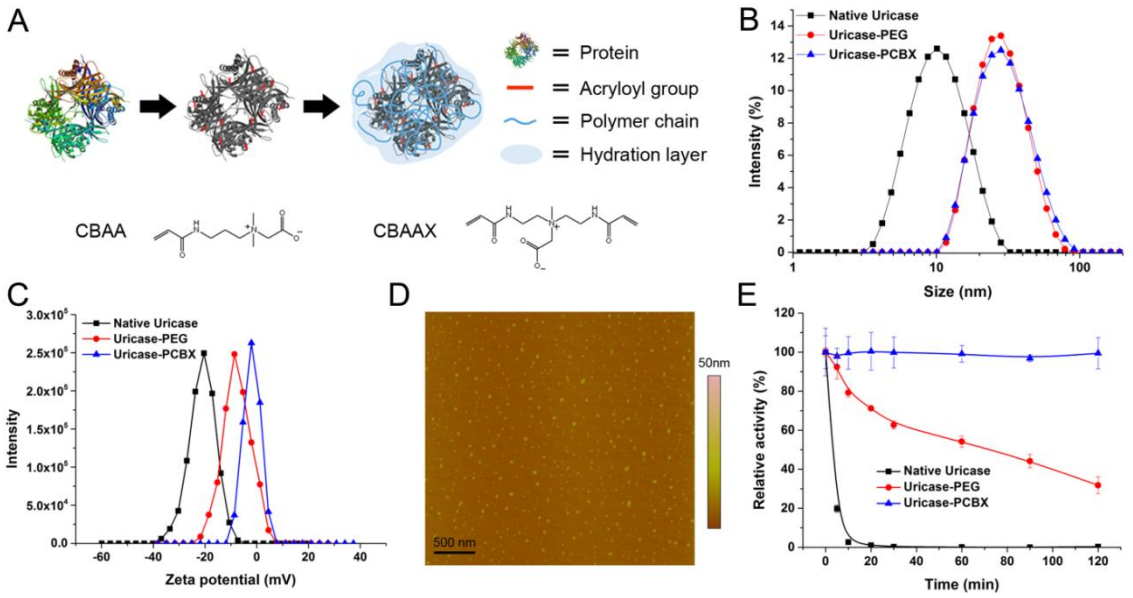

Figure 2.2 Zwitterionic protein encapsulation and characterization. (A) Molecular structure of CBAA monomer and CBAAX crosslinker, and the process of ZPNE modification of a protein surface. (B) Size distributions and (C) zeta potentials of modified uricase *vs.* native uricase. (D) AFM image of formed zwitterionic nanocapsules. (E) Thermal stability study of modified uricase *vs.* native uricase, as retained activity after incubation at 65 ℃

In our hypothesis, there are two crucial aspects to the design of protein protection strategies: the adoption of a super-hydrophilic biomaterial and the comprehensive coverage of protein surface epitopes. A crosslinked carboxybetaine-based gel coating meets these criteria. However, incorporating a conventional crosslinker (e.g., ethylene glycol dimethylacrylate) may introduce unwanted hydrophobicity and compromise the hydrophilicity of the crosslinked gel coating. To avoid this detrimental possibility, we designed a bifunctional CB crosslinker carboxybetaine acrylamide crosslinker (CBAAX) (**Figure 2.2a**) to maximize surface hydration. This carboxybetaine crosslinker has proven to be a key for PCB hydrogels to resist the foreign-body reaction [39] and restrain mesenchymal stem cell differentiation [42]. To realize ZPNE in this work, each protein

was encapsulated in a hydrogel nanoparticle through surface acrylation and *in situ* free radical polymerization reactions. Basic characterization data are shown in **Figure 2.2** and **Table 2.1**. Both PEGylated uricase and ZPNE-modified uricase (denoted as uricase-PCBX) shared a similar hydrodynamic size of around 30 nm, much larger than the ~10 nm diameter of the native uricase tetramer. Zeta potential measurements of uricase-PCBX showed a neutral surface charge (-2.2 mV), indicating more comprehensive surface coverage than that of uricase-PEG (-8.4 mV). Atomic force microscopy (AFM) result showed that uricase-PCBX nanoparticles have a mean diameter of 28.6 ± 6.1 nm, in consistent with those from DLS measurements. Gel permeation chromatography (GPC) results revealed that five PEG molecules were conjugated to each uricase subunit. It should be noted that due to the difficult "graft-to" conjugation of a large polymer to a protein, this was the maximum conjugation number obtained after conjugation condition optimizations. In contrast, it was much easier to achieve higher degrees of surface modification with the ZPNE technique. To maintain a high residual activity (> 90%), we limited the surface conjugation number around twelve. The whole modification process is simple and applicable to a wide variety of proteins. The core-shell structure of these zwitterionic nanocapsules exploits a highly hydrated polymer shell to render the protein core 'stealth' to its surroundings and conceivably to immune system recognition. Compared to conventional protein-polymer conjugates, this core-shell structure provides better protection for its inner cargo.

Table 2.1 Characteristics of uricase samples

Sample	Conjugation number	Hydrodynamic Size (nm)[c]	PDI	Zeta potential (mV)	Activity (%)
Native Uricase	—	10.9	0.17	-20.8	100
Uricase-PEG	5[a]	30.6	0.21	-8.4	93
Uricase-PCBX	12[b]	31.3	0.20	-2.2	91

a Measured by GPC, data expressed as number per subunit
b Measured by matrix-assisted laser desorption-ionization time-of-flight mass spectrometry (MALDI-TOF MS), data expressed as number per subunit
c Measured by dynamic light scattering (DLS)

2.3.2 *In vitro* protein stability

Preparation of therapeutic proteins is often prone to instability during storage and usage. Similarly, enhanced structural stability is a desirable attribute of modification technologies. Thermal stress tests at elevated temperatures are a facile approach to evaluate differences in protein stabilities in a relatively short time [43-45]. A protein conjugate or nanocapsule stable at higher temperatures is likely to be stable at ambient temperatures for a longer period. To test the stability of modified proteins to environmental stressors, their enzymatic activities were assayed after incubation at 65 ℃ for different time periods, and presented as the percentage of pre-heating activity retained. As shown in **Figure 2.2e**, uricase-PCBX has exceptional thermal stability and retained 100% activity after 2 hours of incubation. In contrast, uricase-PEG only exhibited a modest stabilizing effect.

The present result, that uricase-PCBX remains stable at 65 ℃, suggests that it would not require low-temperature storage or formulation with stabilizing excipients as is the case for the native protein. This is important when considering situations in which low-temperature storage or transportation is unavailable, and may help to lower the high cost of therapeutic protein production and usage. In a previous study, PCB was shown to

impart a superior protein-stabilizing effect and increase the substrate affinity to protein binding sites when similar protein conjugation structures were tested [44]. The monomer unit itself is a derivative of glycine betaine, a natural molecule found in many living systems as a stabilizing agent. Encapsulating a protein in a PCB gel network is analogous to placing it into a highly concentrated protein stabilizer solution, equipping it with a protective microenvironment that accompanies the protein both *in vitro* and *in vivo*. Furthermore, the nanocapsule structure has also been reported to stabilize enzymes through multiple covalent attachments between the enzyme core and polymer shell, which effectively hinder conformational changes in adverse environments [45, 46]. Combining these two distinct mechanisms, it is unsurprising that PCB gel encapsulation affords superior stability to protein cargos.

2.3.3 Pharmacokinetics study

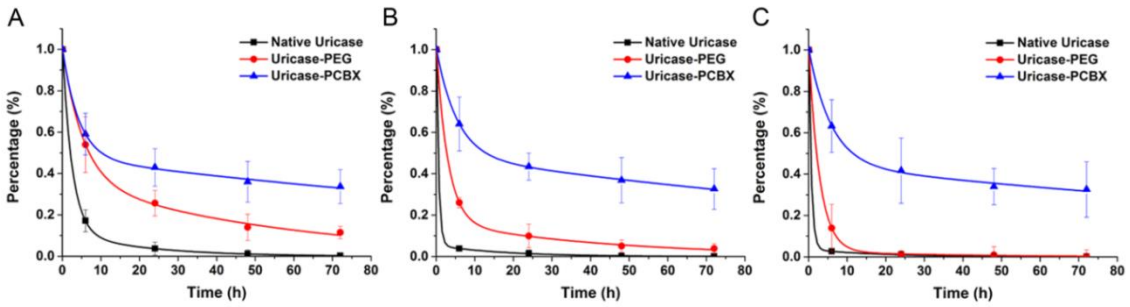

Figure 2.3 Blood circulation profiles of modified uricase *vs.* native uricase. (A) Circulation curves after the first I.V. administration, (B) second administration, and (C) third administration.

Since the 1970s, PEGylation has become the gold standard to alter the PK properties of both proteins and a variety of drug delivery nanoparticle platforms [5, 47]. Surface attachment of PEG significantly prolongs *in vivo* circulation times by increasing

hydrodynamic size to avoid rapid renal clearance (for small particles) and reducing interactions with both blood components (opsonization) and immune cells. The PK profile of ZPNE-modified uricase was compared with the gold standard in healthy Sprague Dawley rats through repeated intravenous injections. **Figure 2.3** shows the circulation profile of native and modified uricase after each injection. All concentration-time curves fit a two-compartment model. Pharmacokinetic parameters are listed in **Table 2.2**. Upon the initial injection, uricase-PEG exhibited an elimination half-life ($t_{1/2}\beta$) of 38.2 h, 3-fold higher than the 13.9 h $t_{1/2}\beta$ of native uricase. The area under curve (AUC_∞) of PEGylated uricase is 5X that of the native enzyme, roughly in agreement with values reported in the literature [48]. By contrast, uricase-PCBX showed exceptionally prolonged circulation behavior, with a $t_{1/2}\beta$ of 134.9 h, a 3.6-fold improvement over uricase-PEG and 10-fold higher than the native enzyme. Moreover, the AUC_∞ of uricase-PCBX was 4.2X that of uricase-PEG, indicating its significantly higher systemic availability.

Table 2.2 Pharmacokinetic parameters after repeated injections

Parameters	Native Uricase (different injections)			Uricase-PEG (different injections)			Uricase-PCBX (different injections)		
	1	2	3	1	2	3	1	2	3
$t_{1/2}\alpha$ (h)	1.7	0.4	0.5	3.7	2.1	1.9	2.9	3.7	4.0
$t_{1/2}\beta$ (h)	13.9	12.5	13.2	38.2	30.6	24.8	134.9	121.3	145.5
AUC_∞ (μg/ml×h)	296	85	90	1394	590	237	5796	5658	6126
CL (ml/h)	3.38	14.17	16.68	0.72	2.03	6.34	0.17	0.21	0.24
MRT (h)	11.6	11.2	9.7	48.1	33.6	11.5	190	170	203

Uricase, used in the present study, is a large tetrameric protein with a molecular weight of ~130 kDa. The rapid clearance of native uricase is considered to be associated with an irreversible uptake process, likely by the reticuloendothelial system (RES), rather

than a renal filtration process [49]. Conjugating a total of twenty large PEG molecules (Mw 10 kDa) to uricase can effectively cover a large portion of its surface, minimizing non-specific uptake clearance. This phenomenon is closely related to material hydration and non-fouling character. As a well-known class of ultra-low fouling materials, zwitterionic polymers have indeed been used to extend the circulation lifetime of nanoparticles [50-52]. Specifically, PCB-coated nanoparticles have demonstrated a longer circulation half-life than PEG-coated counterparts under identical conditions [40]. Similarly, we believe that a PCB polymer would also be able to improve the circulation profile of proteins. Apart from material properties, recent research has shown surface coverage density to be another important factor affecting particle uptake by immune cells and *in vivo* circulation behavior [53]. A high surface grafting density of PEG molecules exceeding the minimum for a brush conformation is required for nanoparticles to evade immune cell uptake and clearance. However, in the case of protein modification, there is a certain limit to conjugation density due to the restricted number of available functional groups on the surface of a protein. A crosslinked hydrogel "mesh", which does not need a high number of conjugation sites, can effectively overcome this problem. A thin hydrogel layer can ideally mask the entire protein surface, making it "stealth" to surroundings and thus slower down the RES clearance. The results of this study confirm our hypothesis that greatly extended circulation profiles of protein therapeutics can be realized by PCB nanocapsule encapsulation. Patients could benefit greatly from this advance by facing reduced administration frequency as compared with PEGylated products.

Uricase is administered chronically in clinical practice to treat refractory chronic gout, so repeated injections were performed to evaluate the long-term performance of

ZPNE-modified and PEGylated proteins. The second and third injections were given at days 7 and 14 after the initial injection. It should be noted that severe infusion reactions were observed 3~5 min post the second and third injections of both native uricase and uricase-PEG, with symptoms including hypopiesia and dyspnea. In contrast, no adverse effects were observed following the uricase-PCBX injections. While the calculated $t_{1/2}\beta$ of native uricase appears comparable after each injection, the sampling frequency was likely inadequate for its rapid elimination; its accelerated elimination after repeated injections is more clearly reflected in the significantly reduced AUC_{∞}. Following the second and third injections of uricase-PEG, an obvious accelerated blood clearance (ABC) phenomenon was noted, with $t_{1/2}\beta$ decreasing to 30.6 and 24.8 h, and AUC_{∞} values dropping 2.8-fold and 5.9-fold, respectively. This accelerated elimination process is most likely due to induction of anti-PEG antibodies, which will be confirmed in the following discussion. Unlike PEGylated uricase, the pharmacokinetic profiles of uricase-PCBX in this study did not show any significant change following three injections, indicating that uricase-PCBX is likely to maintain its superior pharmacokinetic performance in repeated applications.

2.3.4 Detection of antibodies

Serum collected at day 35 after the first injection was tested for both anti-uricase and anti-polymer antibodies using direct enzyme-linked immunosorbent assay (ELISA). As shown in **Figure 2.4a** and **b**, IgG was the major isotype of anti-uricase observed after repeated injections. The measured antibody titers are listed in **Table 2.3**. Due to the strong immunogenicity of the fungal enzyme, the native uricase group developed extremely high IgG antibody titers along with relatively high titers of IgM. In the group

treated with PEGylated uricase, the titers of anti-protein antibodies were significantly less than the native enzyme but still clearly elevated. In contrast, neither anti-uricase IgG nor IgM were detected in the rat group treated with uricase-PCBX. Our results here are consistent with clinical findings, showing that PEGylation cannot completely prevent the generation of anti-protein antibodies, at least for highly immunogenic uricase [19]. This finding supports our hypothesis that comprehensive surface coverage of a protein with a stealth polymer network can effectively render the protein "invisible" to the immune system and thus mitigate antibody induction.

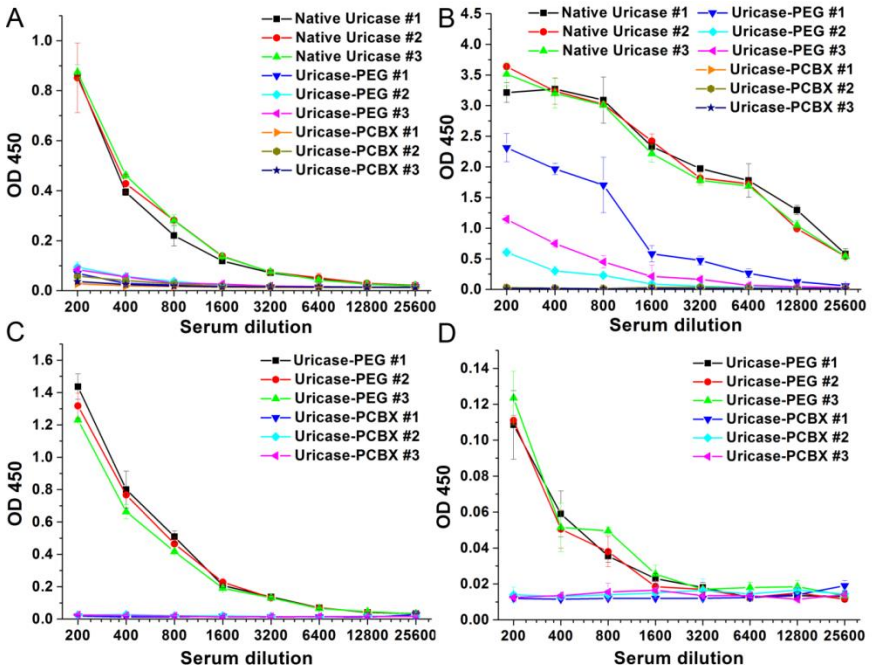

Figure 2.4 Detection of antibodies by direct ELISAs. (A) Anti-uricase IgM, (B) anti-uricase IgG, (C) anti-polymer IgM, (D) anti-polymer IgG. Serum from each rat is plotted separately.

The severe infusion reactions and accelerated drug elimination seen in the native uricase group is apparently related to strong production of anti-uricase antibodies. However, for PEGylated protein therapeutics, clinical trial evidence suggests anti-PEG antibodies rather than anti-protein antibodies to be primarily responsible for infusion

reactions and efficacy loss over chronic injections [17, 19]. Accordingly, strategies to suppress the production of anti-polymer antibodies remain a critical challenge in the development of any therapeutic polymer-protein conjugates. Uricase-PEG and uricase-PCBX groups were tested for anti-PEG and anti-PCB anti-polymer antibodies, respectively, and the results are shown in **Figure 2.4c** and **d**. Notably, at day 35 major anti-PEG response comes from IgM (titers 1:6400) rather than IgG (titers 1:800), suggesting differences in adaptive immunity pathways for the protein and polymer components in the conjugates. Compared with the strong response to PEGylated uricase, no IgG or IgM was detected against the polymeric component of uricase-PCBX.

Table 2.3 Antibody titers detected by direct ELISAs

Sample name	Rat #	Anti-uricase IgM	Anti-uricase IgG	Anti-polymer IgM	Anti-polymer IgG
Native Uricase	#1	1:3200	>1:25600	—	—
	#2	1:3200	>1:25600	—	—
	#3	1:3200	>1:25600	—	—
Uricase-PEG	#1	1:200	1:12800	1:6400	1:800
	#2	1:400	1:1600	1:6400	1:800
	#3	1:400	1:3200	1:6400	1:800
Uricase-PCBX	#1	<200	<200	<200	<200
	#2	<200	<200	<200	<200
	#3	<200	<200	<200	<200

As repeated injections are commonly needed for therapeutic proteins, the antibody response issue cannot be overlooked and should be evaluated carefully. It should be noted that in the earlier work establishing PEGylation to alter protein immunogenicity [9], it was mentioned that neither anti-bovine serum albumin (BSA) nor anti-PEG antibodies were detected after injecting BSA-PEG conjugates into a rabbit model. There are three reasons which may account for their observations. First, BSA shares a large degree of similarity with rabbit serum albumin (RSA) [54], which makes it less immunogenic as a

model protein. In a later study, the generation of antibodies against PEGylated proteins was shown to be strongly related to the protein immunogenicity [14]. This also explains why PEGylated non-human enzymes, e.g., uricase and asparaginase, have been reported to have the most severe issues in clinic trials resulting from anti-PEG antibodies [16, 17, 19]. For this reason, the application of highly immunogenic enzymes *in vivo* still remains a great challenge even with PEGylation technology. Second, a large degree of modification can be easily attained with BSA. The relationship between modification degree and immunogenicity of conjugates was also clearly demonstrated in the later study [14]. Serum albumin is a class of protein with extraordinary ligand binding capacity [54], but this is not the case for most therapeutic proteins. Finally, immunological tests then, e.g., immunodiffusion and complement fixation tests, were not capable of detecting low-titer antibodies.

Since there is no standard method to evaluate anti-polymer antibodies, especially as no positive control is available for the detection of anti-PCB antibodies, we validated our results using a surface plasmonic resonance (SPR) sensor. SPR is an ultra-sensitive technique used in the study of specific/nonspecific protein adsorption on surfaces with detection limits as low as nanogram levels [38]. Compared with ELISA, SPR analysis is more straightforward, as the procedures are simpler and each step can be carefully controlled and monitored. To detect anti-PEG or anti-PCB antibodies, we modified the surface of gold chips with poly(ethylene glycol) methyl ether methacrylate (PEGMA) or PCB polymer brush layers. Both PEGMA and PCB are non-fouling materials that resist non-specific protein adsorption from diluted serum. When serum samples flow over the modified chip surface, only the polymer-specific antibodies can bind to the surface and

generate a SPR signal through specific adsorption (**Figure 2.5a**). The results are shown in **Figure 2.5**. Sera obtained pre-injections were used as a negative control. When sera from uricase-PEG treated rats were flowed over a PEGMA modified chip, adsorption curves showed typical specific binding kinetics with adsorbed mass increasing linearly with time. Protein binding reached 40~50 ng/cm^2 in 15 min under experimental conditions. No nonspecific binding was detected on the same chip from either control serum or uricase-PCBX serum, indicating all adsorption came from anti-PEG antibodies. In contrast, none of the sera showed detectable adsorption on a PCB-coated chip surface, suggesting that there is no antibody in the sera that can recognize and bind to PCB polymers.

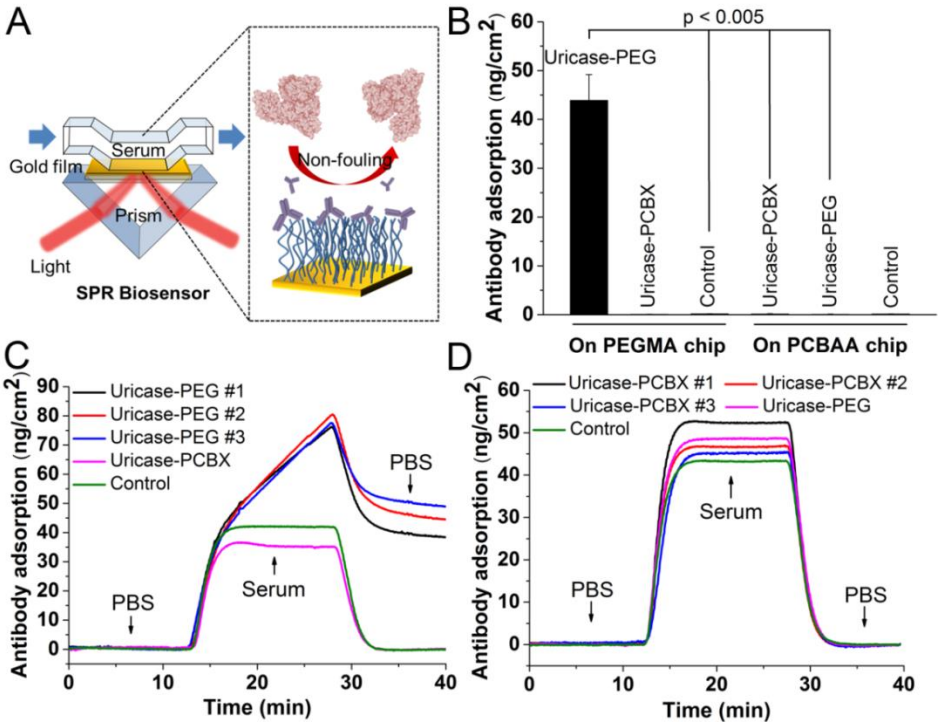

Figure 2.5 Detection of antibodies by a SPR sensor. (A) Scheme showing the detection setup. The gold chip surface was modified with either PEGMA or PCB polymer brushes. The polymer brush serves dual functions, providing a non-fouling background while serving as the investigated antigen. (B) Summary of the SPR detection results. (C) Sensor signal-time curves on PEGMA coated chips, each curve representing one serum sample. No uricase-PCBX serum shows any adsorption onto a PEGMA surface, though only one typical curve is shown here. (D) Sensor signal-time curves on PCB-coated chips.

2.3.5 Biodistribution of modified uricase

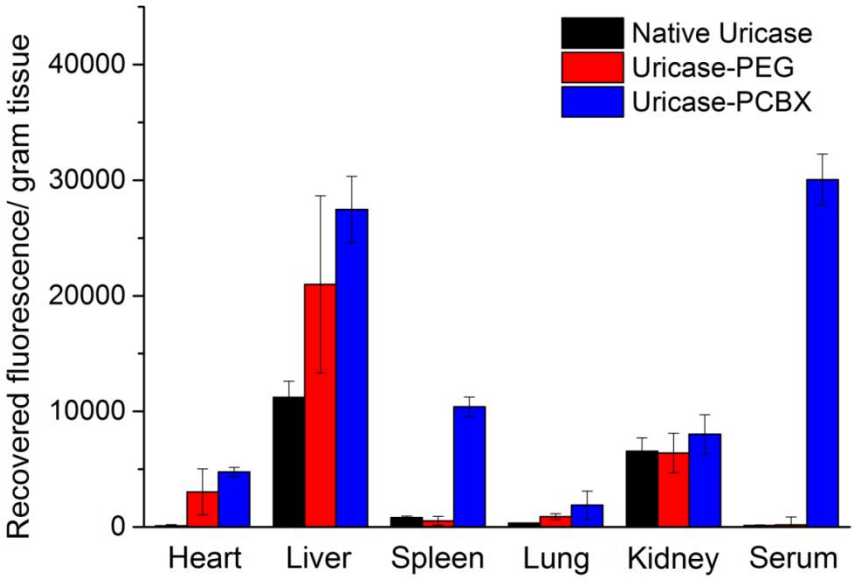

Figure 2.6 Biodistribution of modified uricase *vs.* native uricase after the 3rd injection. Each value is averaged from 3 rats. Standard deviations are shown as error bars.

To examine the biodistribution of modified uricase samples following chronic use, we gathered blood and tissue samples from a treated rat 72 h after the third injection for further analysis. The third doses of uricase, uricase-PEG, and uricase-PCBX were labeled with a fluorescent probe for this test, while unlabeled formulations were given for the initial and second doses to avoid interference. As shown in **Figure 2.6**, the data are presented as recovered fluorescence per gram of tissue. Uricase-PCBX sustained a high serum concentration while all three samples accumulated primarily in the liver. Native uricase was observed to have less organ accumulation compared with protected enzymes three days after injection. This phenomenon can be explained by their different levels of protease stability. Native, unprotected uricase was readily degraded by proteases after liver accumulation, but protected uricase was partially shielded from participation in this

metabolic process. As uricase nanocapsules were prepared using amide-containing crosslinkers, they are expected to degrade through slow hydrolysis. One potential advantage of this persistence is that these nanocapsule constructs may retain their ability to catalyze the oxidation of uric acid even after distribution into organs.

2.4 Conclusions

In summary, we demonstrate here that a polycarboxybetaine polymer network "mesh" coating on a protein effectively improves protein stability, extends pharmacokinetics and mitigates immune response with superior efficacy to PEGylation. PCB-encapsulated uricase did not suffer the accelerated blood clearance encountered by PEGylated uricase during repeated injections in a rat model, and neither anti-uricase nor anti-PCB antibodies were detected in the serum. With its superior ability to mitigating protein immunogenicity, this reported technique makes it possible to adopt highly immunogenic proteins for human therapeutic or protective applications.

Chapter 3 Butyrylcholinesterase nanocapsule as a long circulating bioscavenger with reduced immune response

Butyrylcholinesterase (BChE) is the most promising bioscavenger candidate to treat or prevent organophosphate (OP) poisoning. However, the clinical application of BChE is limited by two obstacles: inadequate circulation half-life and limited sources for production. Although several modification technologies including glycosylation and PEGylation have been developed to improve its pharmacokinetics, none of them was able to outperform blood derived native BChE. In this work, we designed a long-circulating bioscavenger nanogel by coating equine serum-derived BChE with a zwitterionic polymer gel layer. This zwitterionic gel coating protected BChE from denaturation and degradation under harsh conditions. Notably, the nanocapsule exhibited a long circulation half-life of ~ 45 h, 3-fold of the unmodified native version, enabling both therapeutic and prophylactic applications. In addition, the gel coating reduced the immunogenicity of equine BChE, unlocking the possibility to use non-human derived BChE as an OP bioscavenger in humans.

3.1 Introduction

Organophosphates (OPs) are a class of highly toxic synthetic compounds frequently used as pesticides. These compounds, such as dichlorvos and parathion, exert toxicity to insects and other animals, including humans, by inactivating acetylcholinesterase (AChE) in the peripheral and central nervous systems.[55, 56] This rapidly increases acetylcholine levels at cholinergic synapses and produces an acute cholinergic crisis, resulting in neuromuscular paralysis throughout the body and death by respiratory failure.[57, 58] Though their use as pesticides has been regulated in many countries, OPs

remain one of the most common causes of poisoning worldwide. The World Health Organization attributes 200,000 deaths per year in developing countries to OP poisoning.[59] Moreover, many of the most dangerous nerve agents developed as chemical weapons are potent OPs, including soman, sarin, VX and tabun.

Although current anticholinergic antidotes can prevent lethality from OP poisoning, they are unable to mitigate many common post-exposure effects including convulsions, incapacitation, performance deficits and permanent brain damage.[60] Bioscavenger enzymes are a promising alternative treatment, as they can bind to and neutralize OP compounds in the bloodstream before the toxin reaches its physiological target.[61] Plasma-derived butyrylcholinesterase (BChE) has been widely studied as a bioscavenger due to its rapid and irreversible binding to Ops. Exogenously administered BChE from equine or human serum has been shown to protect animals from OP poisoning as well as prevent post-exposure effects.[60, 62] Human plasma-derived BChE is considered as a qualified bioscavenger candidate, having an acceptable circulation half-life *in vivo* to fulfill its mission without causing an immune response or adverse effects.[63] However the production difficulties have hindered the clinical application of human plasma-derived BChE. An extremely large amount of outdated human plasma is needed to generate even a single dose. It was calculated that preparing a small stockpile of plasma-derived BChE (5000 doses) would require dedicating the entire annual U.S. supply of outdated plasma to its production, at a considerable cost.[64] Genetic engineering can produce recombinant human BChE (rh-BChE) at a lower cost, but rh-BChE has a much shorter circulation half-life than the native enzyme.[65] Alternatively, BChE derived from other animal sources such as equine serum may be

used to supplement human BChE, though immunogenicity challenges must first be addressed.[66]

A technique that can effectively improve BChE pharmacokinetics (PK) as well as reduce its immunogenicity is clearly in demand to advance the application of enzyme-based bioscavengers. Glycosylation and PEGylation have been adopted to modify rh-BChE, but the resulting circulation half-life is still unsatisfactory.[67] PEGylation failed to improve the PK of plasma-derived native BChE.[68] Moreover, increasing evidence shows that many PEGylated protein products induce the production of anti-PEG antibodies after administration, challenging the future of this technology.[15, 16, 19] To the best of our knowledge, no modified BChE has PK properties superior to its natural version.

In this work, we have developed a zwitterionic nanogel encapsulation technology to modify BChE from equine serum. Zwitterionic polymers continue to attract growing attention as an important class of super-hydrophilic biomaterials, demonstrating ultra-low levels of protein adsorption and exceptional biocompatibility.[35, 36, 39] Surfaces modified with zwitterionic polycarboxybetaine (PCB) have exhibited protein adsorption below 0.3 ng/cm^2 from 100% blood plasma or serum.[38] In a recent study, conjugating PCB to a protein increased its stability without sacrificing its bioactivity.[44] Moreover, PCB-based nanoparticles and nanogels were shown to have a very long *in vivo* circulation time and not to induce a measurable antibody response in rats after repeated intravenous (IV) injections.[52, 69] Based on these findings, we hypothesized that encapsulating BChE inside a PCB nanogel could enhance its stability and shield it from recognition by the immune system, enabling it to act as a long circulating bioscavenger.

3.2 Experimental Section

3.2.1 Materials and instruments

Butyrylcholinesterase (BChE) from equine serum, N-Acryloxysuccinimide (NAS), tetramethylethylenediamine (TEMED), ammonium persulfate (APS), dimethyl sulfoxide (DMSO) anhydrous, bovine trypsin, bovine serum albumin (BSA), fluorescein isothiocyanate (FITC), and paraoxon-ethyl were purchased from Sigma-Aldrich, and were used as received. Carboxybetaine acrylamide (CBAA) monomer and crosslinker (CBAAX) were synthesized following the same procedure as Chapter 1.

Dynamic light scattering and zeta potential were measured using a Malvern nano zetasizer in PBS 7.4 buffer. Transmission electron microscopy was performed using Tecnai G2 F20 Supertwin TEM, with uranyl acetate as a negative staining agent. All bioassays were done using a BioTek Cytation 3 Multi-Mode Reader.

3.2.2 Protein encapsulation

For zwitterionic nanogel encapsulation, BChE was first modified to introduce acryloyl group onto its surface. Taking the synthesis of n-BChE-50-0.2x as an example, the reaction was performed by dissolving 20 mg BChE into 10 ml 50-mM HEPES buffer (pH 8.5), followed by adding 100 μl of N-acryloxysuccinimide (NAS) DMSO solution (20 mg/ml) dropwise. The reaction was stirred at 4 ℃ for two hours. The polymer encapsulation was done via *in situ* radical polymerization by adding 400 mg CBAA monomer, 80 mg of CBAAX crosslinker, 10 ml HEPES buffer, 15 mg APS and 60 μl TEMED into the former reaction solution. After stirring for another 2 hours, the reaction mixture was concentrated and washed extensively by PBS 7.4 using 150 kDa molecular weight cutoff centrifugal filters. All other samples were prepared in the same way with

adjusted NAS and crosslinker amounts. The protein residue activity was measured by a commercially available activity kit (Arbor assays, USA).

Samples used for *in vivo* test were labeled by FITC. Native or encapsulated BChE was dissolved in 0.1 M sodium carbonate buffer (pH 9) at a protein concentration of 2 mg/ml. Then 50 μl 1mg/ml FITC DMSO solution was added slowly to each milliliter of the protein solution. The reaction was kept at 4 ℃ for 8 h in the dark. After reaction, the labeled samples were concentrated and washed extensively by PBS 7.4 using 100 kDa molecular weight cutoff centrifugal filters.

3.2.3 Measurements of thermal and protease resistance

For thermal stability test, native and encapsulated protein samples (protein concentration 1 ug/mL in 50-mM HEPES buffer, pH 8.5) were incubated at 55 ℃ in water bath. At different time points, each sample was taken out and quenched in ice bath until measurement. After the final samples taken out at 2 h, activities of all samples were measured using the butyrylcholinesterase fluorescent activity kit following the manufacturer's protocol. Values were recorded as percentage of each sample activity before heating.

For protease resistance test, native and encapsulated BChE samples were co-incubated with bovine trypsin at 1:1 weight ratio at 37 ℃ in 50-mM HEPES buffer, pH 8.5. After 0.5 h or 24 h, samples were taken out and measured using the butyrylcholinesterase fluorescent activity kit.

3.2.4 Enzyme inhibition by OP

A model organophosphate toxin paraoxon-ethyl was used to test the binding between native BChE and BchE nanocapsules. The assay was done by mixing BchE

protein or nanocapsule solutions (HEPES, pH8.5) with paraoxon solutions at different concentrations. The mixture was incubated at 37℃ for 30 min and residue activity was measured using the butyrylcholinesterase fluorescent activity kit.

3.2.5 Cell culture and cytotoxicity assay

The cytotoxicity was assessed through MTT assay. NIH3T3 cells were seeded in a 96-well plate, at a density of 2×10^4 cells/well and incubated overnight. The following morning, the culture medium in each well was replaced by 180 μL fresh medium. Proteins or nanogel samples (20 μL in PBS) were then added to each well. After incubation for 24 h, the medium was replaced with 200 μL fresh medium containing 20 μL MTT (5 mg/mL in PBS) and incubated for another 4 h. Finally all medium was removed and 150 μL/well DMSO was added, followed by shaking for 15 min. The absorbance of each well was measured at 490 nm with pure DMSO as a blank. Non-treated cell is used as a control and the relative cell viability (mean%±SD, n=3) was expressed as $Abs_{sample}/Abs_{control}\times100\%$.

3.2.6 Pharmacokinetics and biodistribution study

The pharmacokinetics of native and encapsulated BChE is studied using Spraque Dawley rats (male, body weight 74~100 g) as the animal model. Each sample has six duplicates to generate statistical significance. All animal experiments adhered to federal guidelines and were approved by the University of Washington Institutional Animal Care and Use Committee. For pharmacokinetic studies, each FITC labeled protein sample was administered into the rat via tail vein injection at the dose of 4 mg/kg body weight. Blood samples were collected from the tail vein at 5 min, 6 h, 24 h, 48 h and 72 h after the injection. The blood samples were put in heparinized vials, centrifuged and the enzyme

content in plasma was estimated by fluorescence intensity. The IV injections and bleeding procedure were repeated twice with one week as time interval between each injection.

At 72h post the second injection, three rats in each group were killed and the heart, liver, spleen, lung, kidney and blood were collected for biodistribution analysis. The collected organ tissues were homogenized using a tissue ruptor, followed by centrifugation at 3200 × g for 30 min at room temperature. The fluorescence of particles in the tissues was measured using a microplate reader and compared to a standard curve generated using FITC labeled samples added to untreated homogenized tissues. Two weeks post the second injection, all other rats were killed and 5 mL of blood were drawn by using cardiac punch and serum was prepared for antibody detections.

3.2.7 Enzyme-linked immunosorbent assay (ELISA)

For ELISA experiments, 100 μL antigen solution (10 μg/mL of native BChE) prepared in 0.1 M sodium carbonate buffer, pH 9.5, was used to coat each well of the 96-well plates. During coating procedure, plates were incubated at 4 ℃ overnight. After removing antigen solutions, the plates were washed five times using phosphate-buffered saline washing buffer and then filled with blocking buffer (1% BSA solution in 0.1 M Tris buffer, pH 8.0). After incubation at room temperature for 1 hour, blocking buffer was removed and all wells were washed for another five times. Serial dilutions of rat sera in PBS containing 1% BSA were added to the plates (100 μL/well), which were incubated for 1 h at 37 ℃. The plates were then washed five times. Goat anti-rat IgM or IgG conjugated to horseradish peroxidase (HRP) (Bethyl labs, USA) was used as the secondary antibody for detection of IgM and IgG. After adding the secondary antibody, plates were incubated at room temperature for 1 hour, and then washed five times before

the addition of 100 μL/well HRP substrate 3,3',5,5'-Tetramethylbenzidine (TMB, Bethyl labs). The plates were shaken for 15 min and 100 μL stop solution (0.2 M H_2SO_4) was added to each well. Absorbance at 450 nm (signal) and 570 nm (background) was recorded by a microplate reader. Pre-bleeding sera were used as negative control for all ELISA detections. The positive signal was defined as absorbance significantly larger than corresponding negative control.

3.2.8 Statistics

Student's t test was chosen to compare two small sets of quantitative data when data in each sample set were related, with $P < 0.05$ being considered as statistically significant.

3.3 Results and Discussion

3.3.1 Nanocapsule preparation and characterization

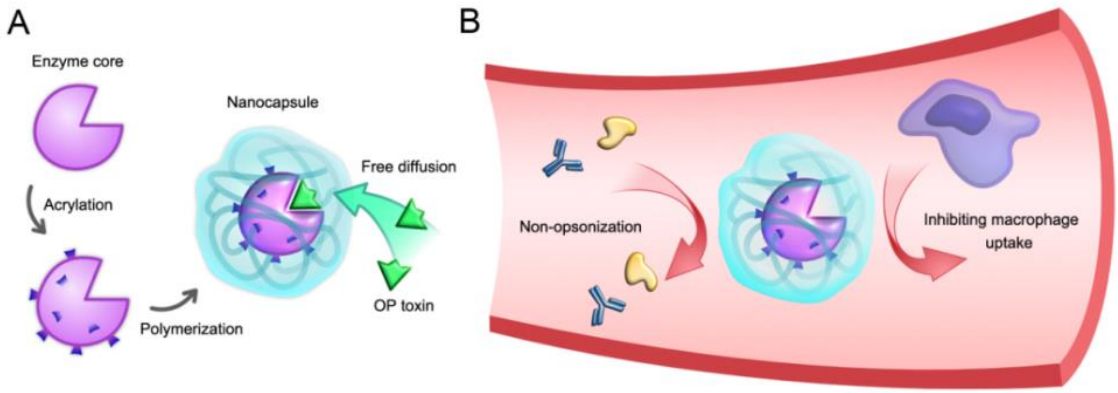

Figure 3.1 (A) Fabrication of BChE nanocapsules. The OP toxins can freely diffuse through the zwitterionic gel layer and (B) The zwitterionic gel layer protects the particle from opsonization and immune cell uptake.

Table 3.1 Characterization of BChE nanocapsules

Sample ID	Surface vinyl group number[a]	Hydrodynamic size (nm)[b]	Zeta potential (mV)	Residue activity (%)
Native BChE	—	14.5	-19.1	100
n-BChE-5-0.2x	3.2	26.4	-1.9	92
n-BChE-50-0.2x	30.3	30.2	-5.2	88
n-BChE-200-0.2x	45.7	30.6	-4.9	53
n-BChE-50-0.1x	30.3	20.6	-10.5	89

a Measured by MALDI-TOF MS; data expressed as number per subunit.
b Measured by dynamic light scattering.

To coat the surface of BChE with a zwitterionic polymer gel, the protein was first chemically modified to introduce surface acryloyl groups, enabling carboxybetaine acrylamide (CBAA) monomer and crosslinker (CBAAX) to be grafted from the surface using free radical polymerization. As shown in **Figure 3.1**, this process covered the enzyme with a non-fouling PCB hydrogel layer. This gel capsule was designed to shield BChE from premature proteolysis and immune system recognition while simultaneously allowing OP toxins to diffuse in so that these toxins can be neutralized by enzyme binding sites. By adjusting reaction feeding ratios, both the number of polymer-protein conjugation sites and thickness of the hydrogel layer could be adjusted. The number of acryloyl groups anchored on the protein surface, which corresponds to the conjugation sites connecting the protein and polymer shell, was adjusted by changing the feeding ratio of N-acryloxysuccinimide (NAS) and BChE. The physical properties of nanogel bioscavengers prepared under different conditions are listed in **Table 3.1**. Sample names are assigned as n-BChE-**a**-**b**x, where **a** denotes the molar feeding ratio between NAS and protein in the acrylation step, and **b** designates the crosslinker content during polymerization. Dynamic light scattering (DLS) measurements confirmed the formation of nanogels, as the encapsulated BChE increased in its hydrodynamic size compared to

the unmodified enzyme. The activity of the enzyme was well maintained at around 90% even when it is conjugated for up to 30 acryloyl groups per subunit. We tuned the crosslinker concentration to control the size of the nanogels, and found 10% and 20% crosslinker content to result in hydrodynamic nanocapsule sizes of ~20 nm and ~30 nm, respectively. The dry size of n-BChE-50-0.2x was measured by transmission electron microscopy (TEM), averaging 15.8 nm in size (**Figure 3.2a**). Encapsulating BChE in zwitterionic nanogels also neutralized the negative surface charge of the native protein (-19.1 mV), as measured by zeta potential. A thicker gel coat corresponded to a more neutral surface, indicating better protein surface coverage and protection.

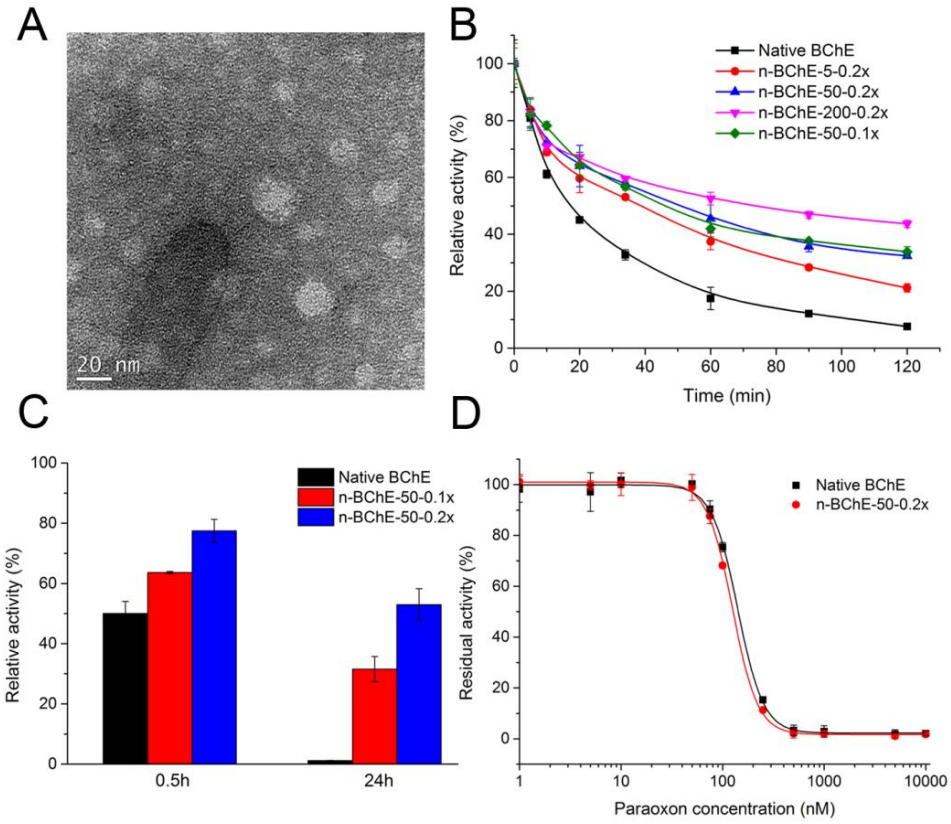

Figure 3.2 Characterization of the Nanocapsules. (A) TEM image of nanocapsules; (B) Relative activities of native BChE and nanocapsules incubated at 55 ℃; (C) Relative activities of native BChE and nanocapsules co-incubated with trypsin and (D) BChE inhibition by paraoxon-ethyl.

Due to their structural complexity, protein therapeutics is often prone to instability during storage, which causes great inconvenience in many applications. We performed thermal stress tests in this work to evaluate the thermal stability of enzymes prepared under different encapsulation conditions. As shown in **Figure 3.2b**, all nanocapsules retained better activity than native BChE when immersed in a 55 ℃ water bath. This protection effect arises from a combination of two distinct mechanisms. For one, the CB monomer has substantial structural similarity to protein stabilizing agent glycine betaine. Encapsulating a protein in a PCB gel network is analogous to placing it into a highly concentrated protein stabilizing solution.[44, 69] The covalent conjugation sites between the protein and polymer gel network work alongside this stabilizing effect to provide additional protection against conformational changes,[45] which was confirmed by observing higher protein stability when a greater number of protein-polymer conjugation sites were present. The higher thermal stability extends the shelf life of this bioscavenger, and reduces the high cost of its production and use.

The *in vivo* stability of a therapeutic protein is not only challenged by its own structural vulnerability, but also by various proteases from organs and tissues. We chose trypsin as a model protease to evaluate the proteolytic stability of native and encapsulated BChE preparations. As shown in **Figure 3.2c**, after co-incubation with trypsin for 30 min, all samples showed an initial activity drop as some BChE was enzymatically degraded. The native protein lost half of its activity, while the nanocapsules maintained ~65% and ~80% of their original activities depending on the nanogel thickness. Notably, while native BChE lost all activity after 24 h of incubation (suggesting complete digestion), the sample encapsulated in a thicker polymer layer still retained ~60% of its activity. This

protection from proteolysis is a major benefit of the non-fouling properties of the gel. The highly hydrated zwitterionic gel sterically hinders contact between BChE and proteases. Such proteolytic resistance contributes to long-term enzyme efficacy *in vivo*. For the following experiments, we chose n-BChE-50-0.2x as the representative nanogel-encapsulated bioscavenger due to its balance between high residual activity and stability.

Improved stability to environmental changes and proteolytic degradation is commonly gained at the expense of bioactivity. However, BChE nanocapsules avoided this compromise, exhibiting high stability with minimal sacrifice to activity. To determine the *in vitro* OP scavenging ability of these nanocapsules, we assayed their activity following incubation with the model OP compound paraoxon, the active ingredient of insecticide parathion. The inhibition profiles of native BChE and nanogel-encapsulated BChE were virtually indistinguishable, with respective EC50 values of 140 nM and 125 nM (**Figure 3.2d**).

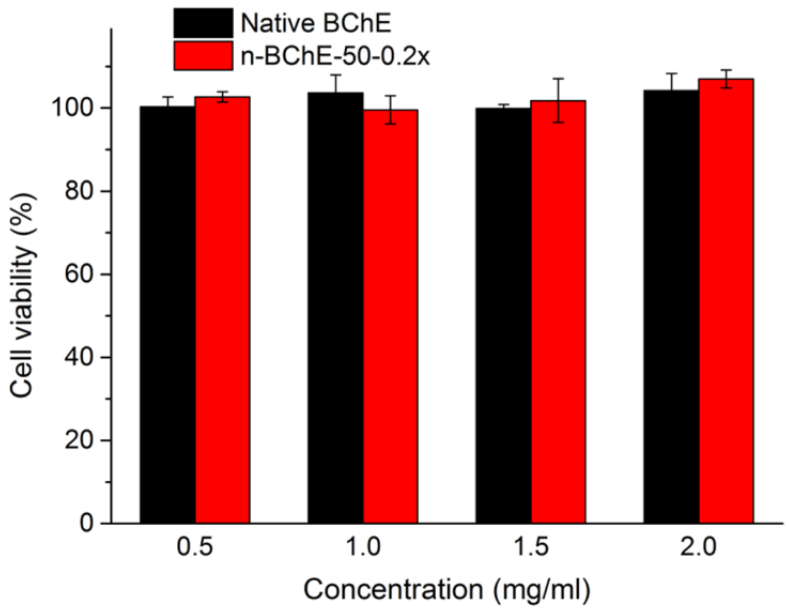

Figure 3.3 Cytotoxicity testing results from an MTT assay. The values represent percentage cell viability (means ± SD, n=3).

As the nanogel-encapsulated BChE demonstrated enhanced stability and maintained OP neutralization ability *in vitro*, we tested its cytotoxicity before further *in vivo* evaluation. Native BChE showed no cytotoxicity to NIH 3T3 cells as expected, since it is derived from mammalian blood (**Figure 3.3**). Critically, the zwitterionic nanogel-encapsulated enzymes remained completely nontoxic, and cells retained 100% viability after incubation with BChE nanogels at very high concentrations, which can be attributed to the superior biocompatibility of PCB.

3.3.2 Pharmacokinetics

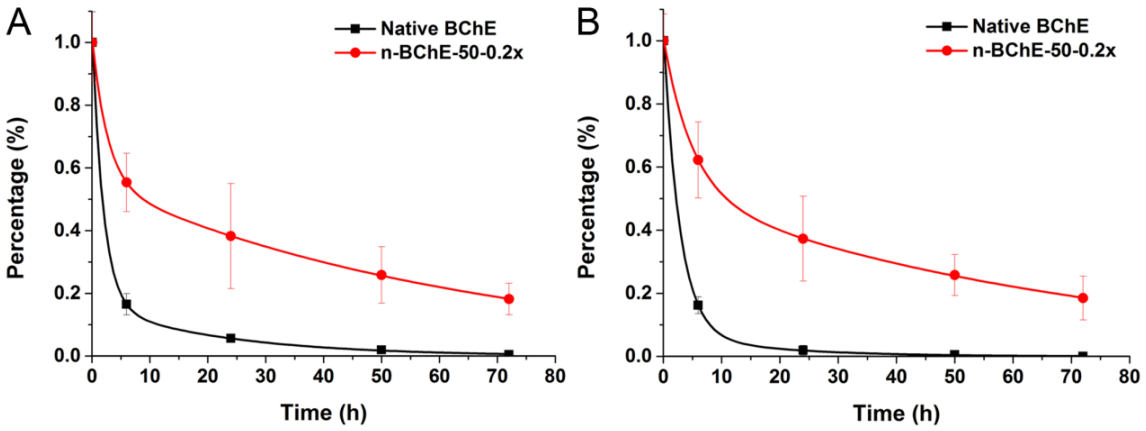

Figure 3.4 Blood circulation profiles of native BChE vs. nanocapsule. Circulation curves after the first *i.v.* administration (A) and second administration (B).

Improving circulation half-life is the core objective of BChE modification technologies. Serum-derived native BChE is highly glycosylated, enabling it to circulate significantly longer than non-glycosylated 'naked' recombinant BChE. Thus, glycosylating rhBChE has been considered a key strategy to boost its circulation time closer to that of the native enzyme.[63] PEGylation has also been applied to modify non-glycosylated rhBChE, and resulted in a similar half-life to glycosylated rhBChE in a mouse model[70]—neither modification could outperform serum-derived native BChE.

In addition, Saxena *et al.* PEGylated native glycosylated BChE, but no improvement in circulation time was observed.[68] In this work, we studied the PK behavior of equine serum-derived BChE before and after zwitterionic nanogel encapsulation through repeated *i.v.* injections of FITC-labeled samples in healthy Sprague–Dawley rats. As shown in **Figure 3.4a**, all concentration-time curves fit a two compartment model. PK parameters are listed in **Table 3.2**. After the initial injection, unmodified native BChE exhibited an elimination half-life ($t_{1/2}\beta$) of 15.6 h, in general agreement with values reported in the literature.[66] Remarkably, the circulation time of BChE nanocapsules demonstrated a threefold improvement over the native enzyme, with a $t_{1/2}\beta$ of 45 h. Moreover, the AUC_∞ (area under curve) of the nanocapsules was 6.7 times that of native BChE, indicating significantly higher systemic availability. Zwitterionic polymers have been shown to have a unique ability to extend the circulation time of nanoparticles beyond that of conventional biomaterials like PEG.[52, 69] The "stealth" characteristics of zwitterionic PCB and the comprehensive surface coverage of nanogel encapsulation appear to work synergistically to help these bioscavengers avoid reticuloendothelial system (RES) clearance and thus circulate for a significantly longer time.

Table 3.2 PK parameters after repeated injections

Parameters	Native BChE		n-BChE-50-0.2x	
	Dose 1	Dose 2	Dose 1	Dose 2
$t_{1/2}\beta$ (h)	15.6	12.0	45.0	48.5
AUC_∞ (μg/mL × h)	344	247	2306	2331
CL (mL/h)	3.5	4.8	0.5	0.5
MRT (h)	16.0	7.5	62.8	65.9

For prophylactic applications, multiple doses of bioscavenger enzymes may be needed to prolong protection against OP toxins. A second injection of encapsulated or

unmodified BChE was thus given one week after the initial administration of each version, and PK profiles were evaluated as before. As shown in **Figure 3.4b**, an obvious accelerated blood clearance (ABC) phenomenon was noted in the group treated with unmodified BChE, with $t_{1/2}\beta$ decreasing to 12 h, AUC_{∞} values dropping by a third and MRT (mean residence time) decreasing by half. This significant decrease is mainly due to the immunogenicity of equine proteins in rats. A similar phenomenon was reported for human plasma derived BChE administered to mice.[68] In contrast, no significant difference in the PK profile was observed between the two injections of BChE nanocapsules, indicating the encapsulated bioscavengers are likely to maintain their superior PK performance through repeated doses.

3.3.3 Immunogenicity tests

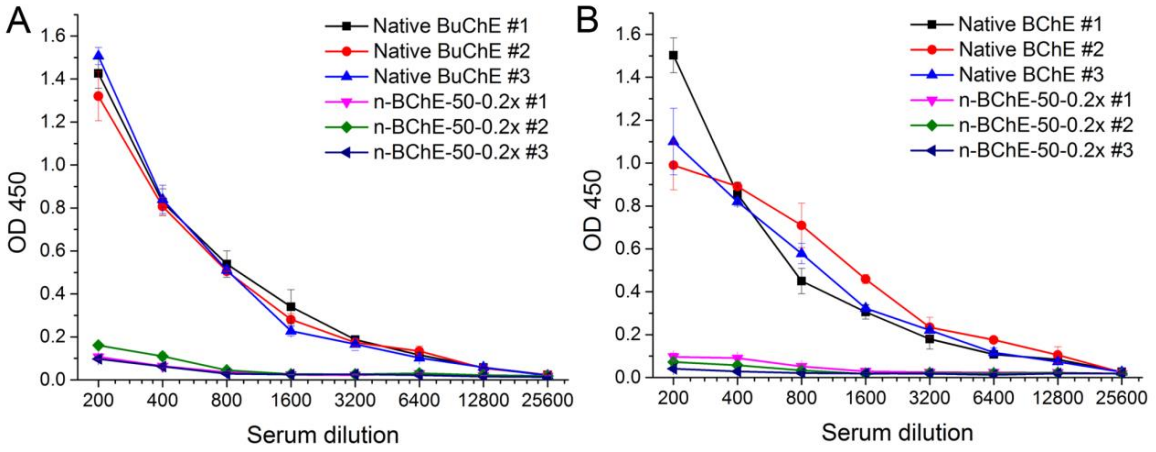

Figure 3.5 Detection of antibodies by direct ELISA: (A) Anti-BChE IgM and (B) Anti-BChE IgG. Serum from each rat is plotted separately.

We explored the immunogenicity of this platform in further detail by collecting serum two weeks after the second injection and testing it for anti-BChE antibodies using direct ELISA. As shown in **Figure 3.5**, high titers of both IgM (titers 1:6400) and IgG (titers 1:12800) were found in the group treated with native equine BChE. Glycosylated

equine serum BChE is expected to be highly immunogenic for rats, due to differences in glycosylation and protein sequences. Likewise, unmodified BChE derived from other species cannot be directly used in humans, as the resulting immune response would certainly reduce its efficacy and potentially induce life-threatening anaphylactic reactions. In contrast, no IgG and negligible IgM were detected in rats treated with BChE nanocapsules, corroborating that the PCB nanogels effectively rendered the protein "invisible" to the immune system and thus mitigated antibody induction.

3.3.4 Biodistribution

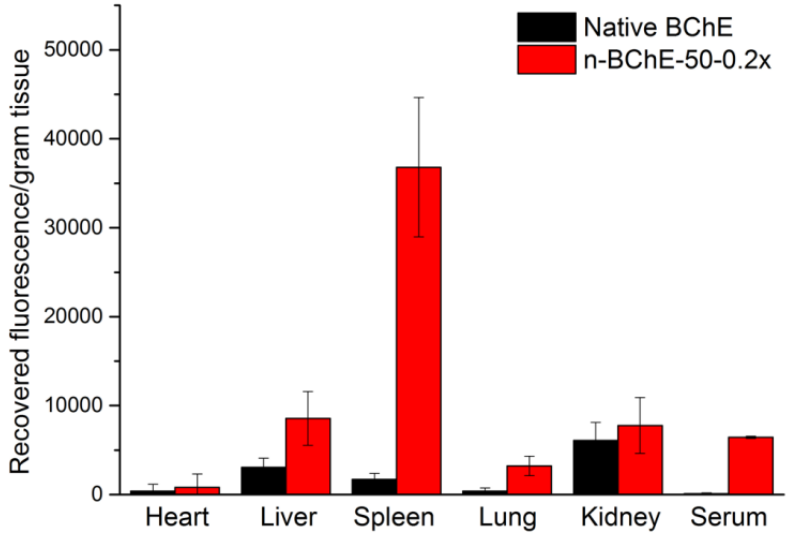

Figure 3.6 Biodistribution of native BChE vs. nanocapsule. Each value is averaged from three rats. SDs are shown as error bars.

To examine the biodistribution of BChE nanocapsules, we gathered blood and tissue samples from treated rats 72 h after the second injection for analysis. These data are presented in **Figure 3.6** as recovered fluorescence per gram of tissue. BChE nanocapsules sustained a high serum concentration, whereas unmodified BChE was completely cleared from blood circulation. Similar as most long circulating nanoparticles, accumulation of

nanocapsules was mainly found in liver and spleen.[52, 53] We observed lower levels of organ accumulation by unmodified BChE compared with the nanocapsules three days after injection. This can be attributed to their differing levels of proteolytic stability. As observed from our *in vitro* tests, unprotected BChE was readily degraded by proteases after organ accumulation, but nanogel encapsulation partially shields BChE from protease recognition, delaying this metabolic process. The BChE nanocapsules in this work were prepared using amide-containing crosslinkers, which are expected to degrade through slow hydrolysis. If faster degradation is needed, ester or disulfide-based crosslinkers could be substituted to facilitate metabolism.

3.4 Conclusions

In summary, toxin-neutralizing enzyme BChE, derived from equine serum, was encapsulated in zwitterionic poly(carboxybetaine) nanogels. Encapsulated BChE exhibited greater proteolytic and thermal stability than its native precursor without sacrificing its ability to neutralize OP toxins. These nanocapsules demonstrated a superior circulation half-life *in vivo*, outperforming the glycosylated native BChE by three times. Furthermore, repeated injections of bioscavenger nanocapsules did not induce antibody production or lose efficacy. This powerful strategy unlocks the possibility to use animal tissue derived BChE as supplement or replacement for the inadequate human native BChE. Enzyme bioscavengers encapsulated in zwitterionic nanogels are a promising strategy to be used in both clinical and military settings.

Chapter 4 Nanoscavenger Provides Long-term Prophylactic Protection against Organophosphates

Nerve agents are a class of organophosphates (OPs) that blocks communication between nerves and organs. Over the past fifty years numerous efforts have been devoted in search for a potent, long-lasting prophylactic bioscavenger to countermeasure the threat from nerve agents, yet few candidates had the potential to fulfill this mission. Herein, we report a nanoparticle-based bioscavenger (or nanoscavenger), which offers long-term protection against OP intoxication. The nanoscavenger, which catalytically breaks down toxic OP compounds, has a long vascular residence time with negligible immune response and has been shown to be effective for protection against OP exposure or rescue after OP exposure. A single prophylactic injection of the nanoscavenger could effectively prevent lethality in the victims that were exposed to $2 \times LD_{50}$ paraoxon or sarin one-week post-administration. Our results suggest that the prophylactic strategy of the nanoscavenger is a promising solution to fulfill the needs in both civilian and military applications.

4.1 Introduction

As one of the most dangerous chemical families, organophosphate (OP) compounds were developed not only as highly effective pesticides but also as chemical warfare agents.[71] Such compounds irreversibly inhibit acetylcholinesterase (AChE) in chemical synapses, causing neuromuscular paralysis throughout the entire body and, subsequently, death by asphyxiation.[56] The most potent nerve agent VX, for example, has a median lethal dose (LD_{50}) of as low as 12.6 μg/kg in mice.[72] These extremely toxic molecules are capable of causing death within minutes when exposed to skin or inhaled, making it

extremely difficult to protect against OP or rescue post OP exposure. OPs appeared in several wars and terrorist attacks. In 2013, thousands of civilians in Syria died due to the usage of sarin in the civil war and additional tragedies have occurred more recently. Even though the state-of-the-art anticholinergic antidotes could prevent lethality if administered in time, post-exposure effects, including convulsions, incapacitation, performance deficits, and permanent brain damage, would still be devastating.[55, 60] OP pesticides, which seem less toxic when compared with the G-series and V-series nerve agents, pose an even greater threat to the public health due to their world-wide applications.[58] According to the World Health Organization, 200,000 deaths per year in developing countries were attributed to OP pesticide poisoning.[59]

In addition to the post-poisoning treatment, researchers have been seeking a prophylactic strategy for decades to counteract OP threats.[57, 73] Protein based bioscavengers are promising candidates due to their ability to scavenge OP compounds in the bloodstream prior to intoxication. This could avoid the potential side effects and exclude the requirement of rapid administration of the antidotes post-exposure.[64] In general, bioscavenger proteins function either by stoichiometric binding to OPs or by catalytic hydrolysis of nerve agents into biologically inactive products. The former category includes proteins that bind to nerve agents at a one-to-one ratio, such as cholinesterases (ChEs) and carboxylesterases (CEs).[74] Although some candidates of this type seem promising due to their natural occurrence in the human blood, such as human butyrylcholinesterase,[63] they have quite low efficiency in OP scavenging due to the stoichiometric binding mechanism. The use of catalytic bioscavengers is considered to be relatively advantageous compared to the use of their stoichiometric counterparts.

However, since most of these proteins are derived from micro-organisms, they suffer from significant immunologic and pharmacokinetic problems.[73] For instance, organophosphate hydrolase (OPH) is highly effective in hydrolyzing OPs, but its circulation half-life is less than an hour in rodents.[75-79] As a result, despite intensive work over the last sixty years, there has yet to be a bioscavenger system that has been able to achieve desired results

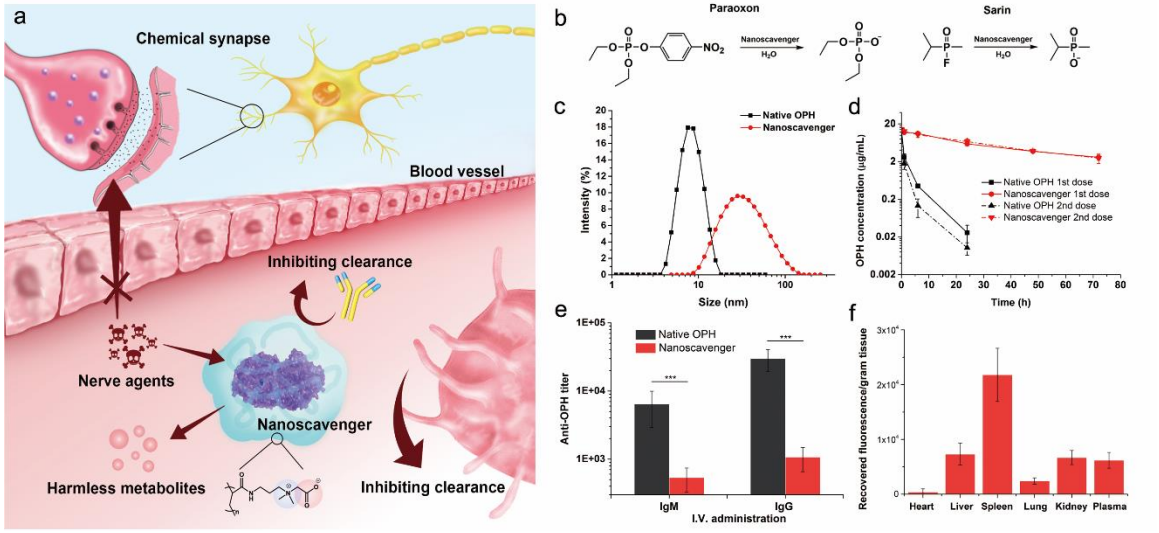

Figure 4.1 Mechanism and characterizations of the nanoscavenger. (a) Schematic demonstrating the protection mechanism of the nanoscavengers. (b) Hydrolysis of paraoxon and sarin mediated by the nanoscavengers. (c) DLS measurement of the nanoscavenger and native OPH. (d) Pharmacokinetic profiles of native OPH *vs.* nanoscavenger after repeated dosing in rats, n=6. (e) Detection of anti-OPH antibodies by direct ELISAs. (f) Biodistribution of the nanoscavengers. Each value is averaged from three rats. SDs are shown as error bars. The Student t test was used to compare two small sets of quantitative data, with *** $p \leq 0.001$.

Herein, we developed a nanoparticulate bioscavenger that utilizes the catalytic advantage of OPH enzyme to offer long-term prophylactic protection against nerve agent poisoning. The two key problems were addressed by coating the enzyme with a zwitterionic poly(carboxybetaine) (PCB) gel network, forming a nanocapsule that confers excellent "stealth" properties upon the protein core. Previously, conjugation of PCB to

model proteins has been shown to stabilize them without sacrificing their affinity to substrates[44], and increase circulation half-life with minimal immunogenicity.[80] The gel encapsulation strategy further promoted these merits by providing complete protein surface coverage.[69] When the OPH enzyme is encapsulated in a hydrated zwitterionic gel nanocapsule, the dramatically prolonged blood residence time makes long-term protection feasible while the porous gel network still allows free diffusion of small OP molecules into the catalytic site (**Figure 4.1a**). By combining the strong catalytic OP scavenging ability of the enzyme core and the extraordinary "stealth effect" from the polymer shell, the nanoscavenger would become an ideal long-lasting bioscavenger.

4.2 Materials and Methods

4.2.1 Materials

All chemicals were purchased from Sigma-Aldrich unless otherwise noted, and were used as received. Carboxybetaine acrylamide (CBAA) monomer and crosslinker (CBAAX) were synthesized following the same procedure as previous chapters.

4.2.2 OPH expression

Gene encoding for OPH A80V/K185R/I274N (VRN) variant was inserted into a pET-20b(+) vector between the NdeI and EcoRI restriction sites as previously described.[77] The expression vector was transformed into E. coli BL21 (de3) cells. Transformants were cultured in 5 mL Terrific Broth (TB) supplemented with ampicillin for 8 hours at 37 ℃. 1 mL of the culture was used to inoculate 1 L TB supplemented with ampicillin and was grown for 16 hours at 30 ℃. The expression culture was then supplemented with 1 mM $CoCl_2$ and expression was induced with 1 mM isopropyl β-D-1-thiogalactopyranoside (IPTG) and allowed to express for 24 hours at 30 ℃. The

culture underwent centrifugation and the cell pellet was resuspended in 100 mL purification buffer (50 mM HEPES 100 μM $CoCl_2$ pH 8.5). The suspension underwent three freeze-thaw cycles and the lysate underwent probe sonication until the lysate was clarified. The lysate underwent centrifugation to remove cellular debris. 0.4 g protamine sulfate dissolved in 20 mL purification buffer was added to the supernatant and incubated for 20 minutes before the precipitate was removed through centrifugation. The supernatant was brought to 60% ammonium sulfate saturation and mixed for 30 minutes before undergoing centrifugation. The pellet was dissolved in up to 5 mL purification buffer and sterile filtered. Further purification was performed on a NGC Quest 10 Chromatography System. The protein solution first underwent size exclusion chromatography utilizing the purification buffer on a HiLoad 16/600 Superdex 200 pg column before undergoing ion exchange chromatography utilizing the purification buffer with an increasing NaCl gradient on an ENrich Q column.

4.2.3 Nanoscavenger preparation

To synthesize the nanoscavenger, OPH was first modified to introduce acryloyl group onto its surface. The reaction was performed by dissolving 10 mg OPH, 100 mg CBAA monomer and 20 mg CBAAX crosslinker into 5 ml 50-mM HEPES buffer (pH 8.5), followed by adding 50 μl of N-acryloxysuccinimide (NAS) DMSO solution (20 mg/ml) dropwise. The reaction was stirred at 4 ℃ for two hours. The polymer encapsulation was done via in situ radical polymerization by adding 4 mg APS and 16 μl TEMED into the former reaction solution. After stirring for another 2 hours, the reaction mixture was concentrated and washed extensively by PBS 7.4 using 150 kDa molecular weight cutoff centrifugal filters. The nanoscavengers were then passed a hydrophobic

interaction column (Phenyl-Sepharose CL-4B, GE) to remove any unencapsulated proteins using PBS 7.4 (50 mM, 0.1 mM $CoCl_2$) as elution buffer. The final products were then concentrated and stored at 4 ℃ for further studies.

4.2.4 Enzyme kinetics measurement

Paraoxon-ethyl was used as the substrate to perform enzyme kinetics measurement. The OPH test samples were diluted to 50 ng/ml in 50-mM HEPES buffer (pH 8.5), while the substrate was dissolved in the same buffer at a range of concentrations from 0.1 to 2 mM. To perform the test, 100 μl of the above OPH sample dilution was added to a 96-well plate, followed by adding 100 μl substrate solution. Upon mixing, the absorption change at 405 nm was monitored using a plate reader (BioTek Cytation 3, USA). The enzyme kinetics parameters were calculated using Michaelis–Menten equation.

4.2.5 *In vivo* experiments in rats

All experiments using rats as the animal model were conducted at the University of Washington, and adhered to federal guidelines and were approved by the University of Washington Institutional Animal Care and Use Committee.

4.2.5.1 Pharmacokinetics study

The pharmacokinetics of native and modified OPH was studied using Spraque Dawley rats (female, body weight 74–100 g) as the animal model. Each sample has six duplicates to generate statistical significance. For pharmacokinetic studies, each protein sample was administered intravenous (I.V.) via tail vein or subcutaneous (S.C.) on the back at the dosage of 1 mg/kg body weight. Blood samples were collected from the tail vein at different time points after the injection. The blood samples were put in heparinized vials, centrifuged and the enzyme content in plasma was estimated by

activity assay. The injections and bleeding procedure were repeated twice with a one week time interval between each injection. Five weeks after the first injection, the animals were euthanized and blood was taken for antibody measurements.

4.2.5.2 Biodistribution study

Samples used for biodistribution test were labeled by fluorescein isothiocyanate (FITC). Nanoscavengers were dissolved in 0.1 M sodium carbonate buffer (pH 9) at a protein concentration of 2 mg/mL. Then 50 μL 1 mg/mL FITC DMSO solution was added slowly to each milliliter of the sample solution. The reaction was kept at 4 ℃ for 8 h in the dark. After reaction, the labeled samples were concentrated and washed extensively by PBS 7.4 using 100 kDa molecular weight cutoff centrifugal filters.

For biodistribution study, rats (n=3) were injected with the FITC labeled nanoscavengers through the tail vein. At 72 h postinjection, all rats were sacrificed and the heart, liver, spleen, lung, kidney and blood were collected for further analysis. The collected organ tissues were homogenized using a tissue ruptor, followed by centrifugation at 3,200 × g for 30 min at room temperature. The fluorescence of particles in the tissues was measured using a microplate reader.

4.2.5.3 Enzyme-linked immunosorbent assay (ELISA)

The antigens used in direct ELISAs consisted of native OPH (for detection of anti-OPH antibody) and BSA-PCB conjugates (for detection of anti-PCB antibody). For ELISA experiments, 100 μL antigen solution (10 μg/mL) prepared in 0.1 M sodium carbonate buffer, pH 9.5, was used to coat each well of the 96-well plates. During coating procedure, plates were incubated at 4 ℃ overnight. After removing antigen solutions, the plates were washed five times using phosphate-buffered saline washing buffer and then

filled with blocking buffer (1% BSA solution in 0.1 M Tris buffer, pH 8.0). After incubation at room temperature for 1 hour, blocking buffer was removed and all wells were washed another five times. Serial dilutions of rat sera in PBS containing 1% BSA were added to the plates (100 μL/well), which were incubated for 1 h at 37 °C. The plates were then washed five times. Goat anti-rat IgM or IgG conjugated to horseradish peroxidase (HRP) (Bethyl labs, USA) was used as the secondary antibody for detection of IgM and IgG. After adding the secondary antibody, plates were incubated at room temperature for 1 hour, and then washed five times before the addition of 100 μL/well HRP substrate 3,3',5,5'-Tetramethylbenzidine (TMB, Bethyl labs). The plates were shaken for 15 min and 100 μL stop solution (0.2 M H_2SO_4) was added to each well. Absorbance at 450 nm (signal) and 570 nm (background) was recorded by a microplate reader. Pre-bleeding sera were used as negative control for all ELISA detections. The positive signal was defined as absorbance significantly larger than corresponding negative control.

4.2.5.4 Detection of anti-PCB antibodies by surface plasmonic resonance sensor

PCB polymer brushes were grafted onto gold-coated SPR sensor chips following previously published methods3. Brush thickness was measured by a spectroscopic ellipsometer (Sentech SE-850). SPR detection of anti-PCB antibodies was optimized at different polymer brush thickness, and ~10-nm film thickness was found to have the best signal/noise ratio. A custom-built SPR sensor was used in this study. All experiments were done following the sequence of flowing PBS for 10 min, 1:20 diluted serum in PBS for 15 min, and PBS for 15 min at flow rate of 30 μL/min. For the SPR sensor used in the

study, a 1-nm SPR wavelength shift represents a surface coverage of ~17 ng/cm^2 for proteins. Detection limit for the SPR sensor used in this work is 0.3 ng/cm^2.

4.2.5.5 Dosage dependent efficacy study

A dosage of 2×LD_{50} paraoxon (0.86 mg/kg) dissolved in pharmaceutical-grade saline was injected subcutaneously into each group of Sprague Dawley rats (n=6) under isoflurane anesthesia. Before the paraoxon administration, 50 μl blood was drawn from tail vein to measure the blood butyrylcholinesterase activity. Immediately after paraoxon injection, different dosages of OPH or nanoscavenger were injected intravenously into each group. The dosages of OPH include 1 μg/kg, 2 μg/kg, 4 μg/kg, 10 μg/kg and 20 μg/kg. Nanogel placebo control was injected at the dosage of 100 μg/kg, and saline control was injected at the same volume. 10 minutes post OPH injection, another 50 μl blood was drawn from tail vein to measure the blood butyrylcholinesterase activity. Symptoms (e.g. tremors, salivation, respiratory depression) were observed and scored within 90 min post injection. Survival rates for 90 min post OP injection were recorded. Any rats that survived a maximum of 90 min after challenge were euthanized immediately by overdose of isoflurane followed with confirmatory thoracotomy.

4.2.5.6 Prophylactic protection efficacy study

The test bioscavengers were injected by I.V. or S.C. first (t = 0 h) at the dosage of 1 mg/kg into rats (n=6) under isoflurane anesthesia, and then 2×LD_{50} paraoxon was injected at different time points later by S.C. administration on the back. 50 μl blood was drawn from tail vein before and 10 min after paraoxon injection to measure the blood butyrylcholinesterase activity change. Symptoms and death rates were observed and

recorded within 90 min post injection. In this set of tests, each animal received one injection of paraoxon.

4.2.5.7 Repeated OP exposure test

The test bioscavengers were injected I.V. via tail vein first (t = 0 h) at the dosage of 1 mg/kg into rats (n=3 in saline control group; n=6 in native OPH and nanoscavenger group). Three hours later (t = 3 h), $2 \times LD_{50}$ paraoxon was injected by S.C. administration on the back. Symptoms and death rates were observed and recorded in the same way as previous tests. At t = 24 h, another injection of $2 \times LD_{50}$ paraoxon was given to the survived animals, and symptoms and death rates were recorded as previously described. The paraoxon administration was repeated every 24 h to the survived rats until all animals died.

4.2.6 *In vivo* experiments in guinea pigs

Animal experiments using guinea pigs as the animal model were conducted at the US Army Medical Research Institute of Chemical Defense (USAMRICD). The experimental protocol utilized for this work was approved by the Animal Care and Use Committee at the USAMRICD and all procedures were conducted in accordance with the principles stated in the Guide for the Care and Use of Laboratory Animals (National Research Council, 2011), and the Animal Welfare Act of 1966 (P.L. 89-544), as amended.

4.2.6.1 Pharmacokinetics

Native OPH and nanoscavenger were administered to male Hartley guinea pigs (n = 3 per formulation; weights 335 g ± 23 g, mean ± SD) via a carotid catheter (5 mg/kg). Blood samples were collected (via toe nail clip) from the animals into heparinized tubes

at multiple time points following administration. The samples were centrifuged to separate the plasma, which was subsequently frozen and stored at -80 ℃ until assay. The activity of OPH was determined in these samples by colorimetric assay; briefly, using MOPS buffer (50 mM at pH 7.0 and 20 ℃), diluted plasma samples (200 μL) were incubated with paraoxon (5 mM) and change in absorbance at 405 nm was measured over 5 min. To determine concentration, standard curves using the stock formulations were constructed, and activities were used to interpolate the concentration. All standard curves and samples were assayed in triplicate. The concentration-time profiles following administration were analysed using PKSolver following instructions.[81] One-compartment model was used to calculate pharmacokinetic parameters.

4.2.6.2 Repeated sarin exposure test

Male Hartley guinea pigs (n = 11; weights 332 g ± 19 g, mean ± SD) were administered 5 mg/kg of either OPH-YT (n=5) or nanoscavenger-YT (n=6) via a carotid catheter (I.V.). Two animals found to be non-patent were utilized as negative controls (no enzyme administered). Animals were exposed to $2\times LD_{50}$ of GB (sarin) in a saline vehicle via subcutaneous injection on the caudal lateral flank area 20 minutes after enzyme administration followed by repeated exposures every 24 hours for 8 days. Survival was assessed every 24 hours with immediate exposure to surviving animals. Negative control animals died due to intoxication within 20 minutes post-exposure.

4.2.7 Statistics

Student's t test was chosen to compare two small sets of quantitative data when data in each sample set were related, with $P < 0.05$ being considered as statistically significant.

4.3 Results and Discussion

4.3.1 Nanoscavenger preparation and characterization

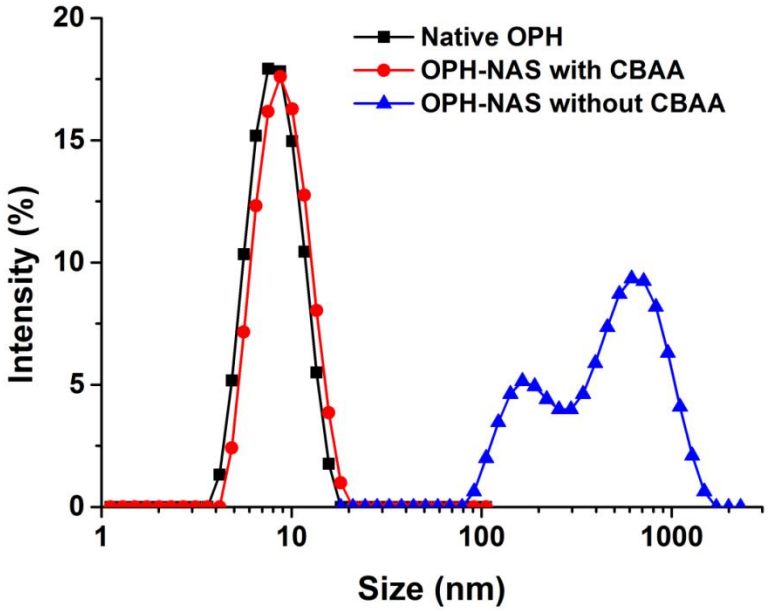

Figure 4.2 DLS shows the OPH protein size change before and after acryloylation. The presence of CBAA stabilized OPH proteins from aggregation during the acrylolation process.

The bioscavenger nanoparticle was fabricated by coating PCB polymer hydrogel onto the surface of OPH protein. The coating process involved two steps – protein surface modification with acryloyl groups and *in situ* radical polymerization with carboxybetaine acrylamide (CBAA) monomer and crosslinkers. The protein coating procedure is similar to what was previously reported[69] but with some critical modifications. Initially, acryloyl groups were introduced onto the protein by reacting surface lysine residues with N-Acryloxysuccinimide, as previously reported. However, serious protein aggregation and precipitation were observed during reaction due to the increased hydrophobicity of the proteins (**Figure 4.2**). Inspired by the fact that glycine betaine, which is the main component of carboxybetaine, is a natural osmolyte and is

used as a protein stabilizer, we changed the feeding order of this reaction - CBAA monomers and crosslinkers were added prior to the first acryloylation step. In the presence of CBAA monomers, OPH protein remained stable throughout the whole reaction process, and the nanocapsules were successfully fabricated by free radical polymerization. Dynamic light scattering (DLS) showed an average hydrodynamic size of 32 nm, with polydispersity index (PDI) of 0.22±0.03 (**Figure 4.1c**). The dry size of these hydrogel nanoparticles was revealed as about 10 nm under transmission electron microscopy (**Figure 4.3**). Enzyme kinetics were studied using paraoxon as the substrate (**Figure 4.4**). The Michaelis constants (Km) were 0.12 mM and 0.10 mM for native OPH and nanoscavenger, respectively. The catalytic efficiency (kcat/Km) was determined to be $2.4\times10^{7}s^{-1}M^{-1}$ for both OPH and encapsulated OPH, indicating that the coated gel layer did not affect the free diffusion of OP molecules into the catalytic center.

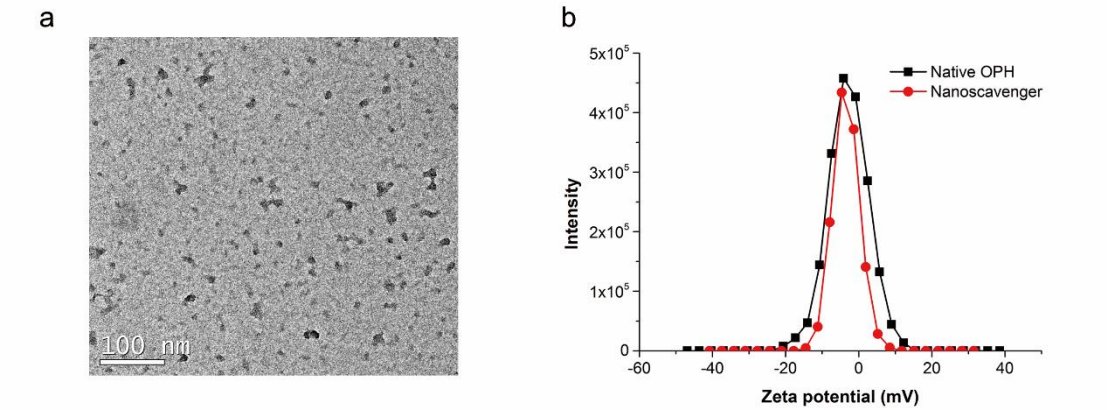

Figure 4.3 (a) TEM image of the dried nanoscavenger. The hydrogel nanoparticle was stained with 5% uranyl acetate for 2 minutes and examined using FEI G2 TF20 (Thermo-Fisher Scientific, Hillsboro, OR) at 200 kV. (b) Zeta potential of the native OPH enzyme and nanoscavenger.

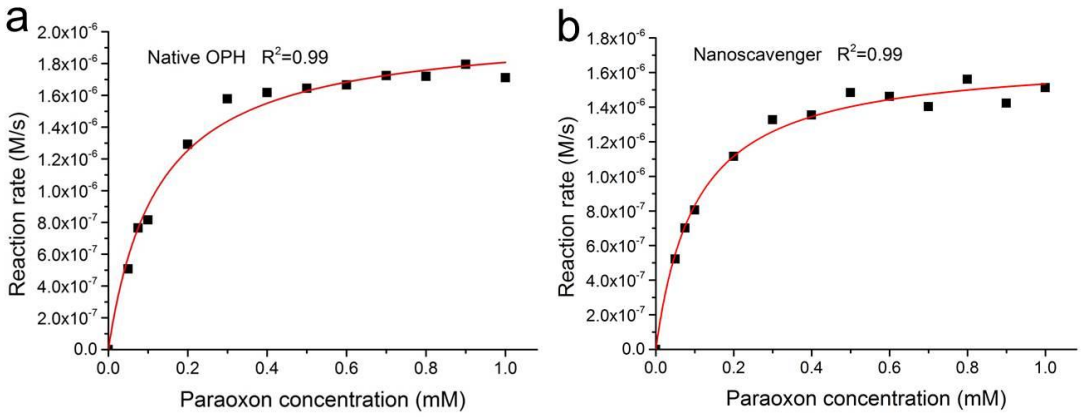

Figure 4.4 Enzyme kinetic measurements of native OPH and nanoscavenger.

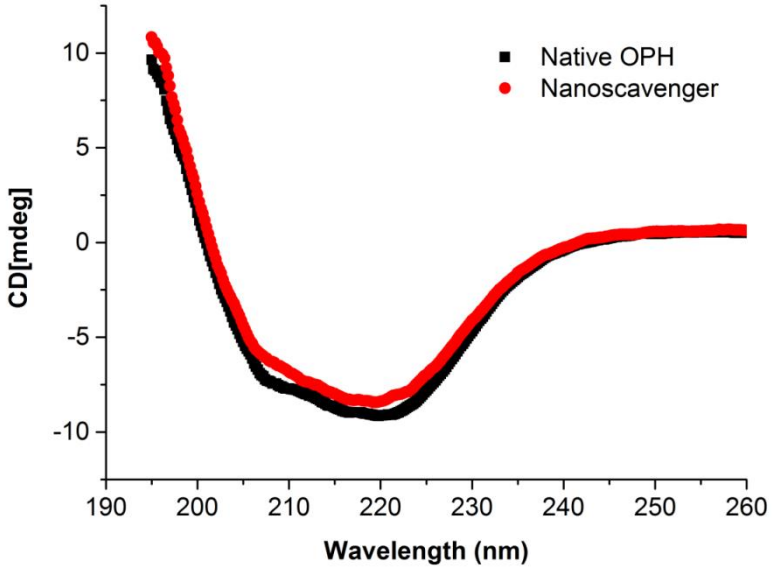

Figure 4.5 Circular dichroism (CD) spectra of the native OPH and nanoscavenger. All spectra were obtained using a Jasco J-720 Circular Dichroism in 1 mM PBS buffer with protein concentrations of 200 μg/mL.

4.3.2 Pharmacokinetics and immunogenicity

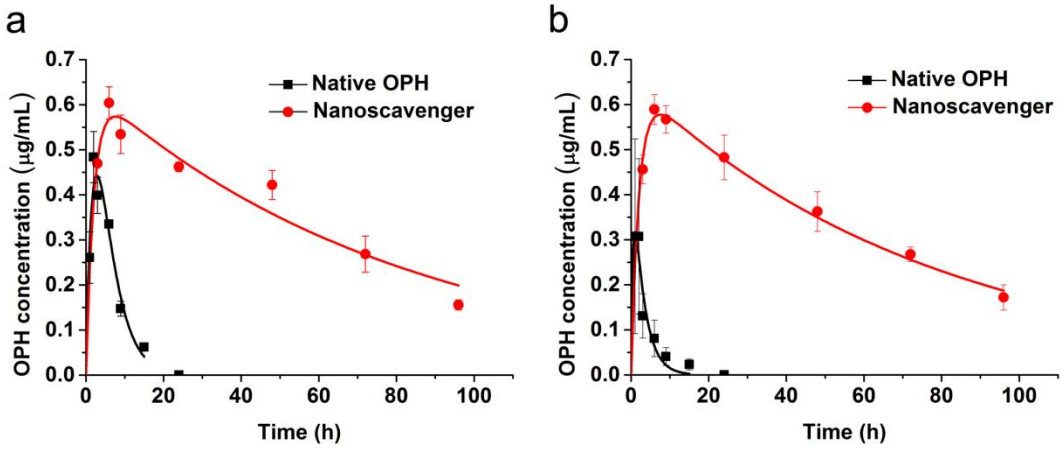

Figure 4.6 Pharmacokinetic profiles of the native OPH *vs.* nanoscavenger after (a) first S.C. injection and (b) second S.C. injection in rats.

Table 4.1 Pharmacokinetic parameters after I.V. and S.C. injections in rats

Parameters		Native OPH (different injections)		Nanoscavenger (different injections)	
		1	2	1	2
I.V.	$t_{1/2}$ (h)	0.4	0.3	26.2	25.9
	AUC_{∞} (μg/mL×h)	8.2	6.6	480	495
	MRT (h)	0.6	0.5	37.8	37.4
S.C.	$t_{1/2}$ (h)	2.8	2.6	56.5	53.2
	T_{max} (h)	2.8	1.4	7.5	7.5
	C_{max} (μg /mL)	0.44	0.32	0.58	0.58
	AUC_{∞} (μg/mL×h)	3.68	1.44	51.4	48.8
	MRT (h)	6.4	4.6	83.5	78.7

As a prophylactic countermeasure against nerve agent poisoning, long vascular residence time is a critical requirement for the bioscavenger candidates.[82] Also, post-exposure therapy in scenarios of percutaneous exposure with ongoing agent transfer from skin into the systemic circulation requires long-lasting therapeutic concentrations of bioscavengers in order to detoxify free agent continuously.[83] The pharmacokinetic (PK)

parameters of unmodified and encapsulated OPH were evaluated by determining the time course of OPH activity in serum following intravenous (I.V.) administration in healthy Sprague-Dawley rats. As shown in **Figure 4.1d**, native OPH was rapidly cleared out from the circulation after administration, while long circulation behavior was observed in the nanoscavenger group. One compartment model was used to analyze the PK parameters, which are listed in **Table 4.1**. After the initial injection, unmodified native OPH exhibited a half-life (t1/2) of 0.43 h, in general agreement with the values reported in the literature.[78, 82] Remarkably, the circulation time of nanoscavenger demonstrated a ~60-fold improvement over the native enzyme, with a half-life of 26.2 h. Moreover, the AUC_{∞} (area under curve) of the nanoscaverger was 58 times that of the native OPH, indicating much higher systemic availability. PK evaluation of subcutaneous (S.C.) injection also demonstrated a similar trend that the nanoscavenger possessed significantly longer vascular residence time and higher bioavailability than the native enzyme (**Figure 4.6a**). As a microorganism-derived protein, the fast clearance remains one of the major obstacles that hinder the translation of OPH into clinical use. OPH has a dimeric structure with a molecular weight of ~72 kDa, slightly larger than the kidney clearance threshold of protein (~60 kDa)[3]. The irreversible uptake by reticuloendothelial system (RES) might be a major culprit for the rapid clearance of native OPH. Coating the native protein with a highly hydrated zwitterionic polymer gel not only dramatically increased its hydrodynamic size, but also hid the enzyme core from immune system, ensuring its long vascular residence. As rodents have much smaller size and faster metabolism when compared to human, we would expect a much longer circulation half-life in human. Consulting the agents that possess comparable circulatory behavior in rodents, it is

reasonable to expect a human half-life of more than 100 h.[84] For prophylactic applications, multiple doses of bioscavenger enzymes may be needed to prolong protection against OP poisoning. However, repeated dosing of biological substances may trigger the accelerated blood clearance (ABC) phenomenon.[85] To test the performance of nanoscavengers after multiple doses, a second injection was given two weeks after the initial administration and PK profiles were evaluated as before (**Figure 4.1d and 4.6b**). No significant difference was found between the two doses of nanoscavengers, indicating the likelihood that they could maintain their superior PK performance after repeated doses.

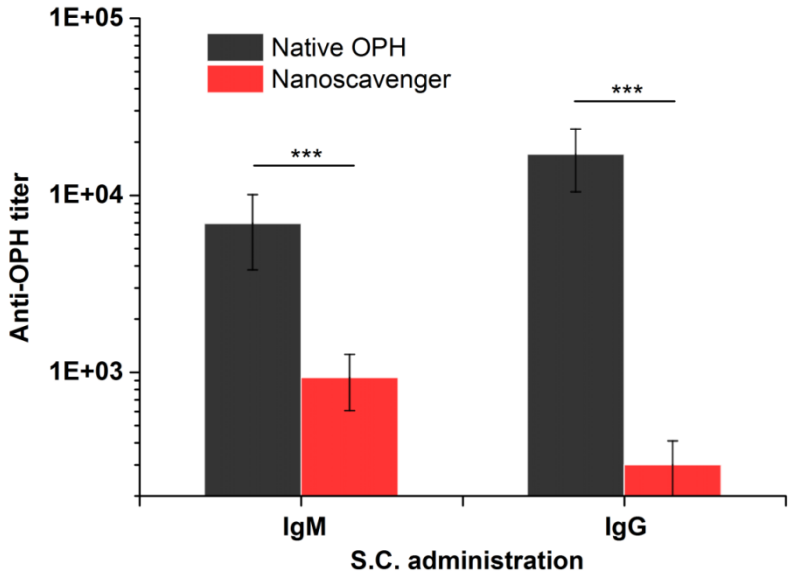

Figure 4.7 Anti-OPH antibody titers after S.C. administration in the rat blood.

We explored the immunogenicity of these protein containing nanoparticles in further detail by collecting and testing sera three weeks after the second injection. As shown in **Figure 4.1e** and **4.7**, high titers of anti-OPH IgM and IgG were found in the groups treated with native OPH via both administration routes (I.V. and S.C.). As a result,

unmodified OPH may not be directly used in humans, as the resulting immune response would reduce its efficacy and potentially induce life-threatening anaphylactic reactions. In contrast, negligible antibody response was detected in rats treated with nanoscavengers, corroborating that PCB gel coating effectively rendered the protein "invisibility" to immune system and thus mitigated antibody induction. As anti-polymer antibodies are becoming a growing concern for protein therapeutic formulations such as pre-existing and therapy induced anti-PEG antibodies,[29, 86-88] the presence of anti-PCB antibodies was tested in this work. As shown in **Figure 4.8-4.9**, no anti-PCB antibodies was observed for either of the administration routes, which is in consistent with our previous findings.[69]

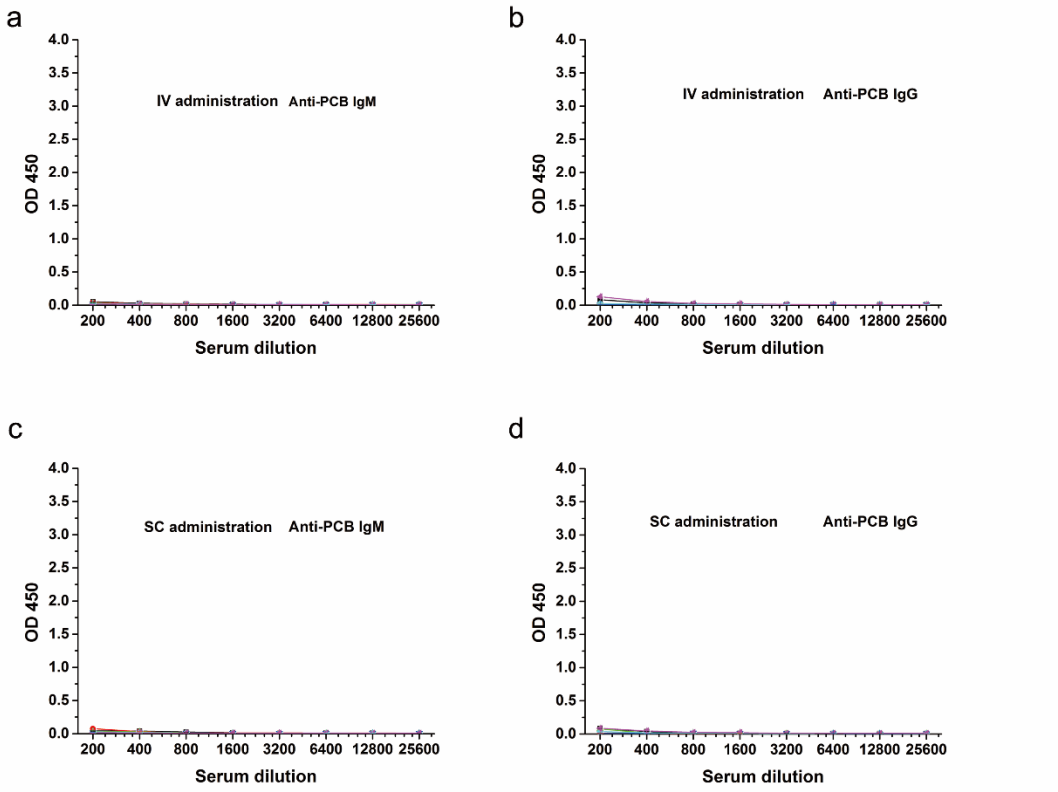

Figure 4.8 Detection of anti-PCB antibodies in nanoscavenger groups by direct ELISAs. (a) IgM after I.V. administration, (b) IgG after I.V. administration, (c) IgM after S.C. administration and (d) IgG after S.C. administration. Serum from each rat is plotted separately.

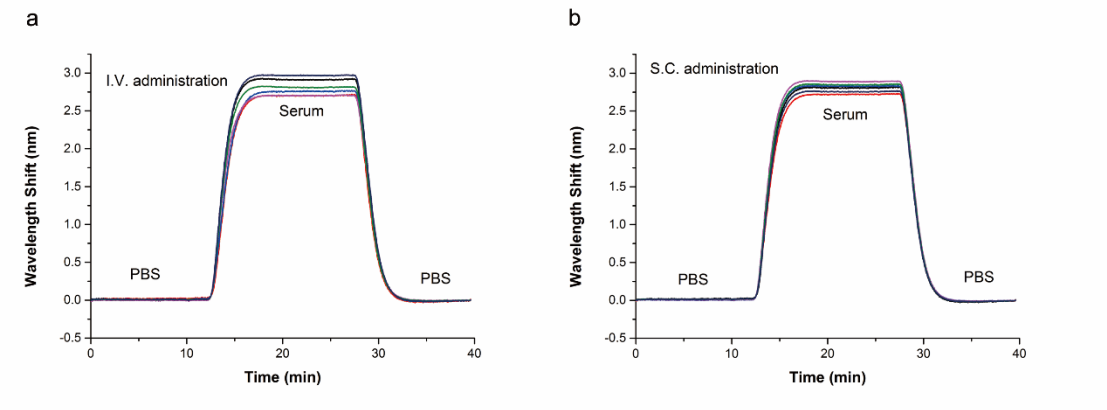

Figure 4.9 Detection of anti-PCB antibodies in nanoscavenger groups by SPR sensors. The gold chip surface was modified with PCB polymer brushes. Sensor signal-time curves of the sera (a) after I.V. administration and (b) after S.C. administration. No adsorption was detected from the tested sera. Serum from each rat is plotted separately.

4.3.3 Detoxification and prophylactic efficacy against paraoxon

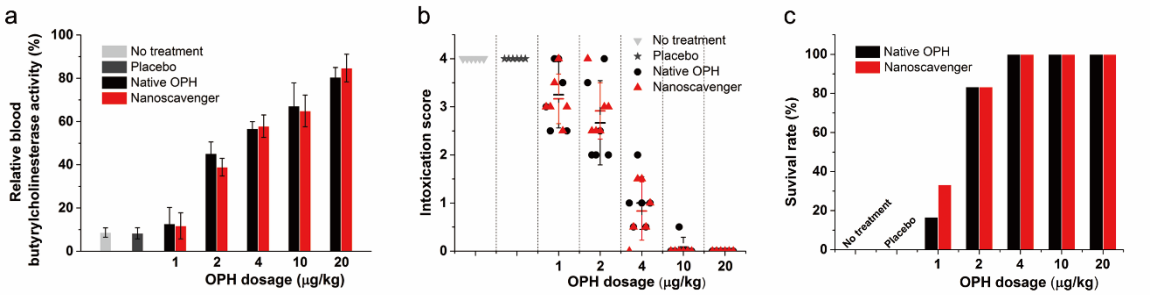

Figure 4.10 Detoxification efficacy study of the nanoscavenger *in vivo*. A dosage of $2 \times LD_{50}$ paraoxon was injected subcutaneously into each group of rats. Immediately after paraoxon injection, different dosages of OPH or nanoscavenger were injected intravenously into each group. (a) Blood butyrylcholinesterase activity, (b) intoxication signs and (c) survival rates post paraoxon administration. Each group consisted of six animals.

Table 4.2 Intoxication score definitions

Intoxication score	Symptoms
1	Slight to moderate muscle twitch
2	Muscle twitch; Salivation
3	Salivation; Tremors
4	Serious tremors; Salivation; Respiratory depression

To explore the detoxification efficacy of the nanoscavenger *in vivo*, we firstly conducted a dosage study in a rat model of OP poisoning. Two times of the median lethal dose ($2 \times LD_{50}$, 0.86 mg/kg)[89] of paraoxon – the active metabolite of the insecticide parathion, was injected subcutaneously on the back of each rat, and different dosages of OPH or nanoscavengers were administered intravenously through the tail vein. Once entered into blood vessels, OP molecules irreversibly inhibit butyrylcholinesterase activity; thus the butyrylcholinesterase activity in blood was measured as the biomarker for OP intoxication.[90] As shown in **Figure 4.10a**, the administered OP compounds almost completely inhibited blood butyrylcholinesterase activity in the untreated groups, while both native OPH and nanoscavenger significantly preserved butyrylcholinesterase from OP inhibition. Five minutes post paraoxon injection, both control groups exhibited serious signs of OP poisoning, including muscle twitch, salivation, tremors and respiratory depression. The clinical signs were scored based of a 0-4 scale, and the score definitions are listed in **Table 4.2**. The administration of bioscavengers at a dosage of 1 μg/kg significantly ameliorated the symptoms induced by paraoxon challenge, while 10-20 μg/kg completely stopped the onset of intoxication. **Figure 4.10c** summarizes the animal survival rate. Both no treatment and nanogel placebo control groups showed rapid death within fifteen minutes after paraoxon administration due to its acute neurotoxicity. In contrast, the administration of 4 μg/kg bioscavengers successfully prevented lethality. Considering that the rat blood volume is approximately 64 mL/kg, it can be roughly estimated that the minimum blood concentration of OPH to prevent lethality is 60 ng/mL while 160 ng/mL is capable of protecting rats from suffering poisoning symptoms. Both

native and protected OPHs behaved similarly in this set of tests, due to their similarity in catalytic activities.

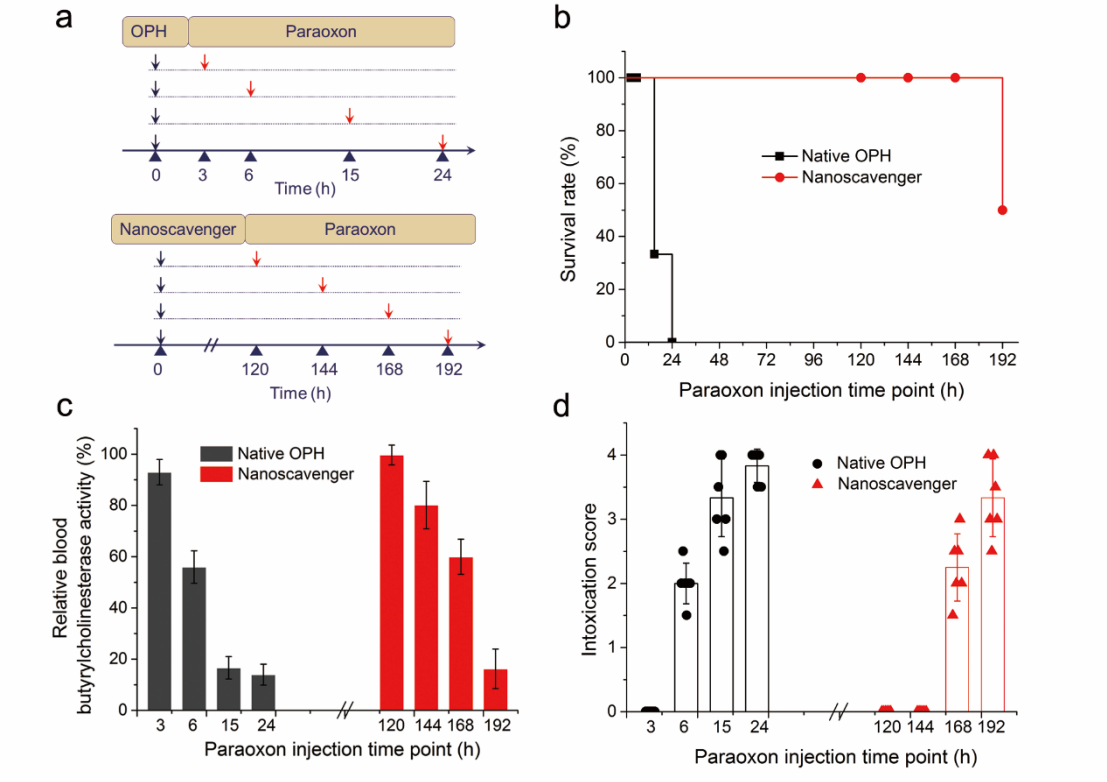

Figure 4.11 Time-dependent prophylactic efficacy test by intravenous administration. The test agents were injected intravenously via the tail veins first (t = 0 h) at the dosage of 1 mg/kg into rats, and then 2 ×LD_{50} paraoxon was injected at different time points later by subcutaneous administration on the back of each rat. (a) Schematic showing of the experiment design. (b) Survival rates, (c) blood butyrylcholinesterase activity, and (d) intoxication signs post each paraoxon administration. Each group consisted of six animals.

Next, a time-dependent prophylactic efficacy test was performed to evaluate the protection time window provided by the nanoscavengers. The experimental design is shown in **Figure 4.11a**. A dosage of 1 mg/kg nanoscavengers was given I.V. at time 0, and 2 ×LD_{50} paraoxon was administered S.C. at different time points post-nanoscavenger administration. Based on the circulatory profiles and the minimum blood OPH concentration required as determined above, it was estimated that the protection time

window lies in 24 hours post injection for native OPH, and around one week for the nanoscavenger. The time points to perform paraoxon challenge were selected based on this estimation. The results are shown in **Figure 4.11b-d**. Due to the fast elimination in blood, unmodified OPH provided complete protection (without symptom and death) against $2 \times LD_{50}$ paraoxon only for 3 hours, and a 6-hour time window for the prevention of lethality. In contrast, the long-circulating nanoscavenger protected animals for 6 days without any signs of intoxication and 7 days without lethality. Such exceptional long-term protection time window provided by nanoscavengers represents the key benefit of their long vascular residence time and high catalytic efficiency. Similarly, another set of experiments showed that S.C. injection of the nanoscavenger also protected the animals for five days (**Figure 4.12**). The successful protection provided by S.C. administration demonstrated its flexibility in administration routes, which is critical under circumstances when I.V. administration is not applicable. To the best of our knowledge, there are no reported bioscavenger analogs that could provide such long-term protection against OP intoxication. The majority of bioscavengers on record was tested prophylactically only minutes to hours post-pretreatment.[45, 57, 60, 79, 91, 92] Since the vascular residence time of modified proteins in human can be several fold longer than in rodents,[84] we can reasonably expect a protection time window of weeks to a month in human prophylactic applications, which should be long enough to fulfill the mission of bioscavengers.

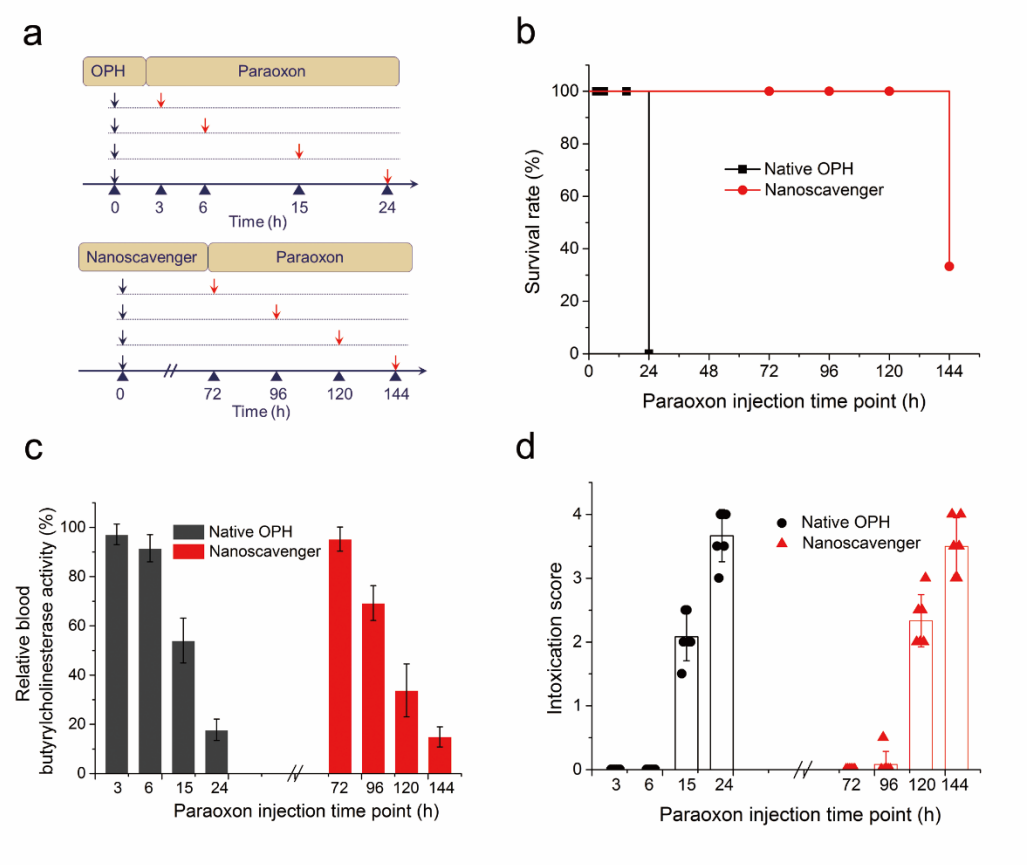

Figure 4.12 Time dependent prophylactic efficacy test by S.C. administration. The bioscavengers were firstly subcutaneously injected (t = 0 h) at the dosage of 1 mg/kg on the back of the rats, and then 2×LD_{50} paraoxon was injected at different time points later by S.C. administration at different sites. (a) Schematic showing of the experiment design. (b) Survival rates, (c) blood butyrylcholinesterase activity, and (d) intoxication signs post each paraoxon administration. Each group consisted of six animals.

To further evaluate the performance of nanoscavenger under different circumstances, as multiple or continuous contacts of OP agents might be encountered in civilian and military settings, a repeated exposure test was performed. In this test, a group of animals received a pretreatment (t = 0 h) of nanoscavenger via I.V. administration, followed by multiple OP challenges at different time points until death. The test results are summarized in **Figure 4.13**. All rats in saline control group did not survive the first

challenge of $2 \times LD_{50}$ paraoxon at the 3h time point, while the other two prophylactically treated groups demonstrated complete protection against intoxication. The second OP challenge was given to survived rats at 24 h, and native OPH failed to protect animals at this time point. Repeated paraoxon injection was then given to the survived rats every 24 hours after the second challenge and complete protection was observed until the sixth challenge performed 5 days after the nanoscavenger pretreatment. Under multiple OP exposure challenges, the nanoscavenger exhibited a slightly shorter protection period compared with single exposure test, which is probably because of a "leakage" phenomenon. In brief, when each time an animal is exposed to nerve agents, the agents will distribute through the blood stream and out into the rest of the body. Although the endogenously administered nanoscavenger will hydrolyze the majority of nerve agent molecules, a small portion will inevitably reach and irreversibly bind to their physiological target AChE without signs of intoxication. This "leakage" will accumulate after multiple OP exposures, and during this process the victim becomes more and more vulnerable to OP intoxication until death occurs. The catalytic mechanism possesses intrinsic advantages over stoichiometric counterparts, particularly in dealing with multiple contact situations, as the nanoscavengers will not be consumed in the detoxification process. These results proved that a long-term protection can also be achieved with pretreatment of nanoscavengers under rigorous multiple OP exposure situations.

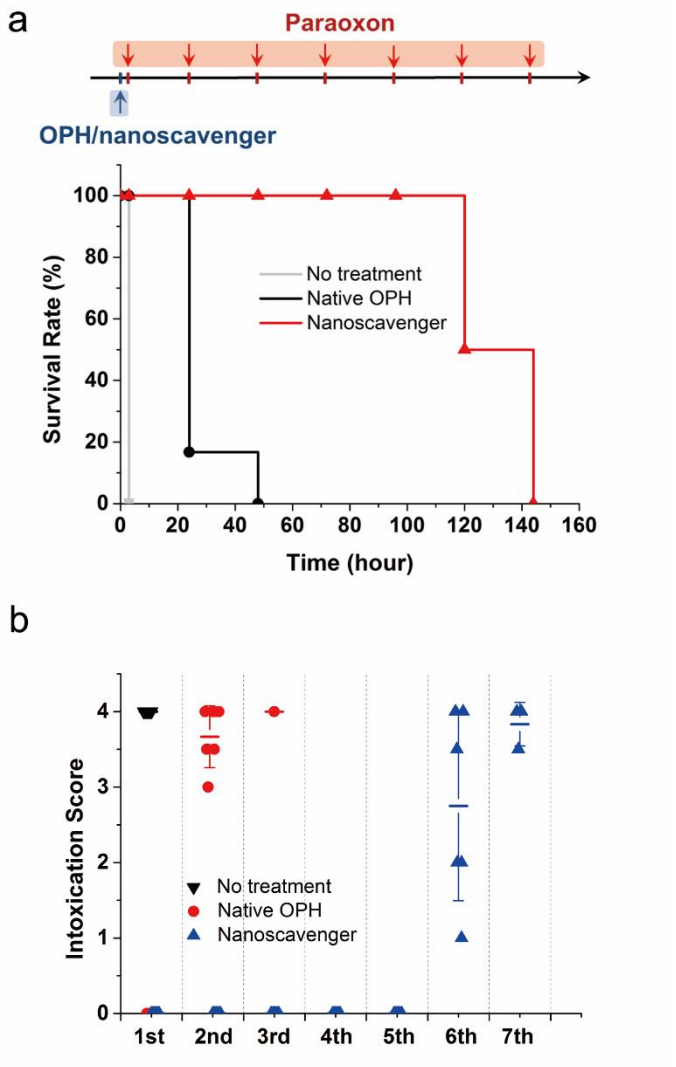

Figure 4.13 Prophylactic protection efficacy under repeated paraoxon exposures. The bioscavengers were injected intravenously via the tail veins first (t = 0 h) at the dosage of 1 mg/kg into rats. Three hours later (t = 3h), 2 ×LD_{50} paraoxon was injected by subcutaneous administration on the back of each rat. The paraoxon administration was repeated every 24 h to the survived rats until all animals died (blue arrow represents the bioscavenger administration, and each red arrow represents one paraoxon exposure). (a) Survival rates and (b) intoxication signs post each paraoxon administration. (n=3 in saline control group; n=6 in native OPH and nanoscavenger group)

4.3.4 Prophylactic efficacy against sarin

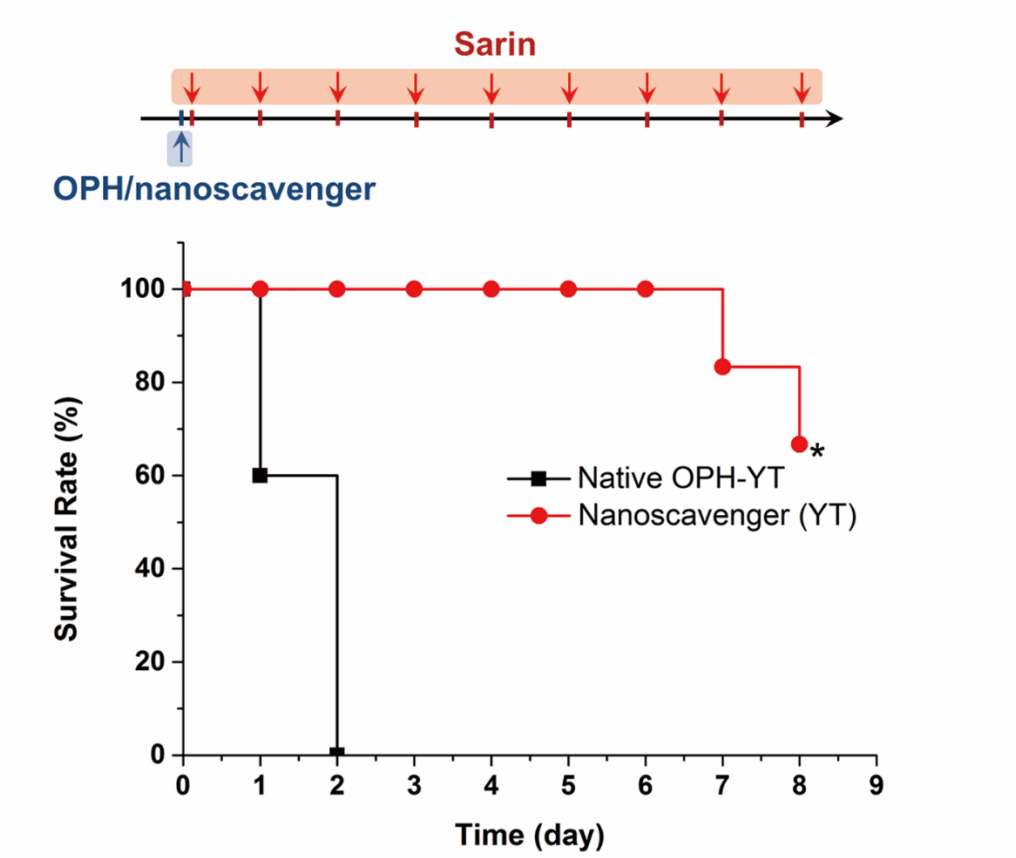

Figure 4.14 Prophylactic protection efficacy under repeated sarin exposure. The bioscavengers were injected intravenously via a catheter (day 0, blue arrow) into guinea pigs at the dosage of 5 mg/kg. Sarin ($2 \times LD_{50}$) was then administered at 20 minutes and then repeatedly every 24 h to the survived animals (red arrows). * Four animals did not show intoxication signs 1 h after the 9th exposure at day 8. (n=5 in native OPH-YT group; n=6 in nanoscavenger-YT group)

Table 4.3 Pharmacokinetic parameters after I.V. administration in guinea pigs

Parameters	Native OPH	Nanoscavenger
$t_{1/2}$ (h)	0.8	36.3
AUC_{∞} (μg/mL ×h)	281	10058
MRT (h)	1.2	52.4

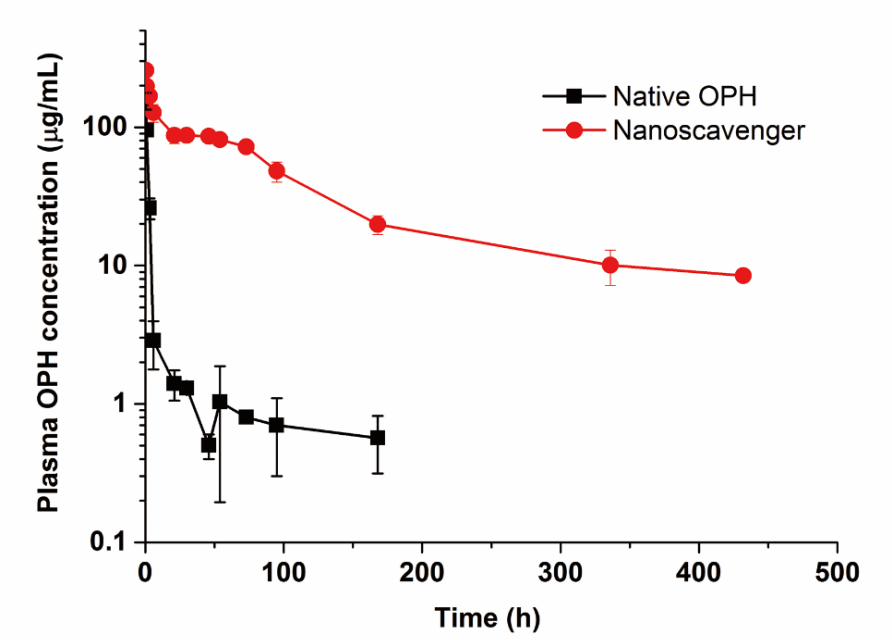

Figure 4.15 Pharmacokinetic profiles of the native OPH *vs.* nanoscavenger in guinea pigs after I.V. administrations. Each group consisted of three animals.

Finally, we tested the protection potency of the nanoscavenger platform against sarin (GB), a chemical weapon. Sarin has appeared in multiple wars and terrorist attacks over the last thirty years, which caused thousands of deaths. The wild-type OPH has relatively lower catalytic activity toward sarin substrate, thus, we used the OPH-YT variant with optimized activities[76] against G-type nerve agents to build the sarin-effective nanoscavenger. This evaluation compared the protective efficacy afforded by both OPH-YT and the nanoscavenger-YT following multiple-exposures to lethal doses of GB in guinea pigs. The pharmacokinetics was firstly evaluated in guinea pigs (**Figure 4.15** and **Table 4.3**). During this test, the animals firstly received a pretreatment of nanoscavenger or OPH-YT (5 mg/kg) via I.V. administration (carotid catheter), followed by one sarin injection (2×LD_{50}, S.C.) 20 minutes after enzyme. Multiple exposures were subsequently administered every 24 hours until death. As shown in **Figure 4.14**, two out

of five animals in the native enzyme group died after the second exposure of sarin, and no animal survived post the third exposure. In contrast, all animals in the nanoscavenger group were well protected until the eighth exposure, and four out of six animals displayed only mild signs of intoxication after the ninth exposure at day 8. Overall, the nanoscavenger provided full protection to guinea pigs receiving a cumulative exposure of $14xLD_{50}$ of GB. These results highlighted the superb protection capacity offered by nanoscavengers against sarin poisoning. As the YT variant has similar catalytic activities across G-type organophosphates (GB, GD, and GF)[76], we can reasonably conclude the effectiveness of nanoscavenger as a prophylactic countermeasure against the threats from this major type of nerve agents.

4.4 Conclusions

OP poisoning remains as a major medical issue for public health while nerve agents intimidate both soldiers and civilians in war zones. The acute poisoning nature demands effective therapeutic and prophylactic interventions. In this study, a nanoscavenger capable of hydrolyzing organophosphates was developed by encapsulating native OPH enzyme into zwitterionic hydrogel nanoparticles. The nanoscavenger demonstrated long vascular residence time with minimal immune responses. In addition to the rescue of animals following lethal OP challenge, a single prophylactic intravenous injection of the nanoscavenger has successfully protected animals from OP poisoning for over a week. By simply changing the enzyme core into different variants, nanoscavenger against different nerve agents can be easily fabricated. A nanoscavenger cocktail against a broad spectrum of OP compounds is also feasible with the rational design of OPH variants. This platform presents the first long-lasting prophylactic bioscavenger, which offers an

applicable strategy to countermeasure OP threatening in both clinical and military settings.

Chapter 5 Rapid, Sensitive and Quantitative Detection of Anti-PEG Antibodies by mPEG-coated SPR Sensors

Pre-existing and induced anti-poly(ethylene glycol) (PEG) antibodies (abs) have been shown to be related with limitation of therapeutic efficacy and reduction in tolerance of several therapeutic agents. However, the current methods to detect anti-PEG abs are tedious and usually lack of quantification. A facile, rapid, sensitive and reliable technique to detect anti-PEG abs is highly desired in both research and clinic settings. In this work, we have presented a surface plasmon resonance (SPR) biosensor technique for the detection of anti-PEG abs and compared three PEG surface chemistries. Methoxy-PEG (mPEG) 5k was found to have the best performance. The detection of anti-PEG abs directly from diluted blood serum was achieved within 40 min. Detection sensitivity is as good as or better than enzyme-linked immunosorbent assay (ELISA). Furthermore, different antibody isotypes can be quantitatively differentiated by adopting secondary antibodies. A pilot study has been performed to analyze clinical blood samples using this technology, demonstrating its potential as a convenient and powerful method to pre-screen and monitor anti-PEG abs in the patients before or after they receive treatment with PEG-containing drugs.

5.1 Introduction

Poly(ethylene glycol) (PEG) is the most widely used synthetic polymer in pharmaceutical industry to conjugate biological therapeutics or as formulation excipients.[1, 5, 10] The attachment of PEG to biomolecules such as recombinant proteins and peptides (or PEGylation) extends their circulation time, reduces immunogenicity and antigenicity and improves therapeutic efficacy.[11] Currently,

twelve therapeutic PEGylated drugs have been approved by the US Food and Drug Administration (FDA), such as PEG-asparaginase for leukemia and lymphoma and PEG-uricase for chronic gout, and more are in the pipeline.[15]

Nevertheless, in contrast to the generally accepted assumption that PEG is non-immunogenic and non-antigenic, an emerging number of studies demonstrated that the immune system can elicit antibody formation specifically against PEG (anti-PEG abs) both in animals and human.[15, 34, 86, 93] The generation of anti-PEG abs can accelerate the clearance of PEGylated therapeutics, thus reducing therapeutic efficacy. For instance, recent clinical investigations of PEG-uricase in refractory chronic gout patients unequivocally showed that anti-PEG abs correlated with a reduction in drug effectiveness.[17, 19] Moreover, the existence of anti-PEG abs threatened patient safety with anaphylaxis and infusion reactions.[17, 87, 94] Re-exposure to PEG containing drugs may greatly increase the chance for adverse effects due to B cell memory of anti-PEG abs.[18] To make things worse, recent findings have indicated the widespread occurrence of anti-PEG abs in general population due to increased daily exposure to PEG containing products.[28, 29] If high titer anti-PEG abs are present in blood, even people without known allergies may have severe hypersensitive reactions when receiving PEG containing therapeutics for the first time.[87, 94] Thus, screening and monitoring the anti-PEG abs in blood before and during the treatment with PEG containing drugs are of particular importance to provide safety and maintain therapeutic efficacy. A facile, rapid, sensitive and reliable technique to detect the anti-PEG abs is highly desired to fulfill the demand.

A variety of methods have been reported to detect anti-PEG abs such as serology[16], flow cytometry[16], Western blotting[20, 95] and enzyme-linked immunosorbent assays (ELISA)[32, 96]. However, these traditional methods usually involve time-consuming and complicated procedures, which hinder clinical applications. In addition, it is difficult to quantify the antibody concentrations using these methods, and the detection results are highly dependent on operation protocols, quality of reagents and even the personal habits of the operator. For these reasons, the detection results from different reports using these methods are often not comparable.

To overcome these shortcomings, we proposed a novel method with high sensitivity, simple operation process, rapid detection time and high throughput using a surface plasmon resonance (SPR) sensor. SPR is a powerful technique to monitor label-free biomolecular interactions and biomolecule/surface interactions.[38] Previously, we modified SPR sensor chips with poly[poly(ethylene glycol) methyl ether methacrylate] (PEGMA) polymer and demonstrated its capacity to detect anti-PEG abs qualitatively.[69] Herein, we compared three different surface coating chemistries and achieved sensitive quantitative detection with methoxy-PEG. The PEG modification simultaneously serves as dual roles: first, it resists non-specific protein adsorption from diluted blood serum and diminishes the background noise; second, it acts as an anchored antigen to catch any anti-PEG abs present in the blood sample to generate strong signals in SPR measurements. With this facile setup, quantitative anti-PEG abs detection could be achieved within 40 mins with a detection limit as low as 10 ng/mL. In addition, antibody isotypes can also be distinguished and quantified using secondary antibodies.

5.2 Experimental Section

5.2.1 Materials

Recombinant uricase from Candida sp., Freund's adjuvants and all chemicals were purchased from Sigma-Aldrich unless otherwise noted and were used as received. Methoxy poly(ethylene glycol) succinimidyl carbonate (mPEG-NHS, 10kDa, 95%), and methoxyl PEG thiol (mPEG, 5kDa) were obtained from Nanocs. 2-(2-(2-(2-(1-mercaptoundec-11-yloxy)-ethoxy)-ethoxy)-ethoxy)-ethanol (EG4) was purchased from ProChimia. Rat monoclonal anti-PEG IgM (26A04) and mouse monoclonal anti-PEG IgG (09F02) were purchased from Abcam. Goat anti-rat IgM antibody, goat anti-mouse IgG antibody, goat anti-human IgM antibody and goat anti-human IgG antibody were purchased from Bethyl labs.

5.2.2 Animal immunization

Uricase-mPEG conjugates were used as the antigen in this study to generate anti-PEG abs in animals. Uricase-mPEG conjugates were prepared following previously published procedure.[69] Two sets of blood samples were generated using different immunization routes. One group of Sprague–Dawley rats was immunized by intravenous injection (IV) as described previously.[69] The other group was immunized by subcutaneous injection (SC) in the presence of Freund's adjuvant. Experimentally, the rats were injected subcutaneously on the back with the immunogens on days 0, 14, and 21. The first immunization was in the presence of Freund's complete adjuvant. Subsequent immunizations were done in the presence of Freund's incomplete adjuvant. Blood was collected prior to immunization (prebleed) and 5 weeks after the first immunization. All the sera were prepared from each bleed by centrifugation and were

kept frozen until use. All animal experiments adhered to federal guidelines and were approved by the University of Washington Institutional Animal Care and Use Committee.

5.2.3 SPR chip coating and detection

PEGMA polymer brushes were grafted onto gold SPR sensor chips following previously published methods.[69] Brush thickness was measured by a spectroscopic ellipsometry (Sentech SE-850). The mPEG and EG4 were modified on the gold SPR chips by immersing the UV-ozone cleaned chips in the corresponding thiol ethanol solution (1 mg/mL for mPEG, and 1 mM for EG4). A custom-built SPR sensor was used in this study. All experiments were done following the sequence of flowing PBS for 10 min, 1:20 diluted serum in PBS for 15 min, and PBS for 15 min at flow rate of 30 μL/min. For the experiment of IgG and IgM differentiation, goat anti-rat IgM or IgG (10 μg/mL) was flowed continuously after anti-PEG detection for 15 min, followed by PBS for 15 min. For the SPR sensor used in the study, a 1-nm SPR wavelength shift represents a surface coverage of ~17 ng/cm2 for proteins. Detection limit for the SPR sensor used in this work is 0.3 ng/cm2.

5.2.4 ELISA experiments

The antigens used in direct ELISAs for plate coating consisted of BSA-mPEG conjugates. BSA-mPEG conjugates were made following the same procedure as uricase PEG samples. For ELISA experiments, 100 μL antigen solution (10 μg/mL of protein concentration) prepared in 0.1 M sodium carbonate buffer, pH 10.5, was used to coat each well of the 96-well plates. During coating procedure, plates were incubated at 4 ℃ overnight. After removing antigen solutions, the plates were washed five times using PBS (PBS 7.4) and then filled with blocking buffer (1% BSA solution in 0.1 M Tris buffer, pH

8.0). It is important to avoid using any buffer that contains PEG-like detergents, e.g., Tween 20 and Tween 80. After incubation at room temperature for 1 h, blocking buffer was removed, and all wells were washed by PBS for another five times. Serial dilutions of monoclonal anti-PEG abs in PBS containing 1% BSA were added to the plates (100 µL/well), which were incubated for 1 h at 37 °C. The plates were then washed five times with PBS, followed by adding secondary antibody HRP conjugates (100 µL/well, dilution 1:50000, Bethyl Labs). After adding the secondary antibody, plates were incubated at room temperature for 1 h and then washed five times using PBS before the addition of 100 µL/well HRP substrate 3,3′,5,5′-tetramethylbenzidine. The plates were shaken for 15 min, and 100 µL stop solution (0.2 M H2SO4) was added to each well. Absorbance at 450 (signal) and 570 nm (background) was recorded by a microplate reader.

5.3 Results and Discussion

5.3.1 Selection of sensor surface chemistry

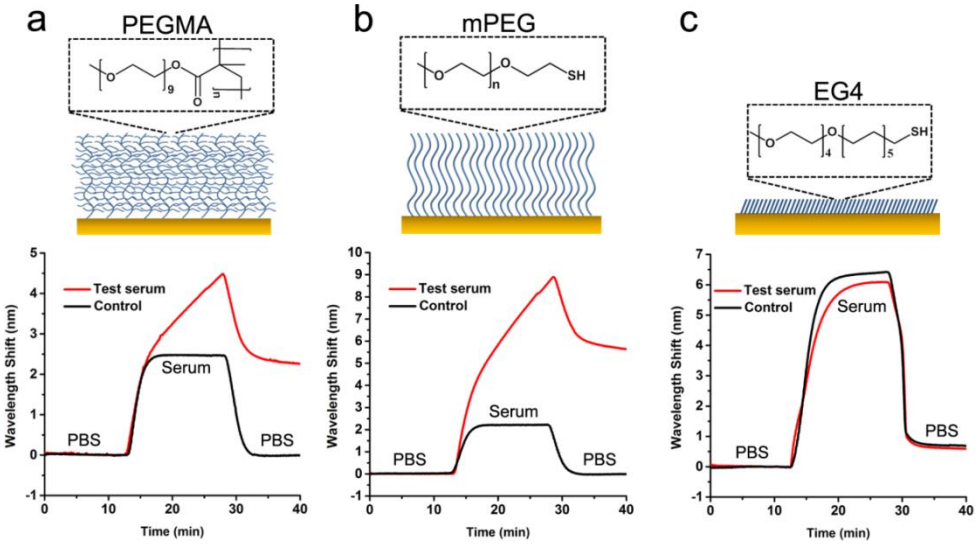

Figure 5.1 The gold chip surfaces were modified by PEGMA polymer brush (a), mPEG (b) or EG4 SAM (c), and tested by both negative control (black) and anti-PEG (red) serum samples.

To effectively detect anti-PEG abs from blood samples, which constitute hundreds of different proteins together, two parameters are crucial in the design of the sensor chips. One is to strongly resist non-specific protein adsorption to ensure a low-noise background while another is to have strong binding affinity to the analyte to produce a high signal. As shown in **Figure 5.1**, three different chemistries were selected to modify chip surfaces with PEG-derived materials and compared for their performance. Oligo(ethylene glycol) (EG4) self-assembled monolayer (SAM) is known to resist non-specific protein adsorption[29] and used in this work. Anti-PEG abs were reported to bind to as few as three oxyethylene groups[32]. Two other methoxy-terminated PEG analogs, mPEG and PEGMA were chosen instead of hydroxyl terminated counterparts due to their stronger binding affinity to anti-PEG abs.[32] EG4 and mPEG were modified onto gold chip surfaces by immersing into corresponding thiol solutions, while PEGMA brushes were synthesized by surface-initiated atom transfer radical polymerization (ATRP). The coating thickness was measured by ellipsometry that the PEGMA layer was 16.5 ± 2.1 nm, mPEG layer was 4.2 ± 0.6 nm, and the EG4 SAM was 1.5 ± 0.2 nm.

The resistance to surface nonspecific protein adsorption from blood proteins was first examined by flowing diluted control serum. The test experiment was done by flowing 5% serum dilution for 15 min, followed by PBS washing for another 10 min. As shown in **Figure 5.1**, a large wavelength shift signal was recorded when serum samples flowed past the chip due to the solution refractive index change. After washed by PBS buffer, the remaining signal represented surface molecular adsorption. Although EG4 SAM is known to reduce nonspecific protein adsorption from single protein solutions, it still showed 0.7 nm wavelength shift biofouling signal when challenged by 5% serum

dilution, which corresponded to ~12 ng/cm2.[38] In contrast, no fouling signal was detected for both mPEG and PEGMA grafted surfaces. The blood sample collected from rats that received three repeated intravenous (IV) injections of uricase-PEG conjugates were used as the test sample to examine the three sensor chips. When flowing 20 times diluted test serum, mPEG modified chip showed the strongest sensing signal (5.6 nm wavelength shift), indicating its highest binding affinity against anti-PEG abs. The PEGMA grafted sensor chip exhibited moderate response (2.3 nm wavelength shift), while the signal from EG4 chip was not distinguishable from biofouling background. As expected, anti-PEG abs have stronger binding affinity toward linear PEGs compared with branched PEGMA polymers,[97] as they were elicited using linear PEG conjugated proteins. mPEG was chosen as the coating material for the following detection studies due to its highest sensitivity in a low-noise background.

5.3.2 Quantitative sensor signal response

Selecting mPEG as the surface coating layer, we next examined the sensor response to different anti-PEG ab concentrations. As shown in **Figure 5.2a-b**, monoclonal rat anti-PEG IgM ab was used to test the SPR sensor at a series of concentrations. As expected, the sensor signals increased with the test antibody concentrations. The detection limit was determined to be 50 ng/mL and the chip surface adsorption reached saturation when antibody solution was higher than 20 μg/mL. As seen in the sensorgram, the background signal generated by the difference in media refractive index between PBS and sample disappeared at ~30 min. To avoid the influence from media refractive index, we took the wavelength shift value at 35 min to represent the sensor signal for each antibody concentration. The sensor signals showed ideal linear relationship with antibody

concentrations in the range of 50 ng/mL to 10 μg/mL. Similar results were also observed for mouse anti-PEG IgG abs, with the detection limit of 100 ng/mL (**Figure 5.2c-d**).

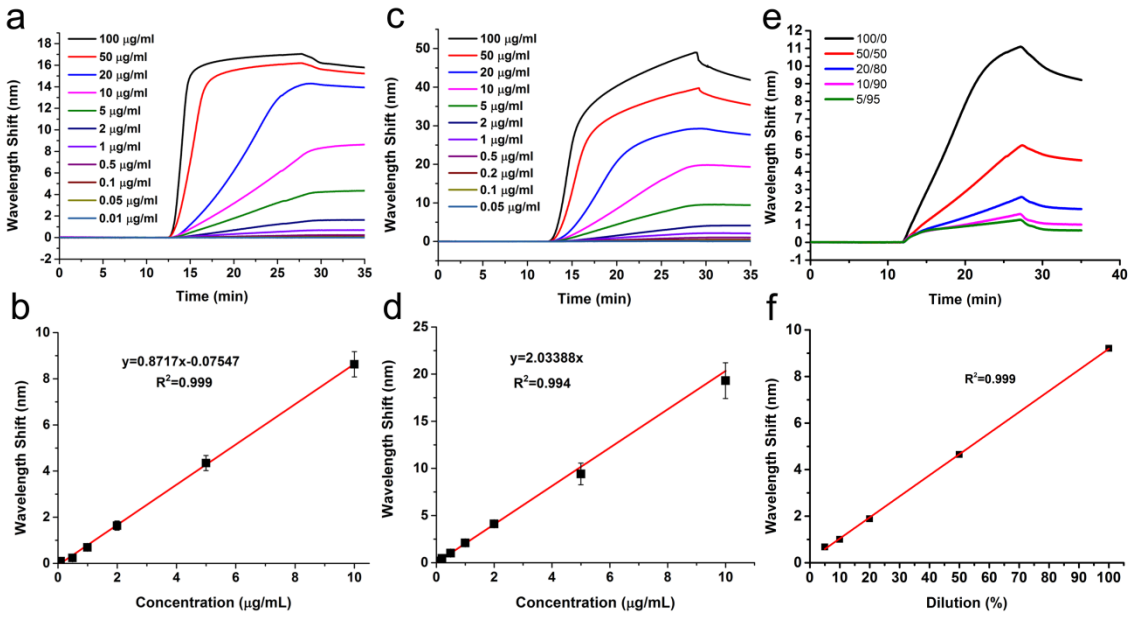

Figure 5.2 SPR sensorgrams of rat monoclonal anti-PEG IgM (a,b) and mouse monoclonal anti-PEG IgG (c, d) detection at different analyte concentrations. The wavelength shift values were correlated with antibody concentrations. A linear dynamic range was found as 0 to 10 μg/mL for both antibodies. (e, f) SPR sensor responses to anti-PEG abs in serum samples. An anti-PEG serum was mixed with control serum at the ratio of 100/0, 50/50, 20/80, 10/90 and 5/95 and examined by the sensor. The wavelength shift values showed excellent linear relationship with the amounts of anti-PEG abs in blood samples.

One intrinsic limitation for currently used antibody detection methods is their non-linearity between the signal responses and analyte concentrations. For example, as the most state-of-the-art immunoassay to quantify anti-PEG abs, ELISA uses enzyme mediated biochemical reactions to generate signals. A four parameter logistic regression is needed to correlate ELISA signals with the anti-PEG abs concentrations, as shown in **Figure 5.3**. With the non-linear relationship, it is always difficult to directly compare two optical density (OD) results without a standard curve. As a result, the antibody titer is

defined as a measurement to facilitate the semi-quantitative comparisons. To determine the titer for a blood sample, a series of sample dilutions need to be tested in parallel which significantly increases the experimental workload. In contrast, the linear relationship demonstrated by SPR analysis provides great convenience when comparing different experiments in the absence of a standard curve. As shown in **Figure 5.2e-f**, we mixed the rat anti-PEG serum with different amount of control serum to simulate a series of different samples. The wavelength signals from serum samples also demonstrated a well fitted linear relationship, showing that the anti-PEG levels from different samples can be directly compared by SPR measurements.

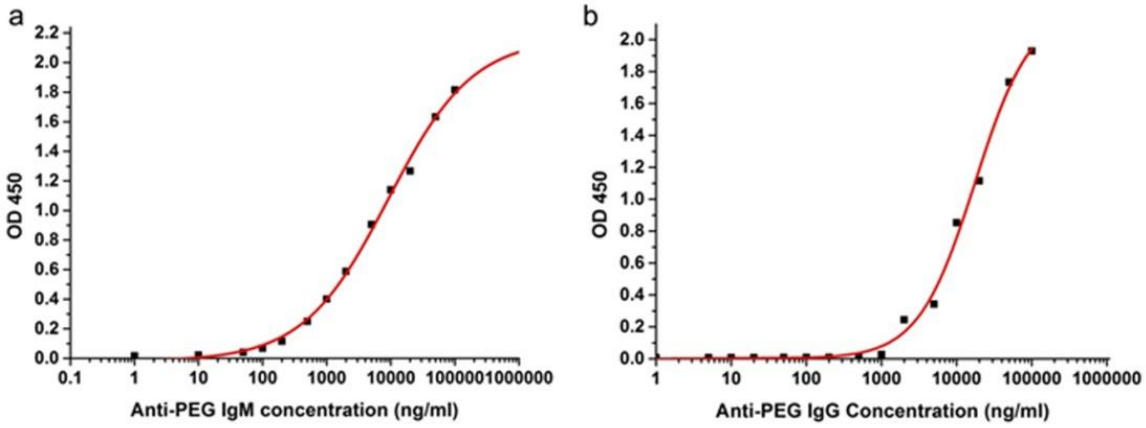

Figure 5.3 Standard ELISA calibration curves generated using rat monoclonal anti-PEG IgM (a) and mouse monoclonal anti-PEG IgG. Each point represents a mean value obtained from three replicates.

5.3.3 Isotype differentiation

Antibodies belong to a family of immunoglobulin that consists of different varieties known as isotypes. In placental mammals there are five antibody isotypes known as IgA,

IgD, IgE, IgG, and IgM, among which IgG and IgM are the most abundant antibodies present in blood circulation. The difference in their heavy chains results in altered complex structures with different molecular weights. For example, IgG appears as a monomer while IgM exists as a much larger pentamer. To accurately monitor the development of immune responses, the detection should be able to differentiate each antibody isotype quantitatively. To identify the isotypes, we adopted secondary antibodies in our experimental settings. As shown in **Figure 5.4a**, taken the detection of anti-PEG IgM as an example, the properly diluted sample was firstly flowed for 15 min, followed by PBS washing, then the goat anti-rat IgM antibody solution (secondary antibody), and finally PBS washing. When anti-rat IgM abs bound to surface adsorbed rat anti-PEG IgM, an increase of wavelength shift showed on the sensorgram. We correlated the wavelength shifts induced by secondary antibody adsorption with a series of analyte samples, and the signal is in linear relationship with the anti-PEG ab concentrations for both IgM and IgG (**Figure 5.4b, c**). Such results demonstrated that blood anti-PEG IgM abs can be quantitatively determined in a wide range of 10 ng/mL to 10 μg/mL and anti-PEG IgG concentrations can be measured in the range of 50 ng/mL to 5 μg/mL. It should be noted that the application of secondary abs amplified the signals, thus increased the signal/noise ratio and extended the detection limits of anti-PEG IgM to 10 ng/mL and IgG to 50 ng/mL. By contrast, direct ELISA tests of the same sets of standard samples showed the detection limits of 100 ng/mL for anti-PEG IgM and 1 μg/mL for anti-PEG IgG abs (**Figure 5.3**).

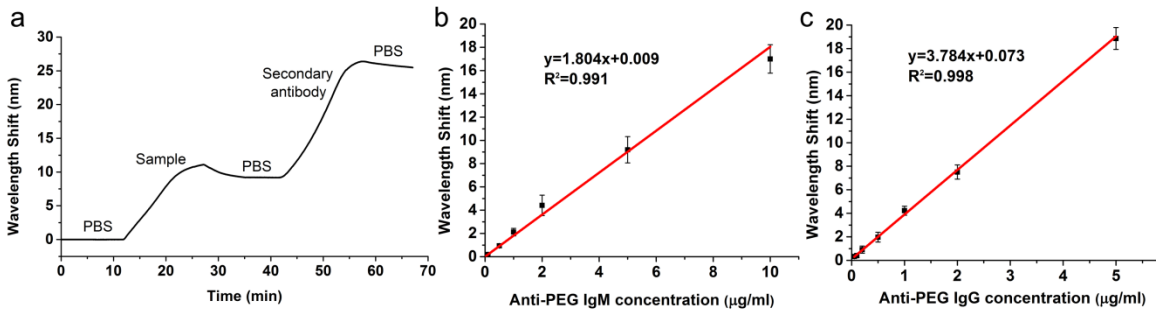

Figure 5.4 (a) A typical SPR sensorgram of anti-PEG antibody isotype detection using secondary antibodies. (b, c) Monoclonal anti-PEG abs were spiked into control serum at different concentrations to prepare standard samples. The wavelength shift signals from secondary antibodies were correlated with concentrations of standard samples to generate standard calibration curves for rat anti-PEG IgM (b) and mouse anti-PEG IgG (c).

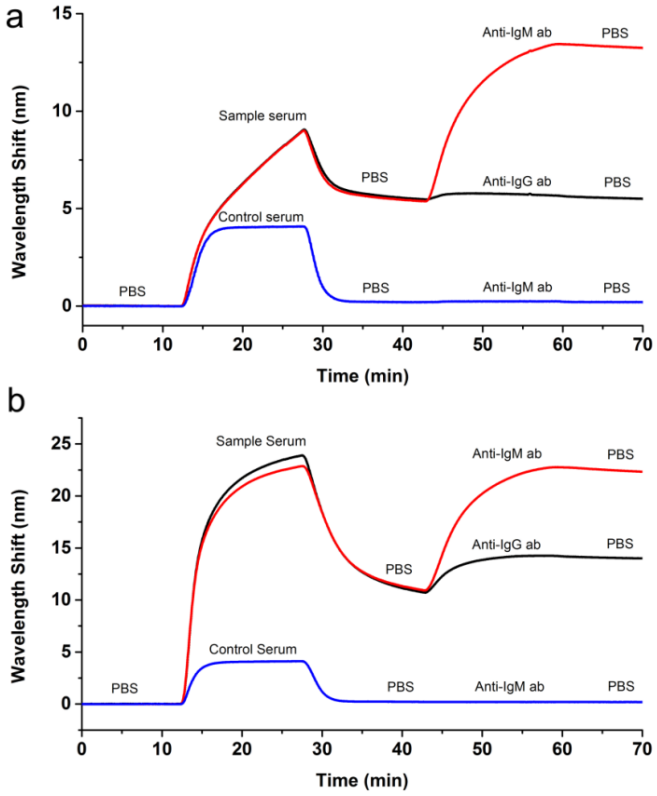

Figure 5.5 SPR sensorgrams of complete anti-PEG ab detections from rat blood samples. (a) Anti-PEG serum generated by IV immunization and (b) anti-PEG serum generated by SC immunization with Freunds' adjuvant.

With the established detection protocol and standard curves generated using monoclonal anti-PEG antibodies, the concentration of each anti-PEG ab isotype can be quantitatively detected. To demonstrate its application to real circumstances, we generated and examined two different anti-PEG antisera from rats to simulate clinical blood samples. One serum was obtained by immunizing a rat with three weekly intravenous (IV) injections of uricase-PEG conjugates, while the other was made by immunizing a rat using uricase-PEG conjugates mixed with Freund's adjuvants subcutaneously (SC). Freund's adjuvant is known to be very effective in stimulating cell-mediated immunity and leads to the production of certain immunoglobulins and effector T cells. As shown in **Figure 5.5**, both serum samples generated strong signals, indicating the abundance of anti-PEG abs in these sera. The wavelength shift when flowed SC sample was much larger than that of IV sample, demonstrating the fact that SC immunization with Freund's adjuvant is much more efficient in generating antibodies. Using the wavelength shift values from secondary anti-IgM abs, we quantitatively determined that the anti-PEG IgM concentrations were 4.3 μg/mL for IV sample and 6.3 μg/mL for SC sample, respectively. Due to lack of availability of the monoclonal rat anti-PEG IgG antibody standard, we were not able to quantify the absolute concentrations of anti-PEG IgG in these serum samples. However, from the wavelength shift values (0.1 nm for IV and 3.3 nm for SC), we can draw the conclusion that SC sample contained 33-fold higher anti-PEG IgG than IV sample, due to the stronger responses and faster anti-PEG isotype switching stimulated by Freund's adjuvant.

5.3.4 Clinical sample analysis

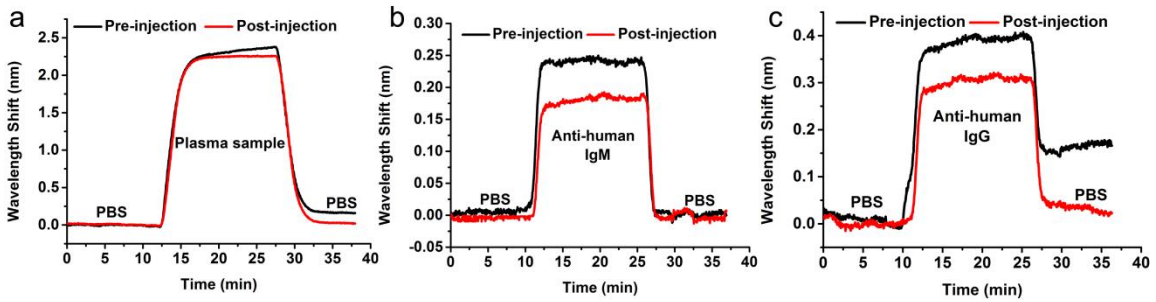

Figure 5.6 Plasma samples from one leukemia patient who received PEG-asparaginase therapy were analyzed by a SPR sensor. (a) sensorgram when flowing plasma samples; (b) sensorgram when flowing anti-human IgM secondary ab; and (c) anti-human IgG secondary ab.

The goal of this study is to provide a convenient high-throughput technology for clinical anti-PEG ab detections. To explore its translational feasibility, we did a pilot study that involves clinical plasma samples from a leukemia patient who received PEG-asparaginase therapy. The study was approved by the Institutional Review Board of the Seattle Children's Hospital. It should be noted that there is no difference in applying serum or plasma as the testing liquid. The patient had no known PEGylated therapeutic exposure history. However, adverse reactions were observed during the fourth administration of PEG-asparaginase. We analyzed two plasma samples from this patient: one was taken before PEG-asparaginase administration and the other was taken ten days post the fourth drug administration. As shown in **Figure 5.6a**, a clear anti-PEG ab response was observed for the pre-injection sample, demonstrating the existence of pre-existing anti-PEG abs. In contrast, the sensorgram showed negative response for the post injection sample, which is possibly because these antibodies bound to the injected PEG-asparaginase and formed immune complexes. The isotype differentiation study

demonstrated the pre-existing anti-PEG abs were mainly IgGs. These samples were validated by ELISA tests, and an anti-PEG IgG titer of 1:400 was found for the pre-injection sample. With these analysis data, we could surmise that the pre-existing anti-PEG IgG might be related with the adverse reactions[87], although a definitive conclusion could only be made based on a larger sample size.

5.4 Conclusions

In conclusion, we demonstrated a simple, rapid, sensitive and reliable technique to directly detect anti-PEG abs in blood samples using SPR sensors. Three PEG derived materials have been tested as the chip coating, and mPEG demonstrated the best analyte signal without fouling background under detection conditions. Compared with traditional methods, the linear response of SPR sensor to anti-PEG ab concentrations greatly facilitates the comparison among different blood samples. By adopting the secondary antibodies in the detection settings, we were able to differentiate and quantitatively determine the concentration of different anti-PEG antibody isotypes in blood samples. This detection method can be readily developed into a high throughput automatic setting, which holds great potential in both academic and clinical applications.

Chapter 6 Polypeptide with High Zwitterion density for Safe and Effective Therapeutics

Stealth materials are widely used in nano-formulations to improve the performance of therapeutics. As the current "gold standard", poly(ethylene glycol) (PEG) polymer effectively promotes the pharmacokinetics of veiled therapeutic cargos while reducing their immune responses. However, recent studies suggested that the usage of PEG could induce adverse reactions, including the emergence of anti-PEG antibodies and PEG-induced tissue histologic changes, therefore casting a shadow over its future therapeutic applications. An alternative material with similar or better therapeutic enhancement effect, but no or less immunogenicity and organ toxicity is urgently needed. Herein, we designed a polypeptide with high zwitterion density (PepCB) as a stealth material for therapeutics. Neither any tissue histologic change in liver, kidney and spleen, nor abnormal behavior, sickness or death was induced by the synthesized polymer after a high-dosage administration regimen for three months in rats. When conjugated to a therapeutic protein uricase, the uricase-PepCB bioconjugate showed significantly improved pharmacokinetics and immunological properties compared with uricase-PEG conjugates.

6.1 Introduction

It is of crucial importance to avoid non-specific protein adsorption and cellular uptake in systemic circulation (so-called "stealth" property) for nanomedicine. Poly(ethylene glycol) (PEG) has been the most commonly used biomaterial in nanomedicine to convey stealth property to biological therapeutics and nanoparticles.[5, 10] It prevents proteins from being adsorbed onto nanoparticle surfaces by its steric

repulsion and high level of hydration.[98] As for biologics, the covalent attachment of PEG (PEGylation) greatly improves their water solubility, stability and circulation half-life while reducing immunogenicity. Over the last four decades, PEGylation has become the “gold standard” for formulating drugs, from small molecules to nanoparticles, liposomes and biologics, in order to achieve higher therapeutic and diagnostic performance. Indeed, a number of PEGylated therapeutics have been approved by the US Food and Drug Administration (FDA) for the treatment of various diseases.[11]

Despite all the success, PEGylation is not without its complications. With its apparent immunogenicity/antigenicity, many studies have demonstrated the generation of anti-PEG antibodies in both preclinical tests and clinical obervations.[15, 19, 34, 88, 93] Repeated administrations of PEGylated proteins, liposomes or nanoparticles triggered accelerated blood clearance phenomenon that was mediated by anti-PEG antibodies. The reduction of vascular residence time greatly limited therapeutic efficacy in chronic applications. In addition, adverse reactions associated with anti-PEG antibodies, including allergic reactions and infusion reactions, were also reported in a number of clinical studies.[18, 86, 87] To exacerbate the situation, high prevalence of pre-existing anti-PEG antibodies were reported in general population.[28, 29] In a recent clinical trial of pegnivacogin, a PEGylated RNA aptamer, pre-existing anti-PEG antibodies caused three serious allergic reactions, one of which was life-threatening, leading to early termination of the trial.[87, 94]

Besides its immunogenicity/antigenicity, the organ accumulation of non-biodegradable PEG molecules was extensively reported to induce intracellular vacuolation.[99-101] Nonclinical toxicology studies showed that 5 out of the 12 approved

PEGylated biopharmaceuticals would cause cellular vacuolation in a series of organs and tissues including adrenal cortex, duodenum, jejunum, liver, heart, spleen and kidney.[102, 103] Although the biological consequences of these cellular vacuoles are yet fully understood, concerns were raised under several particular circumstances. For example, accumulation of PEG associated vacuoles in the proximal tubules of the renal epithelium is of particular concern in patients that have a high incidence of renal failure, such as diabetics.[101] Chronic use of PEGylated substances may add additional risk to patients with organ disorders as a result of the histologic changes. Collectively, these issues raised obvious concerns over the future of PEGylation in the field of nanomedicine.

Alternative stealth materials are apparently desired for the development of safer and more effective therapeutics. Poly[oligo(ethylene glycol) methyl ether methacrylate] (POEGMA), a PEG analog with comb-like architecture, was employed for protein therapeutics modification.[104] POEGMA-protein conjugates showed less immunogenicity and antigenicity compared with methoxy-PEG, but the complication was not fully resolved.[97, 104] Another major class of stealth materials, zwitterionic polymers, showed excellent performance in preventing unwanted protein adsorptions.[35] In particular, poly(carboxybetaine) (PCB) coated surfaces exhibited ultra-low protein adsorption from undiluted blood serum and plasma.[38] PCB nanoparticles presented superior stability in complex media and long circulation half-life *in vivo*.[52, 69] Taken the advantage of its structural similarity with a natural protein stabilizer, glycine betaine, PCB conjugation enhanced protein stability without sacrificing its binding affinity.[44] *In vivo* study showed an increased circulation half-life with negligible antibody responses.[80] Other types of polymers, including biodegradable poly(amino acid)s and

non-biodegradable poly(glycerol), poly(2-oxazoline), poly(acrylamide), poly(vinylpyrrolidone) and poly(N-(2-hydroxypropyl)methacrylamide), have also been proposed as PEG alternatives, however their immunogenicity when conjugated to proteins is not fully studied.[86, 105]

As demonstrated in previous studies, superhydrophilic PCB is a potential non-immunogenic candidate for PEG substitution. It will be interesting to develop a biodegradable zwitterionic polymer. Maynard et al reported a biodegradable zwitterionic polyester by attaching carboxybetaine moieties to an allyl-substituted polycaprolactone (PCL) via thiol-ene chemistry.[106] The PCL-zwitterion was shown to preserve therapeutic protein activities. However, the hydrophobicity of the long caprolactone repeating unit and low zwitterion density might compromise its hydration capacity and its stealth property. Compared with polyesters, polypeptide has a shorter repeating unit with only three atoms and desirable hydrophilic amide bonds, making it an interesting candidate to construct stealth materials. Hence, we report here to incorporate the functionality of carboxybetaine (CB) into polypeptides.

6.2 Experimental Section

6.2.1 Materials

L-glutamic acid, propargyl alcohol, trimethylsilyl chloride, triphosgene, bis(2-dimethylaminoethyl) disulfide dihydrochloride, ethyl bromoacetate, dithiothreitol (DTT), tritylchloride and 1,13-diamino-4,7,10-trioxa-1,13-tridecane were purchased from TCI America. Recombinant uricase from *Candida* sp., Amberlite IRN78 hydroxide resin and all other chemicals were purchased from Sigma-Aldrich unless otherwise noted, and were used as received. BMPS (N-β-maleimidopropyl-oxysuccinimide ester) crosslinker

and Traut's reagent were purchased from ThermoFisher Scentific. Methoxy polyethylene glycol succinimidyl carbonate, MW 5kD (mPEG-NHS, 95%) was obtained from Nanocs Inc., USA.

6.2.2 Analyses via size-exclusion chromatography

All samples were processed in a 1260 Infinity binary high performance liquid chromatography (HPLC) system equipped with a UV detector (Agilent Technologies, Santa Clara, CA), a miniDAWN TREOS light scattering (LS) detector, and a Optilab T-rEX differential refractive index (dRI) detector (Wyatt Technology, Santa Barbara, CA). The flow rate was set at 0.6 mL/min with the mobile phase PBS (pH 7.4) with 0.02% sodium azide as a preservative. A Waters Ultrahydrogel 1000 column (7.8 mm x 300 mm, 12 μm particle size) was used for the analysis.

6.2.3 Chemical synthesis

6.2.3.1 Synthesis of γ-propargyl-L-glutamate N-carboxy anhydride

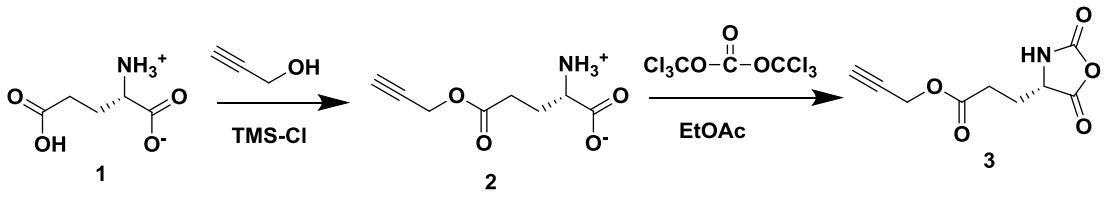

Figure 6.1 Synthesis of the NCA monomer.

The N-carboxyanhydrides (NCA) monomer was synthesized following published protocols (**Figure 6.1**).[107] Firstly, γ-propargyl-L-glutamate was synthesized. L-glutamic acid (5 g, 33.9 mmol) was suspended in propargyl alcohol (180 mL) and the solution was chilled to 0^{o}C. Next, trimethylsilyl chloride (9.5 mL, 74.8 mmol) was added dropwise over a period of 30 minutes and then the reaction contents were stirred at room temperature for another 24 hours. The reaction contents were then filtered to remove any

undissolved starting material, and then poured into 300 mL of diethyl ether. The precipitate obtained were filtered, re-dissolved in 9:1 mixture of acetonitrile:dimethylformamide at 50 ^{o}C and then kept in refrigerator at 4 ^{o}C for overnight. The resulting white crystals were then filtered, washed with cold acetonitrile and dried to give desired compound in 62.4% yield. ^{1}H NMR (300 MHz, DMSO-d_6) δ 8.50 (s, 3H), 4.70 (s, 2H), 3.89 (t, J = 6.5 Hz, 1H), 3.59 (s, 1H), 2.70 – 2.53 (m, 2H), 2.17 – 1.94 (m, 2H).

To synthesize the NCA monomer, compound 2 (4.7 g, 21.2mmol) was suspended in anhydrous ethyl acetate (120 mL) in a three neck flask fitted with a condenser. The reaction contents were refluxed at 85^{o}C in presence of nitrogen atmosphere. Next, triphosgene (2.05 g, 6.9 mmol) dissolved in 15 mL anhydrous ethyl acetate was added dropwise to the reaction mixture over a period of 20 minutes. The reaction was carried out for 4 hours. The reactions contents were cooled to room temperature and filtered to remove any unreacted starting material. The filtrate was quickly washed with cold water, saturated $NaHCO_3$ and saturated NaCl solution. The reaction contents were then dried, filtered and concentrated under vacuum to give desired products as colorless oil in 62.6% yield. ^{1}H NMR (300 MHz, DMSO-d_6) δ 9.10 (s, 1H), 4.71 (s, 2H), 4.56 – 4.41 (m, 1H), 3.56 (s, 1H), 2.56 – 2.41 (m, 2H), 2.16 – 2.00 (m, 1H), 1.97 – 1.85 (m, 1H).

6.2.3.2 Synthesis of 2-ethoxy-N-(2-mercaptoethyl)-N,N-dimethyl-2-oxoethan-1-aminium bromide (Compound 6)

The synthesis scheme is shown in **Figure 6.2**. Bis(2-dimethylaminoethyl) disulfide dihydrochloride (7.4 g, 26.3 mmol) was dissolved in aqueous 1N NaOH (5.6 mL, mmol). The free base, bis[2-(N,N-dimethylamino)ethyl] disulfide was then extracted with

dichloromethane (3x100 mL), dried, concentrated in vacuum and used directly without further purification. To a stirred solution of bis[2-(N,N-dimethylamino)ethyl] disulfide (5.4 g, 25.9 mmol) in 50 mL acetonitrile, ethyl bromoacetate (8.6 mL, 77.7 mmol) was added dropwise over a period of 15 minutes and the reaction contents were further stirred for one hour at room temperature. The precipitates formed were filtered, washed with cold acetonitrile, ether and dried to give desired compound 5 in 90.1% yield. ^{1}H NMR (500 MHz, D_2O) δ 4.32 (s, 4H), 4.27 (q, J = 13.9, 7.1 Hz, 4H), 3.95 – 3.89 (m, 4H), 3.29 (s, 12H), 3.17 – 3.11 (m, 4H), 1.25 (t, J = 7.1 Hz, 6H).

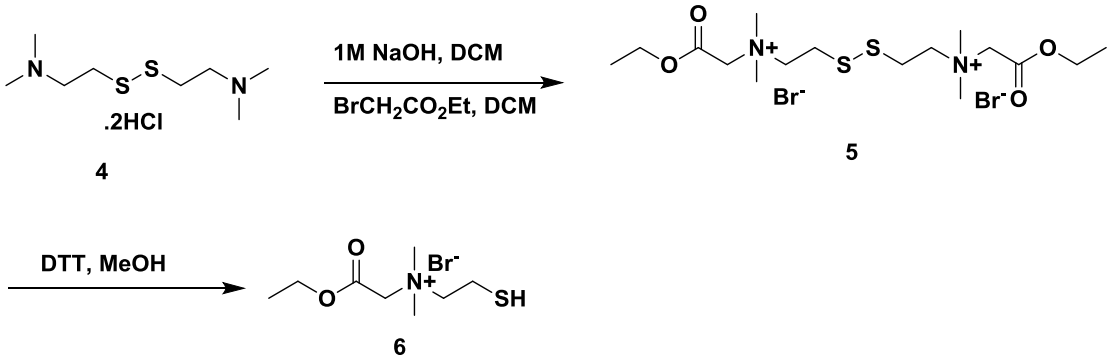

Figure 6.2 Synthesis of 2-ethoxy-N-(2-mercaptoethyl)-N,N-dimethyl-2-oxoethan-1-aminium bromide.

Compound 5 (5.0 g, 9.2 mmol) was dissolved in 30 mL methanol and DTT (1.5 g, 9.7 mmol) was added to it. The reaction was stirred for 12 hours and concentrated to one-tenth of volume. The concentrated solution was then poured slowly over 100 mL diethyl ether. The precipitates formed were further washed with diethyl ether, filtered and dried in vacuum to give desired compound 6 in 87.8% yield. ^{1}H NMR (500 MHz, D_2O) δ 4.29 (s, 4H), 4.28 – 4.24 (m, 4H), 3.77 – 3.70 (m, 4H), 3.26 (s, 12H), 2.94 – 2.88 (m, 4H), 1.25 (t, J = 7.1 Hz, 6H).

6.2.3.3 Synthesis of initiator

Briefly, 1,13-diamino-4,7,10-trioxa-1,13-tridecane starting material (10.2 mL, 46.2 mmol) was dissolved in dichloromethane and the reaction contents were cooled to 0 ^{o}C. Tritylchloride was dissolved in 5 mL dry pyridine and added to the reaction contents over a period of one hour. The reaction was stirred at room temperature for 3 hours. After completion of reaction, 3 mL methanol was added and the reaction contents were concentrated.

The residue was dissolved in 100 mL dichloromethane and the resulting solution was washed with water (50 mL), saturated $NaHCO_3$ (30 mL) and brine (20 mL). The organic contents were dried, filtered and concentrated to give crude residue which was purified by flash chromatography to give desired compound 12 in 76.2% yield. ^{1}H-NMR (300 MHz, $CDCl_3$): δ 7.07 -7.39 (m, 15H) 3.40-3.55 (m, 12H), 3.40 (s, 1 H), 2.75-2.80 (bs, 4H), 2.13-2.18 (t, 2H), 1.65 – 1.75 (m, 4H).

6.2.3.4 Synthesis of the polypeptides

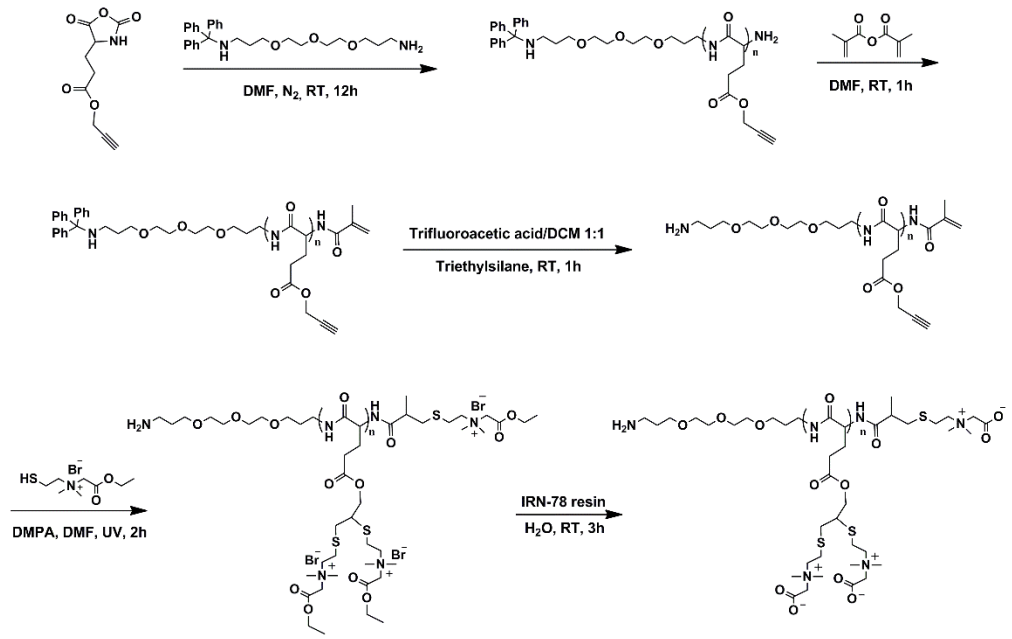

Figure 6.3 Synthetic procedure of PepCB.

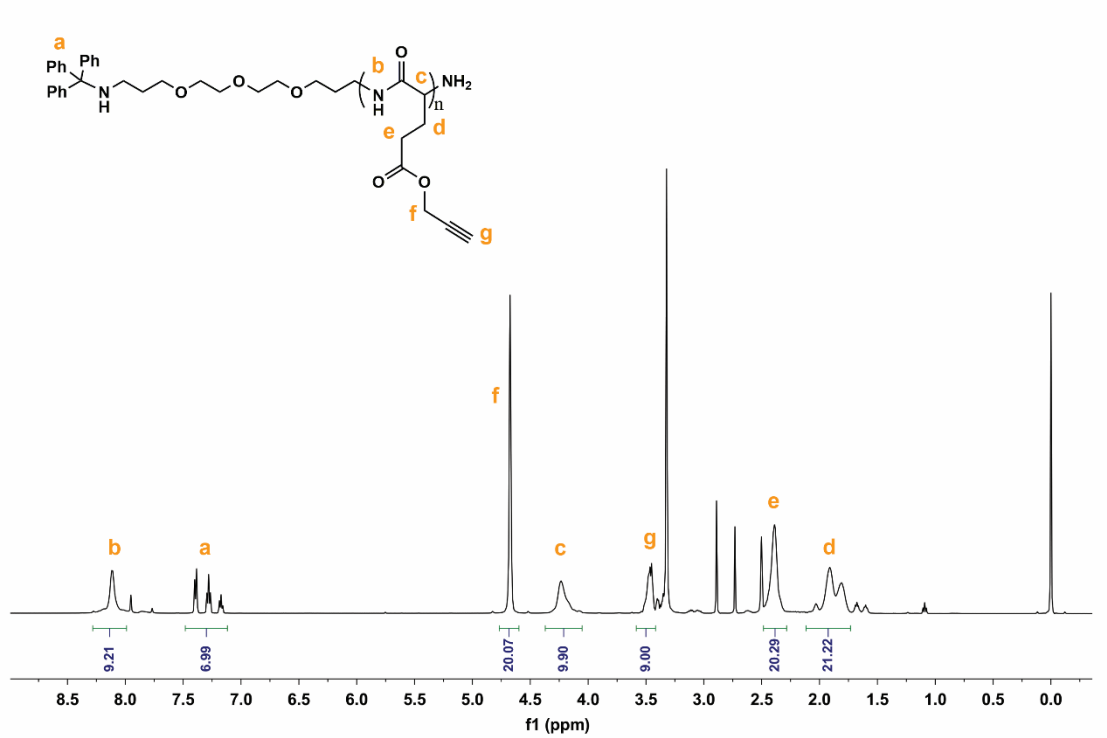

Figure 6.4 ^{1}H NMR spectrum of Poly(γ-propargyl-L-glutamate) (DP21) (DMSO-d_6).

The synthesis procedure of PepCB is shown in **Figure 6.3**. Poly(γ-propargyl-L-glutamate) is firstly synthesized by amine-initiated ring-opening polymerization of the NCA monomer. For example, a polypeptide with a degree of polymerization of 20 was produced by dissolving 3 (1.7 g, 8 mmol) in anhydrous DMF (3 mL) and adding the initiator in anhydrous DMF (0.4 mmol in 1 mL) with stirring under nitrogen. After a reaction time of approximately 24 hours, methacrylic anhydride (120 µL, 0.8 mmol) was added to the reaction mixture to cap the end amine groups. After reaction for another 1 hour, the solution was precipitated in 50 mL diethyl ether to yield the crude product, which was then re-dissolved in a minimal amount of dichloromethane (DCM) and precipitated into a 10x volume of diethyl ether. The resulting precipitate was rinsed with diethyl ether, and dried to yield the pure poly(γ-propargyl-L-glutamate) as a white powder (70% yield). The degree of polymerization was calculated to be 21 using ^{1}H

NMR (**Figure 6.4**). The trityl protection group was then removed by dissolving the polypeptide in 5 mL trifluoroacetic acid/DCM 1:1 mixture, followed by adding 50 µL triethylsilane and stirred for one hour. The acid solution was then precipitated in 50 mL diethyl ether to yield the crude product, which was then re-dissolved in a minimal amount of dichloromethane (DCM) and precipitated into a 10x volume of diethyl ether. The resulting precipitate was rinsed with diethyl ether, and dried to yield the product. ^{1}H NMR spectrum is shown in **Figure 6.5**

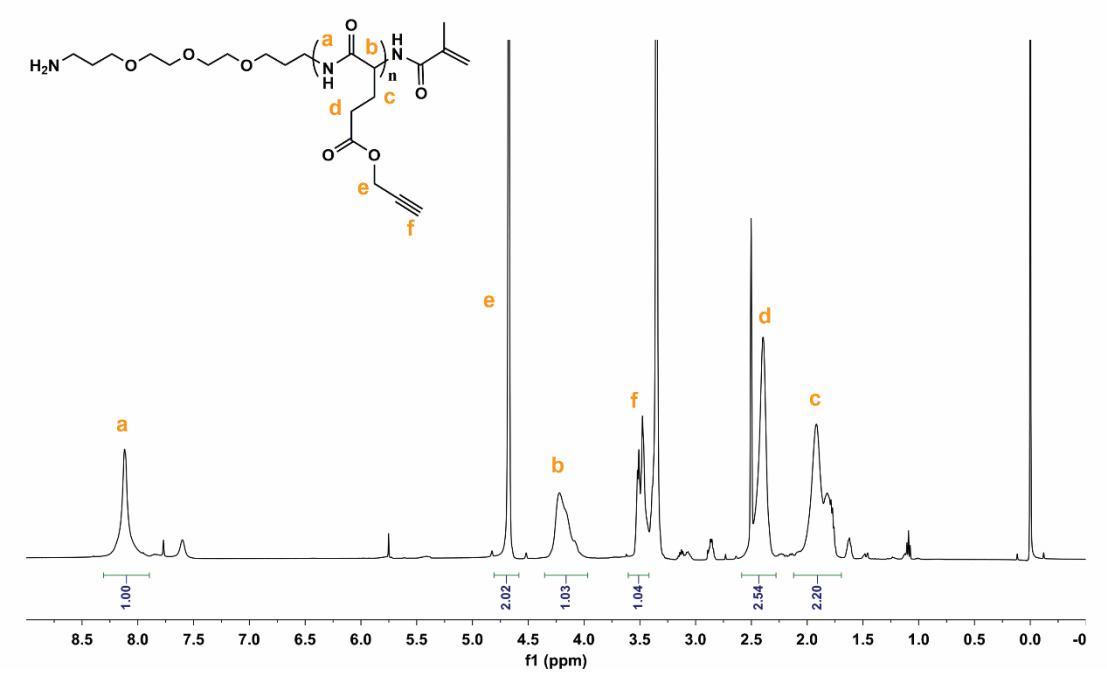

Figure 6.5 ^{1}H NMR spectrum of Poly(γ-propargyl-L-glutamate) (DP21) after end-group modification and deprotection (DMSO-d_6).

A solution of Poly(γ-propargyl-L-glutamate) (0.20 g), compound 6 (2 g), and DMPA (40 mg) in 12 mL of DMF was bubbled with nitrogen for 5 min and then irradiated under UV light (365 nm) for 2 h. After reaction, the mixture was then dissolved in water and dialyzed against DI water (MWCO 3500) for five days. The aqueous

solution was then lyophilized to yield white solid products (yield 65%). ^{1}H NMR spectrum is shown in **Figure 6.6**

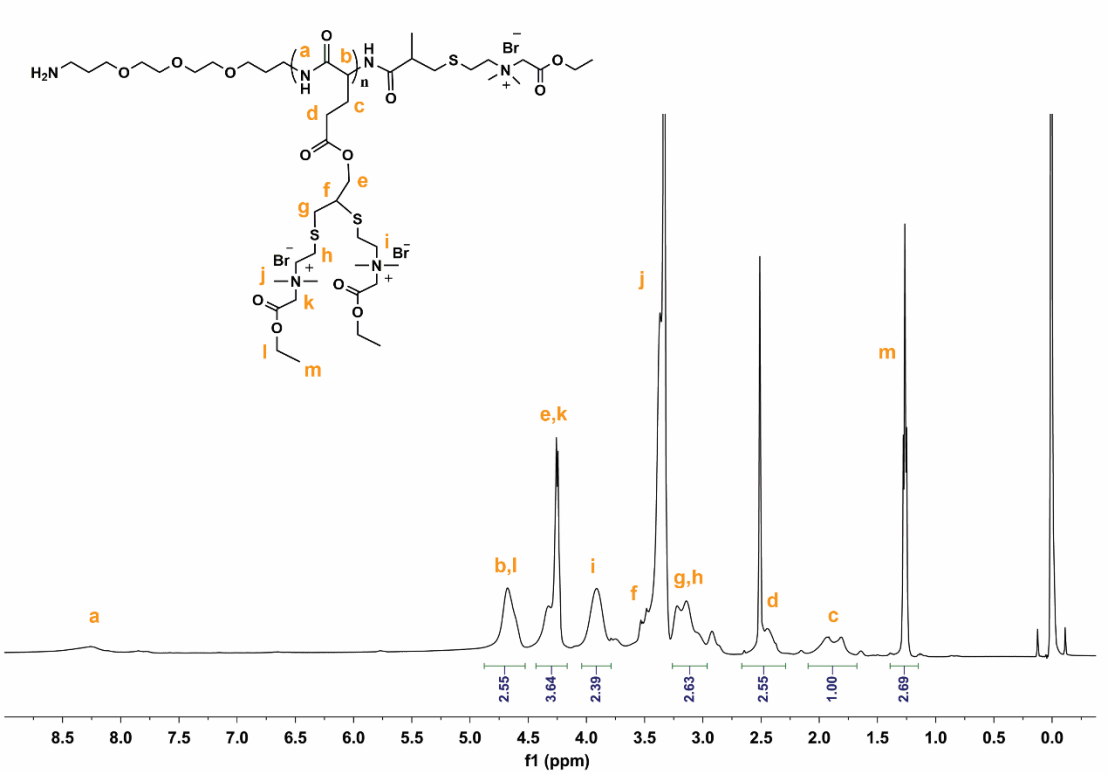

Figure 6.6 ^{1}H NMR spectrum of polypeptide (DP21) after thiol-yne click chemistry (DMSO-d_6).

To yield the final product, 100 mg PepCB-ethyl ester from last step was dissolved in 5 ml DI water followed by adding 500 mg Amberlite IRN78 hydroxide resin. The mixture was gently shaken for 4 hours, and the aqueous solution was filtered and lyophilized to yield final PepCB product as white solid (yield 85%).

6.2.4 Protein conjugation

The procedure of protein-polymer conjugation is shown in **Figure 6.7**. To conjugate uricase, 1 mg uricase solid was dissolved in 0.5 mL PBS 7.4 and BMPS (0.175mg, 40 mg/mL in DMSO) was added into the above solution. The reaction mixture was stirred at room temperature for 1 h. At the same time, 10 mg PepCB was reacted with Traut's

reagent (molar ratio 1/1) in 0.5 mL PBS 7.4. Then, the protein reaction solution was concentrated and washed with PBS using an Amicon ultra centrifugal filter (MWCO50k) for 3 times. The protein solution concentrated residue after centrifuge was then added into the polymer solution. The reaction was kept for 2 h at room temperature and then the mixture was washed extensively using PBS with an Amicon ultra centrifugal filter (MWCO100k) to remove unreacted polymers. The product was concentrated to 1 mg/mL and stored at 4 ^{o}C before use.

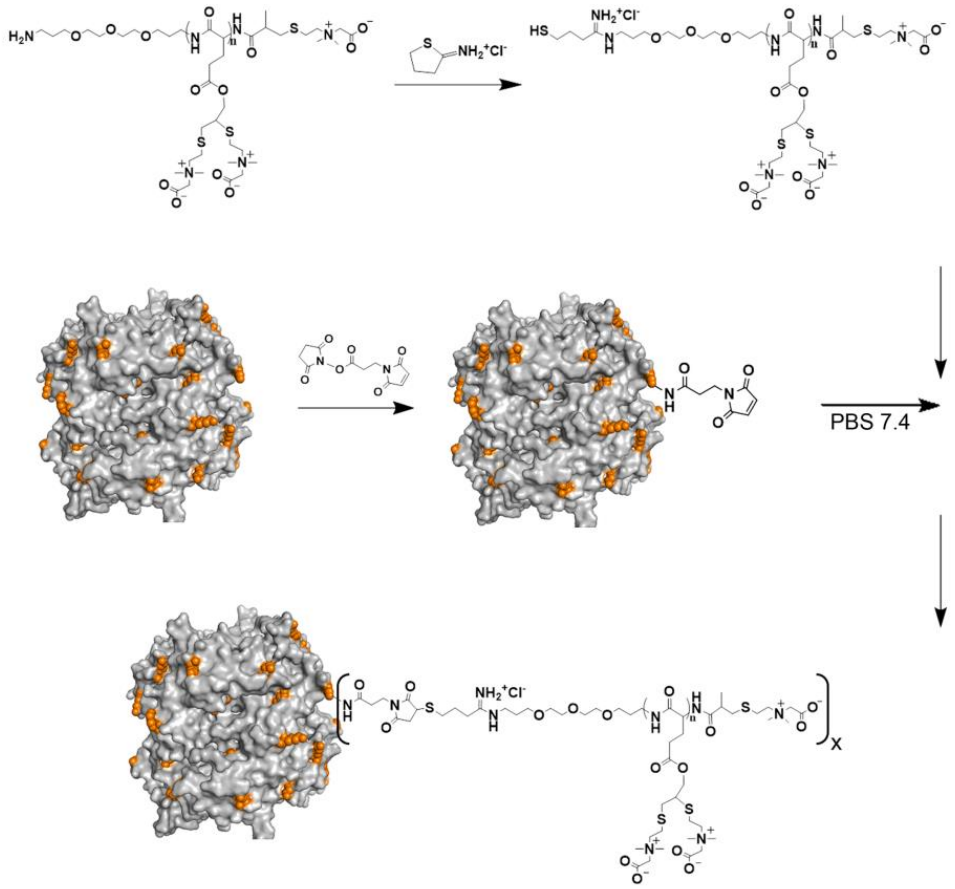

Figure 6.7 Protein-polymer conjugation procedures.

Uricase-PEG conjugates were prepared in PBS buffer (pH 7.4), with uricase concentration at 1 mg/mL and mPEG-NHS concentration at 10 mg/ml. The reaction was stirred at 4 ℃ overnight. Then the conjugates were concentrated and washed extensively by PBS 7.4 using a 100 kDa molecular weight cutoff centrifugal filter. The protein residue activity was measured by a commercially available uricase activity kit (Life technologies, USA).

6.2.5 Hemolytic activity test

A total of 200 μl rat blood was added to the polymer solutions and the volume was adjusted to 1 mL with sterile PBS (pH = 7.4). The final polymer concentration was 20 mg/ml. 200 μl rat blood mixed with 800 μl PBS served as the negative control, and 200 μl blood mixed with 800 μl PBS containing an excess amount of ammonium chloride to cause complete hemolysis was used as the positive control. After the vials were incubated at 37 °C for 90 min, the solutions were centrifuged at 2000 rpm for 10 min. 200 μl supernatant was collected into each well of a 96-well plate. The absorbance at 543 nm was recorded using a plate reader. The percentage hemolysis (PH%) (mean% ± SD, n = 3) was calculated using the following formula: $PH\% = (As - An)/(Ap - An) \times \%$, where As, An and Ap represent the absorbance of sample, negative and positive controls, respectively.

6.2.6 Cell culture and cytotoxicity assay

NIH 3T3 cells were cultured in Dulbecco's Modified Eagle Medium (DMEM) with high glucose, containing 10% fetal bovine serum (FBS), 100 U/mL penicillin and 100 μg/mL streptomycin at 37 ℃ in 5% CO_2 humidified atmosphere.

The cytotoxicity of polymers and conjugates was assessed through MTT assay. NIH 3T3 cells were seeded in a 96-well plate, at a density of 2×10^4 cells/well and incubated overnight. The following morning, the culture medium in each well was replaced by 180 μL fresh of DMEM/FBS. Polymers and conjugates solutions were then added to each well. After incubation for 24 h, the medium was replaced with 200 μL fresh medium containing 20 μL MTT (5 mg/mL in PBS) and incubated for another 4 h. Finally all medium was removed and 150 μL/well DMSO was added, followed by shaking for 15 min. The absorbance of each well was measured at 490 nm using a plate reader with pure DMSO as a blank. Non-treated cell (in DMEM) was used as a control and the relative cell viability (mean% $\pm$ SD, n = 3) was expressed as Abssample/Abscontrol $\times$ 100%.

6.2.7 *In vivo* experiments

All animal experiments adhered to federal guidelines and were approved by the University of Washington Institutional Animal Care and Use Committee.

6.2.7.1 Evaluation of tissue cytoplasmic vacuolation

In vivo vacuole formation assessment was studied in Spraque-Dawley rats (Female, body weight ~100g). PEG (40kDa) and PepCB (80kDa) were formulated in sterile pharmaceutical grade saline. Three animals were involved in each group. The animals received one dose (200mg/kg) of the substance every week by IV injection via the tail vein for three months (12 doses). The injection was performed under isoflurane anesthesia. One week after the final dosage, the animals were euthanized. Liver, kidney and spleen were fixed in 10% neutral buffered formalin by immersion. Fixed tissues were dehydrated and embedded in paraffin. Tissues were sectioned and stained with hematoxylin and eosin (H&E), followed by microscopy examination.

6.2.7.2 Pharmacokinetic and immunogenicity studies

The pharmacokinetics of native and polymer conjugated uricase was studied using Spraque Dawley rats (male, body weight 74~100 g) as the animal model. Each sample had six duplicates to generate statistical significance. Each protein or bioconjugate sample was administered into the rat via tail vein injection at the dose of 25 U/kg body weight. Blood samples were collected from the tail vein at 0 min, 2h, 6 h, 24 h, 48 h and 72 h after the injection. The enzyme content in serum was estimated by enzyme activity. The IV injections were repeated three times with one week as time interval between each injection. Five weeks after the first injection, 5 mL of blood were drawn by using cardiac punch and serum was prepared for antibody detections.

6.2.8 Enzyme-linked immunosorbent assay (ELISA)

The antigens used in direct ELISAs consisted of native uricase (for detection of anti-uricase antibody), BSA-PEG conjugates (for detection of anti-PEG antibody) and BSA-PepCB conjugates (for detection of anti-PepCB antibody). BSA-polymer conjugates were made following the same procedure as uricase samples. For ELISA experiments, 100 μL antigen solution (10 μg/mL of protein concentration) prepared in 0.05 M carbonate-bicarbonate buffer, pH 9.6, was used to coat each well of the 96-well plates. During coating procedure, plates were incubated at 4 ℃ overnight. After removing antigen solutions, the plates were washed five times using phosphate-buffered saline (PBS 7.4) and then filled with blocking buffer (1% BSA solution in 0.1 M Tris buffer, pH 8.0). It is important to avoid using any buffer that contains PEG-like detergents, e.g. Tween 20 and Tween 80. After incubation at room temperature for 1 hour, blocking buffer was removed and all wells were washed by PBS for another five times.

Serial dilutions of rat sera in PBS containing 1% BSA were added to the plates (100 μL/well), which were incubated for 1 h at 37 °C. The plates were then washed five times with PBS. Goat anti-rat IgM or IgG conjugated to horseradish peroxidase (HRP) (Bethyl labs, USA) was used as the secondary antibody for detection of IgM and IgG. After adding the secondary antibody, plates were incubated at room temperature for 1 hour, and then washed five times using PBS before the addition of 100 μL/well HRP substrate 3,3',5,5'-Tetramethylbenzidine (TMB, Bethyl labs). The plates were shaken for 15 min and 100 μL stop solution (0.2 M H_2SO_4) was added to each well. Absorbance at 450 nm (signal) and 570 nm (background) was recorded by a microplate reader. Pre-bleeding sera were used as negative control for all ELISA detections. Commercially available rat anti-PEG antibodies (Abcam 26A04) were used as positive control for anti-PEG detections.

6.3 Results and Discussion

6.3.1 Polymer synthesis and characterizations

Poly(γ-propargyl-l-glutamate) (PPLG) is a well-studied polypeptide platform that can integrate various functionalities via “click” chemistry.[108] Still, the classic azide-alkyne cycloaddition can only attach one functional group per side chain. To maximize the hydration capacity of the stealth polypeptide, we adopted the thiol-yne type reaction which allows the addition of two functional moieties using one alkyne group.[109] As shown in **Figure 6.3**, the molecule of design presented a branched macromolecular architecture and maximized zwitterion density. A backbone with functional end-groups is needed for the conjugation of the polymer onto nanoparticles or proteins. We choose to use primary amine as the conjugation motif since it can be easily

converted into various functional groups via simple chemistries. We attempted to use the N-terminal amine group of the polypeptide for conjugation as it is readily available after ring-opening polymerization. Yet, one issue was encountered after several attempts that the N-terminal group is too close to the branched side chain, therefore hindering the conjugation due to steric effects. Thus, we introduced a primary amine group using a hydrophilic linker as the polymerization initiator instead. A protected amine which is distanced from the bulky side chains was then incorporated at the C-terminal of the polypeptide. To avoid interference during conjugation, the N-terminal was capped by methacrylamide which was then converted into a CB group in the following thiol-yne reaction. After the following steps of trityl deprotection, thiol-yne "click" and ethyl ester hydrolysis, the final carboxybetaine polypeptide (PepCB) with a free amine end group was synthesized, as shown in **Figure 6.8**. The N-carboxyanhydrides (NCA) ring-opening polymerization resulted in well-controlled molecular weight and polydispersity (PDI) (**Table 6.1**). PepCB with two molecular weights (10 kDa and 80 kDa) were synthesized and compared with PEG (5 kDa and 40 kDa) using gel permeation chromatography (GPC). **Figure 6.9** showed that the hydrodynamic size of a PepCB molecule is similar to a PEG molecule with half of its molecular weight, due to its compact comb-like architecture. Hemolytic activity and cytotoxicity tests demonstrated the superior biocompatibility of the PepCB polymers (**Figure 6.10**).

Table 6.1 Characterization of polymers

Samples	Monomer:Initiator (Molar ratio)	Mn (NMR) [a]	Mn (GPC)[b]	PDI[b]
PepCB 10k	20	10400	10300	1.02
PepCB 80k	160	75400	71200	1.11
PEG 5k	—	—	5400	1.06
PEG 40k	—	—	35200	1.05

[a]Mn was calculated from the repeating unit to trityl group based on ^{1}H NMR after polymerization. [b]Mn and PDI were measured by an aqueous GPC/light scattering system.

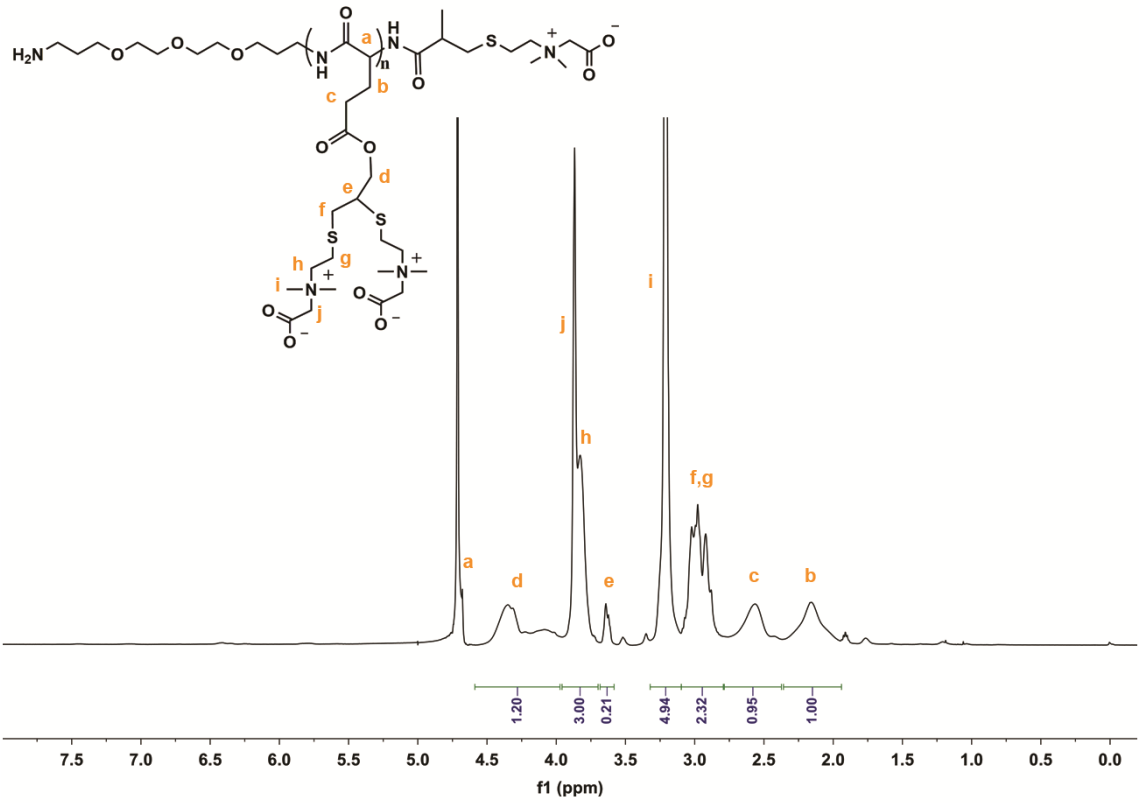

Figure 6.8 Molecular structure and ^{1}H NMR spectrum (D_2O) of the PepCB polymer (Mw 10 kDa).

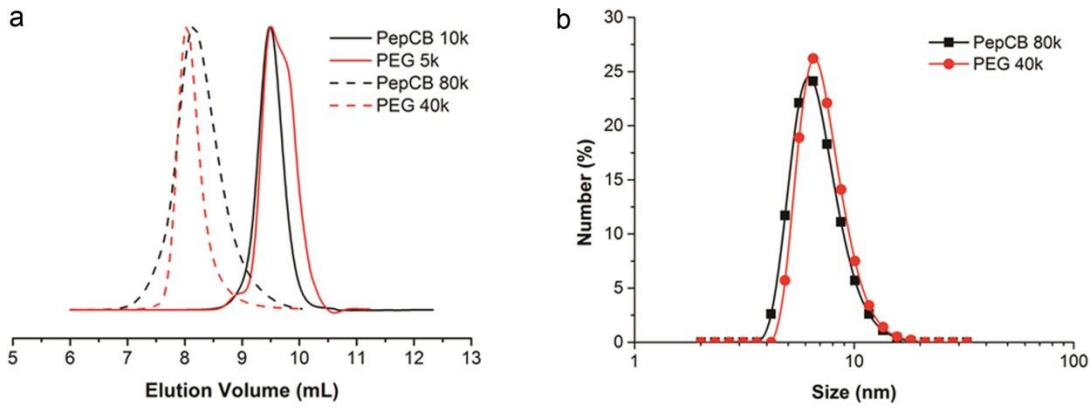

Figure 6.9 Hydrodynamic size comparisons between the polymers. a) GPC traces of synthesized PepCB polymers and PEG control samples. b) Dynamic light scattering (DLS) measurement of PepCB 80k and PEG 40k. Both polymers shared similar hydrodynamic size.

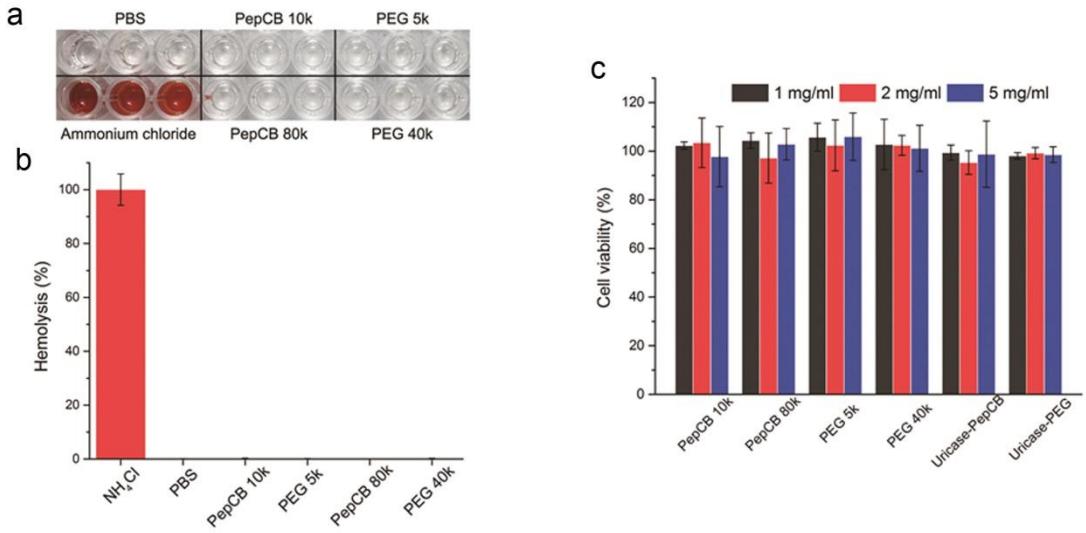

Figure 6.10 Biocompatibility assays. a) Hemolytic activity tests of the polymers, and b) Cytotoxicity of the polymers and bioconjugates.

6.3.2 Tissue cellular vacuolation

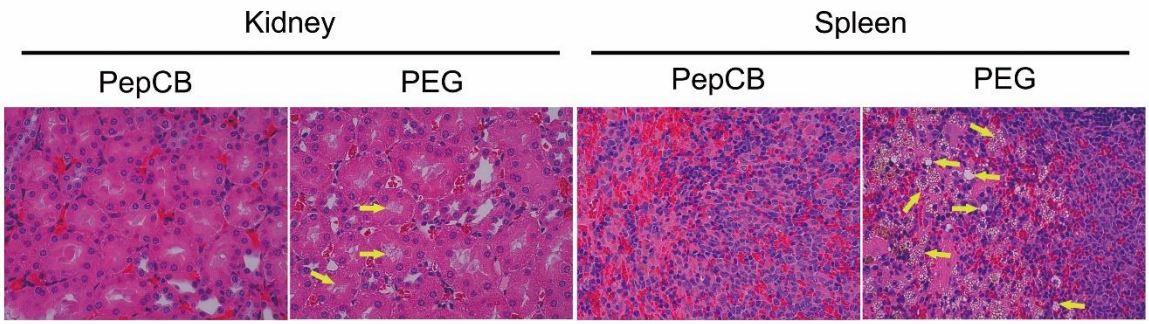

Figure 6.11 Histologic examinations of rat organs. The tissue sections were stained with hematoxylin and eosin (H&E). Representative cytoplasmic vacuoles are shown by arrows. Magnification = 200×.

As a potential biocompatible stealth material, we firstly evaluated the organ toxicity of PepCB via intravenous (I.V.) injections in a rat model. Rudamnn et al. reported that PEG-associated cytoplasmic vacuolation is molecular-weight dependent and does not require conjugation to proteins.[99] In their study, the long-term administration of 40 kDa PEG induced significant tissue cellular vacuolation in multiple organs. Thus, we adopted a similar administration regimen in our study, comparing 80 kDa PepCB to 40 kDa PEG as they have similar hydrodynamic size. The animals were injected with 200 mg/kg polymers per week. Livers, kidneys and spleens were harvested and examined after three-month treatment. As shown in **Figure 6.11**, cytoplasmic vacuolation was clearly observed in kidney and spleen tissues in the PEG group after three months. No vacuolation was found in liver tissues (**Figure 6.12**). Vacuoles formed in the renal tubule epithelium were on the order of microns in size, which were unstained by hematoxylin and eosin. The histologic changes in renal tubule were suggested to be consistent with tubular degeneration.[99] As for splenic tissues, the vacuoles were mainly found in the red pulp, possibly due to its blood filtration functions. By contrast, PepCB did not cause

any detectable histologic changes, demonstrating its excellent biocompatibility. Although the mechanism of cytoplasmic vacuolation remains unknown, we suspected that it is associated with PEG amphiphilicity. It is well-known that PEG interacts with cellular membranes and proteins[110, 111], thus these amphiphilic macromolecules might interfere with cytoplasmic proteins or membranes once accumulated intracellularly and subsequently induce histologic changes. PepCB, on the other hand, is consisted of superhydrophilic CB functional groups, which has been proven to have minimal effects on proteins.[112] Accumulation of PepCB in cytoplasm is likely to be harmless due to its superhydrophilic property while polypeptide backbone will further facilitate its elimination.

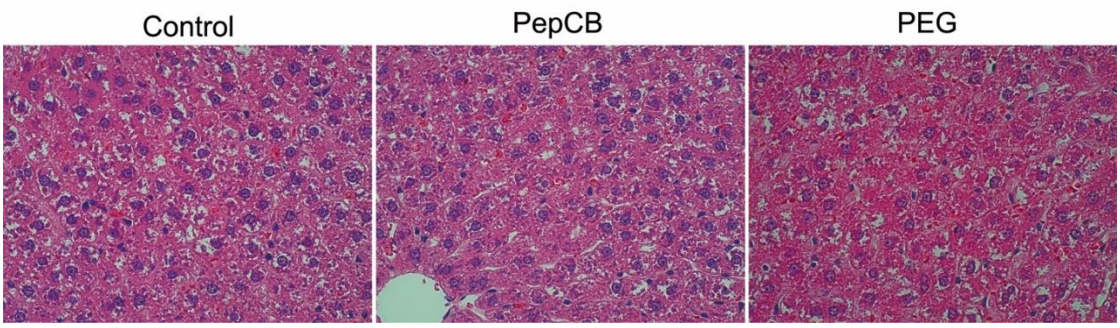

Figure 6.12 Histologic examinations of rat livers. The tissue sections were stained with hematoxylin and eosin (H&E). Magnification = 200×.

6.3.3 Protein conjugation

Table 6.2 Physical parameters of uricase and bioconjugates derived from GPC and activity measurements

Samples	Molecular Weight (kDa)	# polymer per monomer protein	Relative Activity (%)
Native Uricase	140	0	100
Uricase-PepCB	360±10	5-6	97
Uricase-PEG	290±10	6-8	98

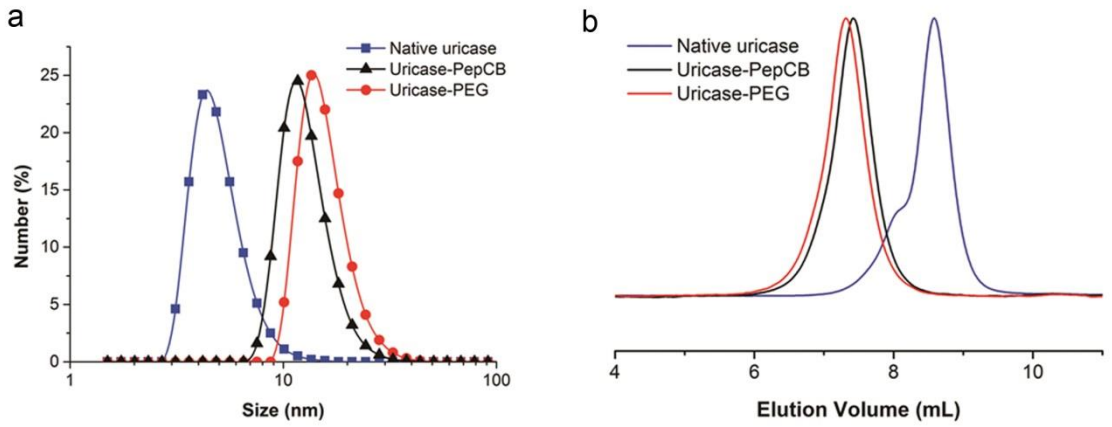

Figure 6.13 Characterization of the uricase-polymer conjugates. a) DLS measurements of the polymer conjugated and native uricase. Both conjugates demonstrated much larger hydrodynamic size compared with the native uricase. The zeta potential values of native uricase, uricase-PEG and uricase-PepCB were measured to be -20.2 mV, -7.4 mV and -1.8 mV, respectively. b) GPC traces of the native uricase and uricase conjugates.

Next, we evaluated the performance of PepCB as a stealth coating for protein therapeutics. Uricase derived from *Candida sp.* was selected as a representative since it has the following properties, (1) sufficient conjugation sites available on its surface; (2) easily measurable activity; (3) poor pharmacokinetics; (4) strong immunogenicity. Native uricase was reported to have very short circulation half-life, but strong immunogenicity in a rat model. FDA approved PEGylated uricase (pegloticase) induced the generation of anti-PEG antibodies in a large percentage of patients in a clinical study, which led to loss of therapeutic response in 43% of the patients.[17] These facts make uricase a meaningful model for testing the immunogenicity of the conjugated polymers. Polymer-protein conjugation was carried out via thiol-maleimide chemistry, as shown in **Figure 6.7**. A PEGylated uricase was also prepared for the purpose of comparison. In order to fairly compare PepCB and PEG, both polymers were controlled at the same hydrodynamic volume rather than molecular weight, since the hydrodynamic volume plays the key role

in determining *in vivo* behavior. GPC analysis showed that each subunit of uricase reacted with similar numbers of PEG or PepCB chains (**Table 6.2**) and the final conjugates were similar in hydrodynamic size (**Figure 6.13**). Activity assay showed that both polymer conjugates retained similar enzyme activities (>95%) with respect to the native protein. Some studies reported bioactivity loss after polymer conjugation, possibly due to steric blockage of active sites. However, this was not observed for uricase, as its substrate is small and can diffuse through the polymer coating readily.

6.3.4 Pharmacokinetics

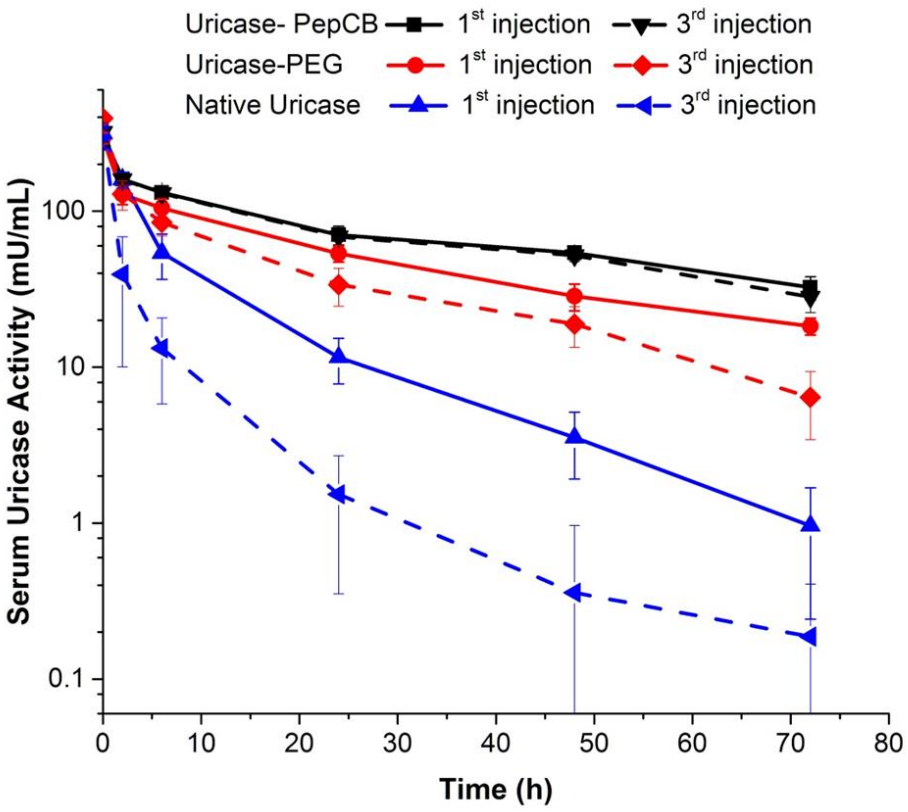

Figure 6.14 Circulatory profiles after multiple injections, n = 6.

Having demonstrated that polymer conjugation did not affect the catalytic activity of uricase, we then conducted in vivo pharmacokinetic experiments. Here 25 U/kg of native

uricase, uricase-PEG or uricase-PepCB were administered in saline by intravenous injection to groups of Spraque–Dawley rats. Blood was collected at regular time intervals from the tail vein for the analysis of residual uricase catalytic activity. Native uricase was rapidly cleared from the body, as evidenced by the nearly complete loss of activity within 24 hours (**Figure 6.14**). Both uricase-PepCB and uricase-PEG displayed sustained activity in over 72-hour time period. It should be noted that uricase-PepCB demonstrated a prolonged half-life compared to uricase-PEG, although both conjugates possessed similar hydrodynamic size. Native uricase is a large tetrameric protein which exceeds the renal filtration limit.[49] Hence the clearance mechanism of native uricase and conjugates is considered mainly to be associated with an irreversible uptake process, likely by the reticuloendothelial system (RES). Conjugating polymers onto protein can effectively cover a large portion of its surface. The hydration and nonfouling characteristic of the material would provide the protein "stealthness" to minimize nonspecific uptake clearance. As a well-known class of ultra-low fouling materials, zwitterionic polymers have been reported to extend the circulation lifetime of nanoparticles and proteins.[51, 80] CB group is proven to have stronger hydration effect than ethylene glycol units.[113] Together with the branched comb-like architecture, PepCB coating successfully protected the underlying cargo against body clearance by its exceptional stealth characteristic.

6.3.5 Immunogenicity

Immunogenicities of PepCB and the bioconjugates were evaluated by three injections of the conjugates at a dosage of 25 U/kg with 1-week intervals. Blood was drawn on day 35, and both IgM and IgG titers against either uricase or the polymers were measured. In comparison to the native protein, uricase-PEG and uricase-PepCB

conjugates stimulated significantly less anti-uricase antibodies (**Figure 6.15a**). The results also revealed that immunization of uricase-PepCB stimulated 16-fold lower anti-uricase IgG titers than the immunization of uricase-PEG, and 160-fold lower than with the native protein. ELISA was conducted to compare the relative levels of antibodies raised against the conjugated polymers (Figure **6.15b**). Three injections of PEGylated uricase stimulated the generation of anti-PEG antibody, mainly in the form of IgM, which is in consistence with previous reports.[69] In comparison, anti-polymer response observed for PepCB conjugates was negligible, demonstrating its effectiveness in ameliorating humoral immune responses. Furthermore, the circulation time of uricase-PEG was significantly shortened after the third injection, while no accelerated clearance was observed for uricase-PepCB (**Figure 6.14**). The prevention of anti-protein antibodies generating by coated polymers mainly depends on their epitope shielding capabilities. PepCB is composed of superhydrophilic carboxybetaine groups, which has much stronger hydration effects than ethylene glycol repeating units. In addition, the high grafting density of CB groups makes the polymer a comb-like architecture, which promotes the protein protection capability.[104] Benefited from the non-immunogenic CB groups and reduced protein immunogenicity, anti-polymer response is also greatly ameliorated for uricase-PepCB conjugates. Hershfield et al. demonstrated that the generation of anti-PEG antibodies is the major cause of rapid efficacy loss and increased risk of infusion reactions of PEGylated uricase in clinic.[17] It is also reported that pre-existing anti-PEG antibodies can induce severe allergic reactions when PEG containing drugs were administered.[94] With significantly reduced antibody responses

and improved long-term efficacy, we believe protein-PepCB conjugate is a safer alternative to its PEGylated counterpart.

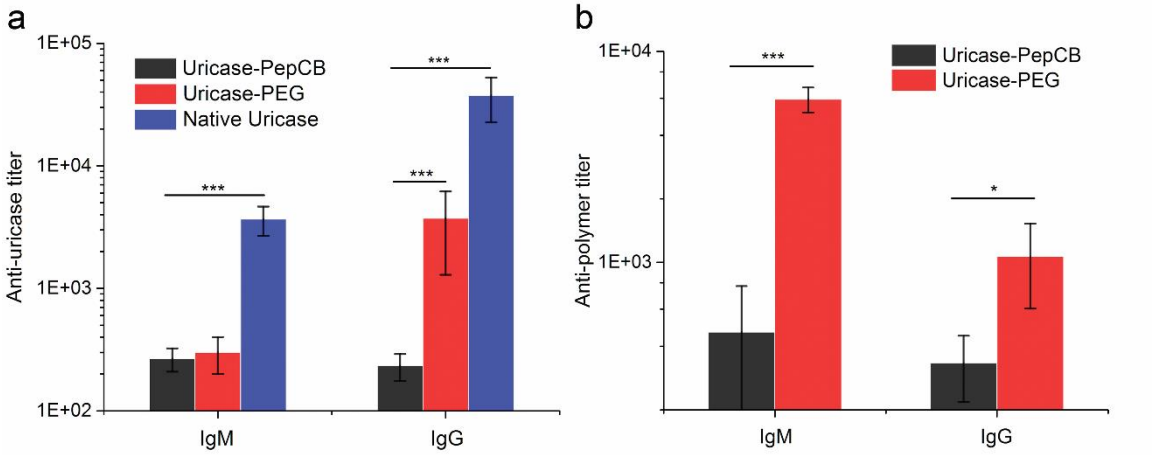

Figure 6.15 Antibody responses measured by enzyme-linked immunosorbent assay (ELISA), a) anti-uricase antibodies and b) anti-polymer antibodies, with ***p≤0.001.

6.4 Conclusions

PEGylation is broadly applied in nanomedicine to bestow stealth property to therapeutics. Its success already brought more than ten FDA approved drugs into clinics, and many more are in pipeline. However, recent studies indicate that the immunogenicity and organ toxicity of PEG are the two major concerns to the safety of PEGylation technology. Alternative materials are in urgent need to formulate the next generation of nanomedicine and biologic therapeutics. Herein we developed a superhydrophilic polypeptide with high density of zwitterionic carboxybetaine groups as a stealth polymer. Benefited from the superior biocompatibility of CB groups and polypeptide backbone, PepCB does not induce any tissue histologic change in liver, kidney and spleen after three months of toxicity test in rats. No abnormal behavior, sickness or death was observed in the test period. PepCB can be readily conjugated to therapeutic protein drugs using its terminal primary amine group. Owing to its superhydrophilicity and high zwitterion

density, PepCB-uricase conjugate exhibits a better circulation profile with significantly reduced immunogenicity than PEG-uricase conjugate. The outstanding stealth capability, biocompatibility and non-immunogenicity make PepCB a promising material in nanomedicine, not only for biologic therapeutics, but also for liposomes, nanoparticles and small molecule drugs. With all these merits, PepCB holds great potential as the next generation of stealth polymer to formulate safer and more effective therapeutics.

Chapter 7 Proactively Reducing Anti-Drug Antibodies via Immunomodulatory Bioconjugation

The generation of anti-drug antibodies (ADAs) is the major cause of biotherapeutic treatment failure and adverse reactions. Although PEGylation reduces the immunogenicity of several protein drugs to some extent by "stealth effect", more and more reports demonstrated its limitations when dealing with highly immunogenic biotherapeutics. Here we describe a proactive strategy to alleviate the development of ADAs against protein drugs by immunomodulatory bioconjugation. An immunomodulator rapamycin was conjugated to PEGylated uricase via a cleavable disulfide linker. The conjugated rapamycin was shown to inhibit dendritic cell maturation when co-incubating the bioconjugates with DC 2.4 cells. Repeated administration of the immunomodulatory bioconjugates in rats resulted in significantly reduced ADAs titers compared with regular PEGylated protein. Importantly, the inhibition of immune responses is a result of induced antigen-specific immune tolerance. Co-injecting ovalbumin with the uricase bioconjugates did not alter the generation of anti-ovalbumin antibodies. The immunomodulatory bioconjugation represents a robust approach to advance the PEGylation chemistry.

7.1 Introduction

Anti-drug antibodies (ADAs) remain as one of the major obstacles that limit the widespread applications of biologic therapeutics.[4] Although naturally derived biologic macromolecules, including enzymes, antibodies, hormones, cytokines and nucleic acids, comprise a broad reservoir of drug candidates with exceptional medicinal potency and specificity, they carry an inherent risk of eliciting ADAs that can adversely affect the

efficacy and safety of the treatment.[1, 4] Virtually all biologics can elicit an ADA response, even fully human growth factors and human antibodies.[114, 115] The generated ADAs may negatively affect treatments by neutralizing drug pharmacological activity, expediting blood clearance or causing hypersensitivity reactions (including life-threatening anaphylaxis).[17, 19, 116]

Various approaches have been developed to reduce the immunogenicity of biologic therapeutics.[2, 11, 69, 98, 117] Among which, the conjugation of polyethylene glycol (PEG) (known as PEGylation) has successfully brought a number of PEGylated therapeutics into market.[11] PEGylation has significantly improved the pharmacokinetics and immunogenicity of biologic macromolecules by sterically shielding their antigenic epitopes from immune system recognition. However, more and more reports demonstrated its limitations when dealing with highly immunogenic biotherapeutics.[86, 93] For example, Pegloticase (PEGylated uricase) induces ADAs in ~90% of the refractory chronic gout patients, resulting in a reduction in drug effectiveness and increased risk of infusion reactions.[17, 19] Similarly, clinical hypersensitivity occurred in a subset of acute lymphoblastic leukemia patients received Pegaspargase with reported incidence rates of up to 24%.[118] Recently, the US Food and Drug Administration (FDA) has advocated that the biopharmaceutical industry take a proactive risk-based approach to mitigate unwanted immunogenicity of the biologic therapeutics.[119] An effective approach to improve PEGylation to further reduce ADAs is apparently desired.

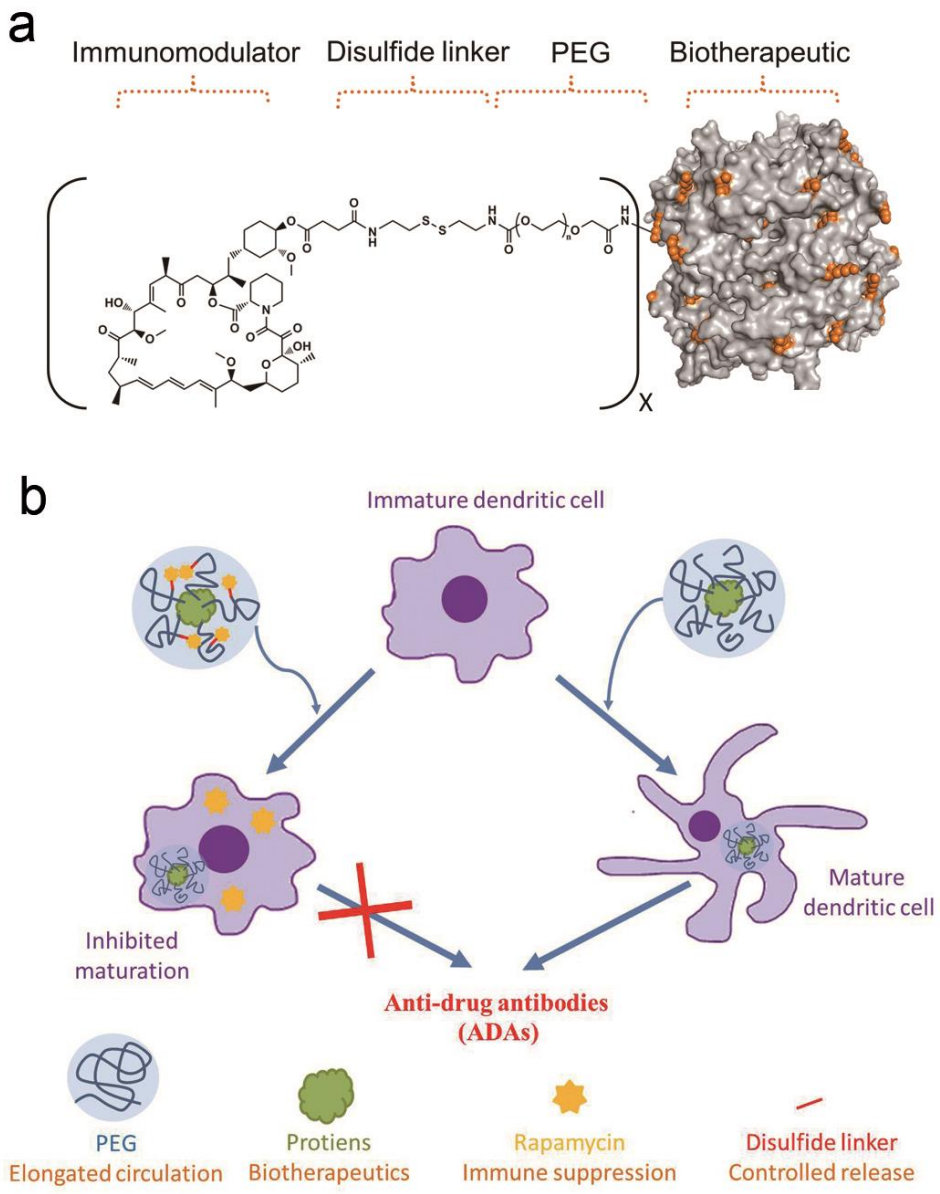

Figure 7.1 a) Schematic showing of the immunomodulatory protein bioconjugate structure. b) When uptaken by dendritic cells, rapamycin released from the bioconjugate inhibits dendritic cell maturation and prevents ADA generation.

Traditional methods, e.g. PEGylation, passively reduce ADAs by physically hiding the underlying protein cargos from immune recognition. However, such passive strategies may suffer from particular limitations, such as material immunogenicity and insufficient protein surface epitope coverage.[86] A proactive strategy that endows the therapeutic

itself with the ability to modulate the immune system may be a new choice to further alleviate unwanted immune responses. Rapamycin, a commonly used immunosuppressant to prevent organ transplant rejections, has been shown to inhibit dendritic cell (DC) maturation and induce tolerogenic DCs.[120-122] Rapamycin encapsulated PLGA nanoparticles have been used to induce antigen-specific immunologic tolerance.[123, 124] Herein, we report an immunomodulatory bioconjugation chemistry to proactively mitigate ADA responses, by conjugating rapamycin to PEGylated therapeutic proteins. When circulating in blood, the bioconjugate will play its therapeutic role as normal PEGylated drugs; while the conjugated rapamycin can be released and prevent immune responses once the bioconjugate is uptaken by antigen presenting cells.

7.2 Experimental Section

7.2.1 Materials

Rapamycin was purchased from Wuxi AppTec, China. SC-PEG-COOH (10kDa) and NH_2-PEG-COOH (10kDa) were purchased from Biochempeg Scientific Inc., USA. Methoxy polyethylene glycol succinimidyl carbonate (10kDa, mPEG-SC) was obtained from Nanocs Inc., USA. N,N,N',N'-Tetramethyl-O-(N-succinimidyl)uronium Tetrafluoroborate (TSTU) was obtained from TCI Chemicals, Japan. Recombinant uricase from *Candida* sp., and all other chemicals were purchased from Sigma-Aldrich unless otherwise noted, and were used as received.

7.2.2 Chemical synthesis

7.2.2.1 Synthesis of rapamycin 42-hemisuccinate

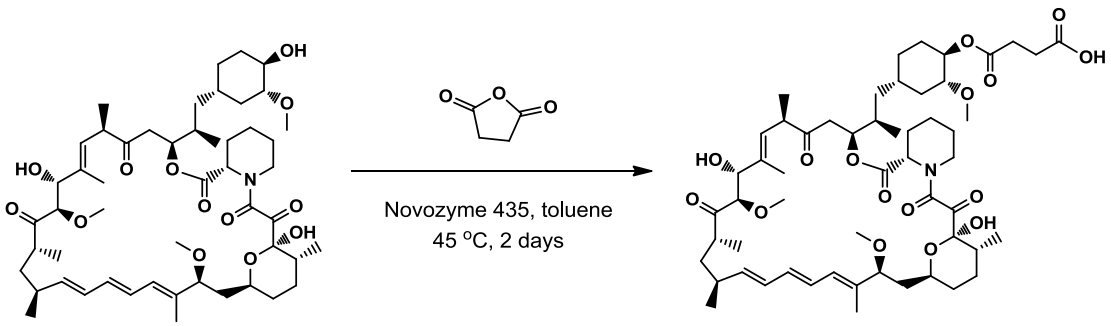

Figure 7.2 Synthesis of rapamycin 42-hemisuccinate

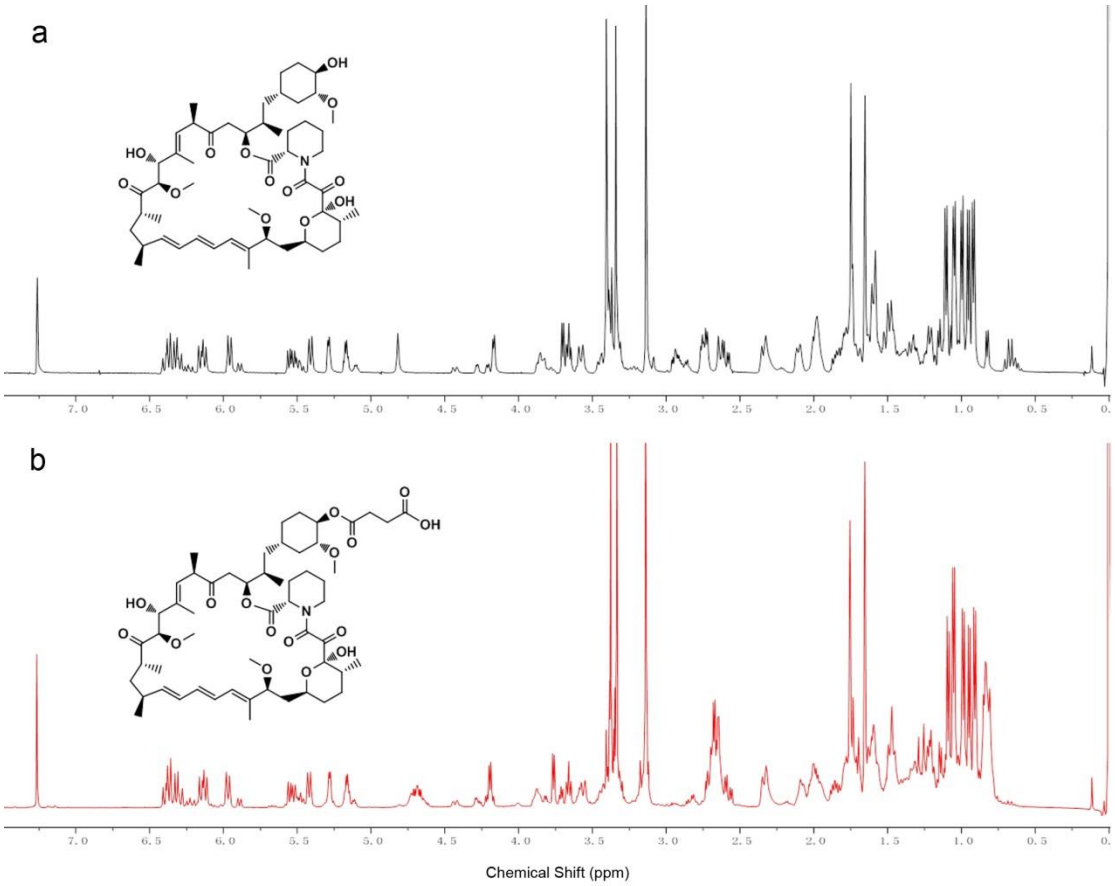

Figure 7.3 ^{1}H NMR spectrum of rapamycin 42-hemisuccinate, in comparison with that of rapamycin. ($CDCl_3$)

Rapamycin 42-hemisuccinate was synthesized following an established procedure.[125] A mixture of 500 mg rapamycin, 250 mg succinic anhydride (4.5 eq) and Novozyme 435 (1.2 g) was stirred in toluene (20 mL) at 45 ^{o}C. After stirring for about 2

days, the resin was filtered off using a sintered funnel and washed with toluene (2x 10 mL). The combined organic solvent was removed by a rotavapor and the resulting mixture was purified by flash chromatography using DCM:MeOH as the eluent. The resulting compound was obtained as white solid, 70% yield. ^{1}H NMR spectra (500 MHz, $CDCl_3$) are shown in **Figure 7.3**.

7.2.2.2 Synthesis of the disulfide linker (Compound 1)

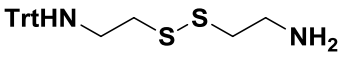

Cystamine dihydrochloride (7.0 g, 27.31mmol) was dissolved in 1:1 mixture of water:dioxane (60 mL). Next, trimethylamine (11.4 mL, 81.9 mmol) was added to the reaction mixture. A solution of trityl chloride (2.54 g, 9.1 mmol) was then added dropwise over a period of 30 minutes and the reaction contents were stirred for two days. The dioxane from the reaction mixture was removed in vacuum and the aqueous mixture was further diluted with another 20 mL water followed by extractions with $CHCl_3$ (3x25 mL). The organic contents were then separated and washed with saturated $NaHCO_3$ (1x20 mL) and water (1x20 mL). The organic layer was then dried, filtered and concentrated to give the crude compound 1 as oil. The crude compound was then purified by flash chromatography to give the desired compound 1 in 75.3% yield. ^{1}H NMR (300 MHz, $CDCl_3$) δ 7.57 – 7.16 (m, 15H), 2.97 – 2.81 (m, 4H), 2.58 (t, J = 6.1 Hz, 2H), 2.50 (t, J = 6.0 Hz, 2H), 1.64 (s, 2H).

7.2.2.3 Synthesis of the rapamycin-PEG conjugate

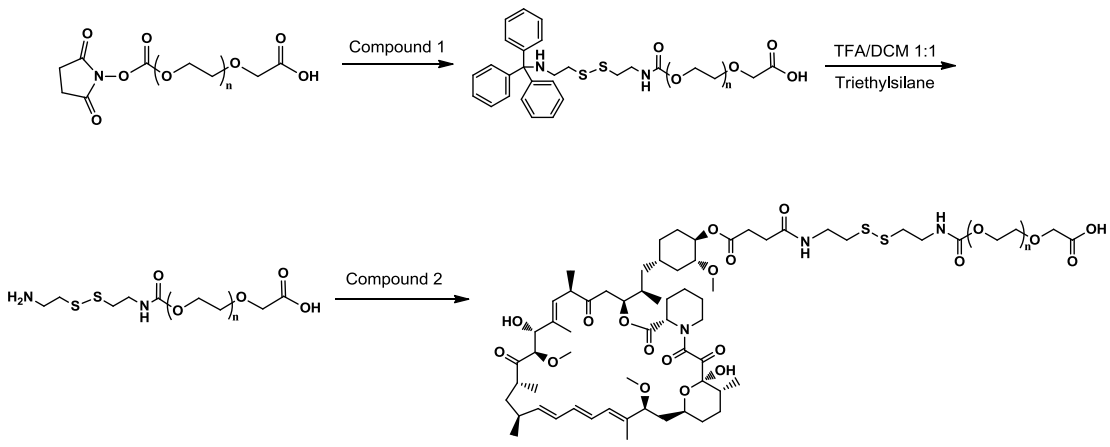

Figure 7.4 Synthesis of the PEG-ss-rapa conjugate

The rapamycin 42-hemisuccinate was firstly activated as an N-hydroxysuccinimide (NHS) ester (compound 2). Rapamycin 42-hemisuccinate (360 mg) was dissolved in 15 mL acetonitrile and TSTU (112 mg, 1.05 equivalent) was added followed by addition of N,N-diisopropylethylamine (DIPEA, 1.2 eq). The mixture was stirred at room temperature for 2 hours and the resulting crude mixture was purified using flash chromatography.

SC-PEG-COOH (200 mg) was firstly dissolved in 1 mL dichloromethane (DCM). Compound 1 (40 mg) and triethylamine (TEA) 4.2 μL was then added to the PEG solution. The reaction mixture was stirred at room temperature for 4 h, followed by precipitation in 10 mL of diethyl ether. The precipitated white solid was collected by a centrifuge and re-dissolved in a minimal amount of DCM. The solution was then precipitated again into a 10x volume of diethyl ether and the white solid was collected and dried under vacuum. The product was characterized by ^{1}H NMR (Fig. S2). The trityl protection group was then removed by dissolving the polymer in 2 mL trifluoroacetic acid/DCM 1:1 mixture, followed by adding 20 μL triethylsilane and stirred for one hour.

The acid solution was then precipitated in 20 mL diethyl ether to yield the crude product, which was then re-dissolved in a minimal amount of DCM and precipitated into a 10x volume of diethyl ether. The resulting precipitate was rinsed with diethyl ether, and dried to yield the product.

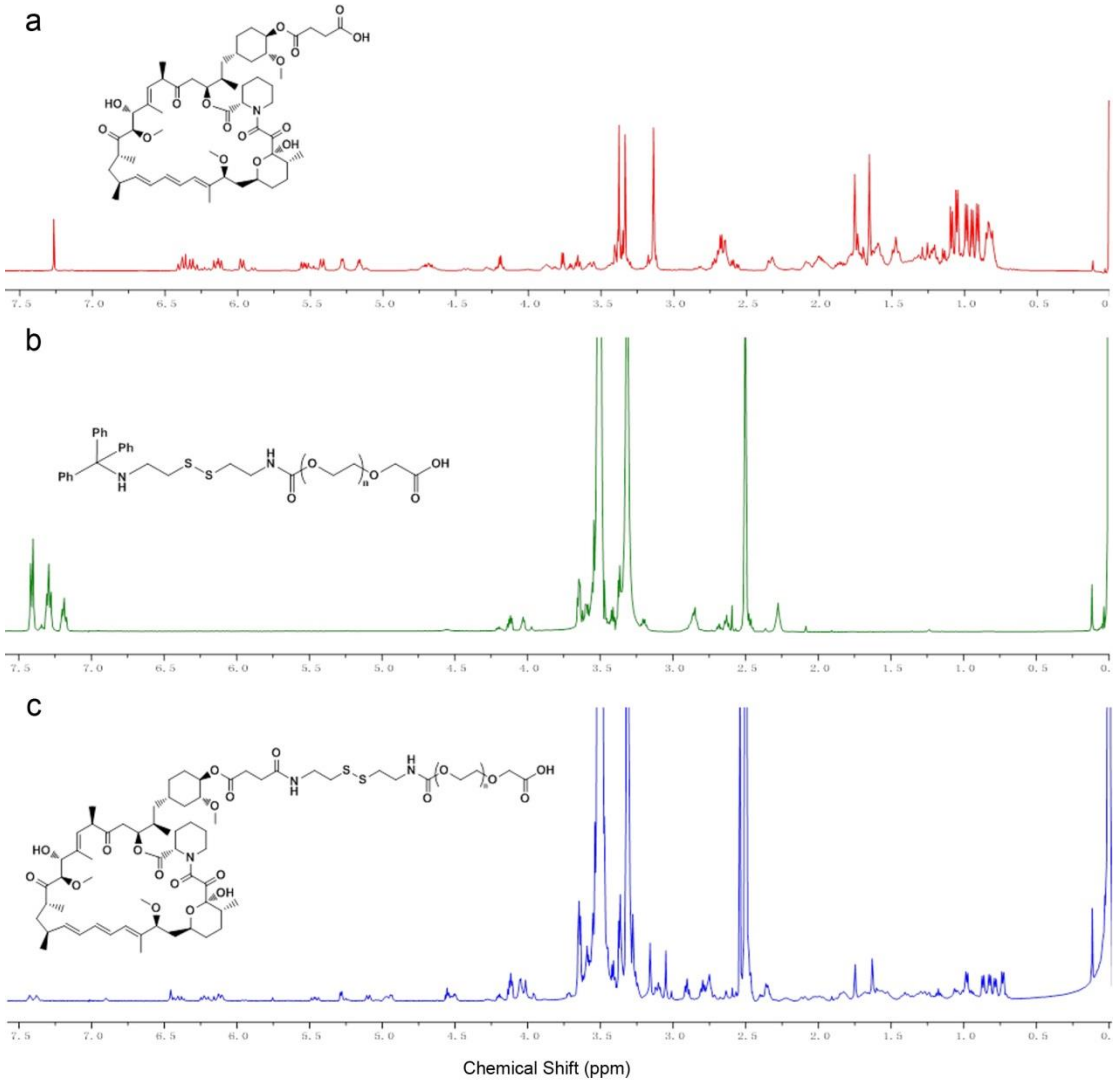

Figure 7.5 ^{1}H NMR spectrum of PEG-ss-rapa conjugate (DMSO-d_6), in comparison with that of rapamycin 42-hemisuccinate ($CDCl_3$) and the PEG precursor (DMSO-d_6).

To synthesize the PEG-ss-rapa conjugate, 200 mg of the above product was dissolved in 2 mL DCM. Compound 2 (40 mg) and TEA (10 μL) was then added to the solution. The reaction mixture was stirred at room temperature for 4 h, followed by precipitation in 10 mL of diethyl ether. The product was collected by a centrifuge, and then re-dissolved in DI water. The solution was then dialyzed against DI water for three days. The final product was obtained by lyophilization and characterized by ^{1}H NMR (**Figure 7.5**).

7.2.3 Measurement of the conjugation density

The conjugation density was calculated based on the characteristic absorption peak at 280 nm. Firstly, the rapamycin substitution degree was obtained by comparing the UV absorption of PEG-ss-rapa with an established rapamycin absorption standard curve. The substitution degree was then calculated to be 87%. For the protein bioconjugates, the absorption values of native uricase and Ur-PEG-ss-rapa solution (protein concentration 2 mg/ml in PBS 7.4) at 280 nm was recorded, respectively. The absorption of conjugated rapamycin can then be obtained by subtracting the absorption of uricase from that of the bioconjugates. The rapamycin concentration was then calculated by comparing the result with the rapamycin standard curve. With the known uricase concentration, the rapamycin conjugation density can then be determined to be 18.6 rapamycin molecules per uricase tetramer. With the PEG substitution degree of 87%, the PEG conjugation density was calculated to be 21.4 polymer chains per uricase tetramer.

7.2.4 Rapamycin release test

PEG-ss-rapa (2 mg) was dissolved in 1 mL PBS 7.4 buffer, followed by adding 1 mg dithiothreitol (DTT). The solution was incubated at 37 ^{o}C for 30 min, and then

concentrated and washed five times by PBS 7.4 using a 3 kDa molecular weight cutoff centrifugal filter (Amicon, Milliporesigma, USA). The resulted residue was then reconstituted to 1 mL by adding PBS 7.4 buffer. A control sample was treated in the same way without adding DTT. The UV-Vis spectra of both samples were recorded using a microplate reader.

7.2.5 Protein conjugation

The carboxyl group of PEG-ss-rapa was firstly activated as an NHS ester. PEG-ss-rapa (200 mg) was dissolved in 2 mL DCM. TSTU (12 mg) and DIPEA (7 μL) were then added to the solution. The mixture was stirred at room temperature for 2 hours and then precipitated in 10 mL of diethyl ether. The product was collected by a centrifuge, and dried under vacuum.

Polymer conjugated uricase samples were prepared in 50-mM PBS buffer (pH 7.4), with uricase concentration at 1 mg/ml and the corresponding polymer concentration at 10 mg/ml. The reaction was stirred at 4 ℃ overnight. Then the conjugates were concentrated and washed extensively by PBS 7.4 using a 100 kDa molecular weight cutoff centrifugal filter (Amicon, Milliporesigma, USA). The protein residue activity was measured by a commercially available uricase activity kit (Life technologies, USA).

7.2.6 Analyses via size-exclusion chromatography

All samples were processed in a 1260 Infinity binary high performance liquid chromatography (HPLC) system equipped with a UV detector (Agilent Technologies, Santa Clara, CA), a miniDAWN TREOS light scattering (LS) detector, and a Optilab T-rEX differential refractive index (dRI) detector (Wyatt Technology, Santa Barbara, CA). The flow rate was set at 0.6 mL/min with the mobile phase PBS (pH 7.4) with 0.02%

sodium azide as a preservative. A Waters Ultrahydrogel 1000 column (7.8 mm x 300 mm, 12 μm particle size) was used for the analysis.

7.2.7 Cell culture and flowcytometry tests

DC2.4 cells, a murine dendritic cell line[126], were kindly provided by Dr. Kenneth Rock (University of Massachusetts Medical Center, Worcester, MA). Cells were grown in complete media comprised of RPMI1640 (Gibco, USA), supplemented with 10% FBS (Hyclone, USA), 25 mM HEPES, 2 mM L-glutamine and 1x non-essential amino acids (Hyclone, USA). DC2.4 cells were maintained at 37 ℃ in a humidified incubator with 5% CO_2.

DC2.4 cells (5×10^5/well) were seeded in 6-well plates and incubated overnight. The culture medium was then replaced with fresh medium containing 0.1 mg/ml of the test samples. After 24 h incubation, the cells were then stimulated with 5 μg/ml lipopolysaccharide (LPS from E. coli, Invitrogen, USA) for an additional 24 hours. For flow cytometric evaluation of the costimulatory molecules, the cells were harvested and suspended in 0.5 mL ice cold PBS, containing 10% FBS and 1% sodium azide. Purified anti-mouse CD16/32 antibody (clone: 2.4G2, BD Biosciences, USA) was added for Fc receptor blocking. 7-AAD solution (25μL, Invitrogen) was added for dead cell exclusion. After incubating for 30 min in dark at 4 ℃, BV421 conjugated Hamster anti-Mouse CD80 (Clone: 16-10A1, BD Horizon) and PE conjugated anti-mouse CD86 (Clone: GL-1, Biolegend) was added. The cells were incubated for another 30 min in dark at 4 ℃ and washed three times before analysis. Data were acquired with a FACSCanto II (BD Biosciences) flow cytometer.

7.2.8 *In vivo* experiments

All animal experiments adhered to federal guidelines and were approved by the University of Washington Institutional Animal Care and Use Committee.

7.2.8.1 Pharmacokinetic and immunogenicity studies

The pharmacokinetics of native and polymer conjugated uricase was studied using Spraque Dawley rats (male, body weight 74~100 g) as the animal model. Each sample had six duplicates to generate statistical significance. Each protein or bioconjugate sample was administered into the rat via tail vein injection at the dose of 25 U/kg body weight. Blood samples were collected from the tail vein at 0 min, 2h, 6 h, 24 h, 48 h and 72 h after the injection. The enzyme content in serum was estimated by enzyme activity. For immunogenicity tests, each agent was injected via the tail vein following the described regimen. Two weeks after the last injection, blood was collected to measure the antibody levels.

7.2.8.2 Enzyme-linked immunosorbent assay (ELISA)

The antigens used in direct ELISAs consisted of native uricase (for detection of anti-uricase antibody), the bioconjugates (for detection of each anti-bioconjugate antibody, the corresponding bioconjugate was used to coat the plate) and ovalbumin (for detection of anti-OVA antibody). For anti-bioconjugate test, a standard backbone-specific anti-PEG antibody (monoclonal mouse anti-PEG Ab, Life Diagnostics 1D9-6) was used as a control to ensure that each different bioconjugate (Ur-PEG, Ur-PEG-rapa and Ur-PEG-ss-rapa) has the similar immobilization density.

For ELISA experiments, 100 μL antigen solution (10 μg/mL of protein concentration) prepared in 0.05 M carbonate-bicarbonate buffer, pH 9.6, was used to coat each well of the 96-well plates. During coating procedure, plates were incubated at 4 ℃

overnight. After removing the antigen solutions, the plates were washed five times using the washing buffer (PBS 7.4, 0.05% Tween20) and then filled with blocking buffer (1% BSA solution in 0.1 M Tris buffer, pH 8.0). After incubation at room temperature for 1 hour, blocking buffer was removed and all wells were washed for another five times. Serial dilutions of rat sera in PBS containing 1% BSA were added to the plates (100 μL/well), which were incubated for 1 h at 37 °C. The plates were then washed five time. Goat anti-rat IgG conjugated to horseradish peroxidase (HRP) (Bethyl labs, USA) was used as the secondary antibody. After adding the secondary antibody, plates were incubated at room temperature for 1 hour, and then washed five times before the addition of 100 μL/well HRP substrate 3,3',5,5'-Tetramethylbenzidine (TMB, Bethyl labs). The plates were shaken for 15 min and 100 μL stop solution (0.2 M H_2SO_4) was added to each well. Absorbance at 450 nm (signal) and 570 nm (background) was recorded by a microplate reader. Pre-bleeding sera were used as negative control for all ELISA detections.

7.3 Results and Discussion

7.3.1 Rapamycin conjugation and characterization

Rapamycin is a macrocyclic polyketide whose biological activities are dependent on the binding of the left-hand portion of the molecule, from C8 to C31 (so-called “binding domain”), to FKBP12 (FK-506 binding protein) and the subsequent formation of a tertiary complex with mTOR (mammalian target-of-rapamycin) protein.[127] Modification of the 42-OH position has led to a series of derivatives with good activity.[125, 128] Thus, the 42-OH position was selected in our study to introduce the reactive moiety for bioconjugations. Rapamycin 42-hemisuccinate was firstly synthesized

via lipase-catalyzed regioselective esterification following a published procedure.[125] The carboxyl group was then activated and conjugated to PEG molecules (10 kDa) through a disulfide linker, denoted as PEG-ss-rapa. The successful conjugation was verified by both NMR (**Figure 7.5**) and UV-Vis spectra (**Figure 7.6a**). A rapamycin substitution degree of 87% was calculated from the UV absorption intensity. The disulfide bond was introduced as the environmental triggering mechanism to release the immunostimulators intracellularly. As shown in **Figure 7.6a**, when treated with dithiothreitol (DTT), the characteristic absorption peak of rapamycin around 280 nm rapidly disappeared, indicating its release from the conjugate.

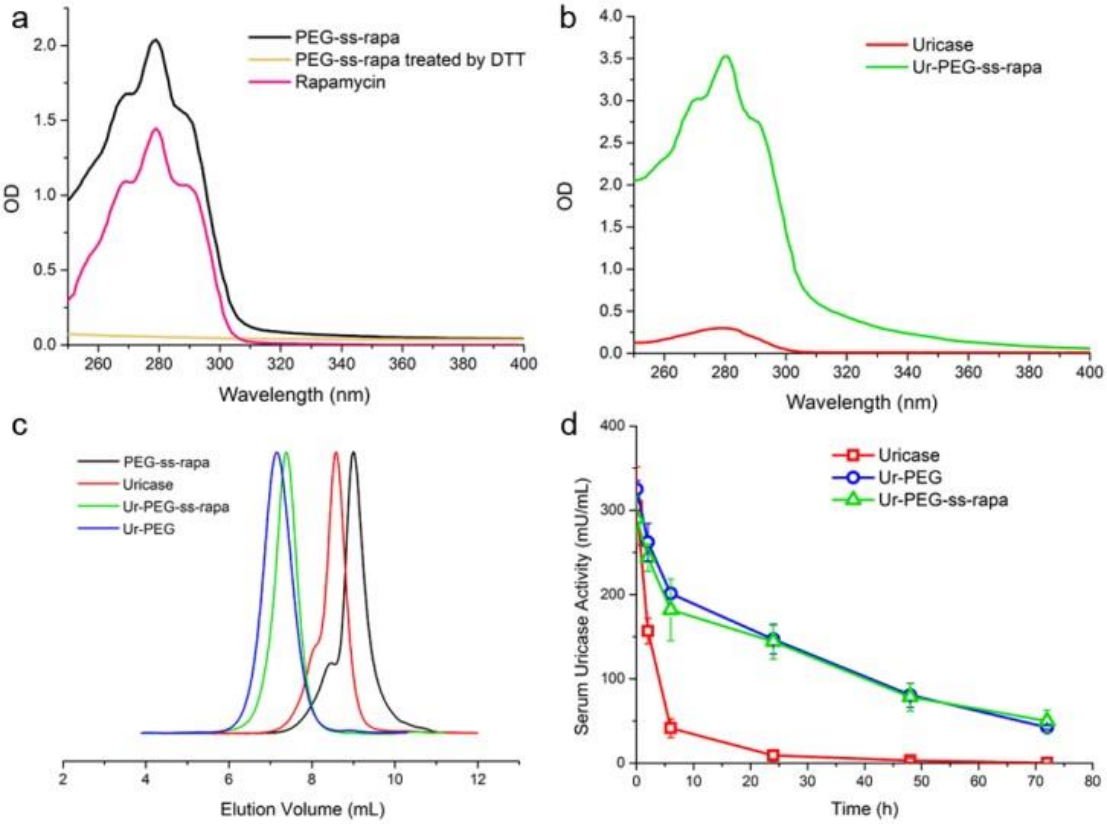

Figure 7.6 Characterization of the immunomodulatory conjugates. a) UV-Vis spectra of the PEG-ss-rapa polymer before and after DTT treatment (in PBS), in comparison with the spectrum of rapamycin (DMSO solution). b) UV-Vis spectra of the native uricase and bioconjugate, at a protein concentration of 2 mg/ml. c) Gel-permeation chromatography (GPC) traces of uricase and the bioconjugates. d) Circulatory profiles of uricase and bioconjugates (n=6).

PEG-ss-rapa was subsequently conjugated to uricase to test its performance both *in vitro* and *in vivo*. Uricase derived from *Candida sp.* was selected as the model protein in this study due to its strong immunogenicity. Previous reports demonstrated that PEGylated uricase induced significant ADA responses in both pre-clinical and clinical studies,[17, 19, 69] which make it a meaningful model to evaluate the ADA mitigation strategies. To perform the protein conjugation, the carboxyl end-group of PEG-ss-rapa was activated as N-hydroxysuccinimide (NHS) ester, and then bioconjugation was completed by reacting with the protein lysine residues. The successful protein conjugation was revealed by UV-Vis spectra (**Figure 7.6b**), as the bioconjugate (denoted as Ur-PEG-ss-rapa) showed an 11-fold stronger absorption at 280 nm compared with the native uricase. Based on the UV absorptions, the conjugation density was calculated to be 18.6 rapamycin molecules with a total of 21.4 PEG polymer chains per uricase tetramer. A PEGylated uricase (Ur-PEG, 22 PEGs per protein tetramer) was also prepared using 10 kDa PEG-NHS for the purpose of comparison. GPC analysis showed that Ur-PEG-ss-rapa possessed a slightly smaller hydrodynamic size than the Ur-PEG bioconjugate at a similar polymer conjugation density (**Figure 7.6c**). Both uricase bioconjugate showed residue activities of > 95% with respect to the native enzyme. The *in vivo* circulation behavior of Ur-PEG-ss-rapa was evaluated in a rat model. As shown in **Figure 7.6d**, no significant difference was observed between the serum concentration-time curves of Ur-PEG-ss-rapa and the regular PEGylated uricase, indicating that the conjugation of rapamycin did not sacrifice its circulation half-life.

7.3.2 Inhibition of dendritic cell maturation

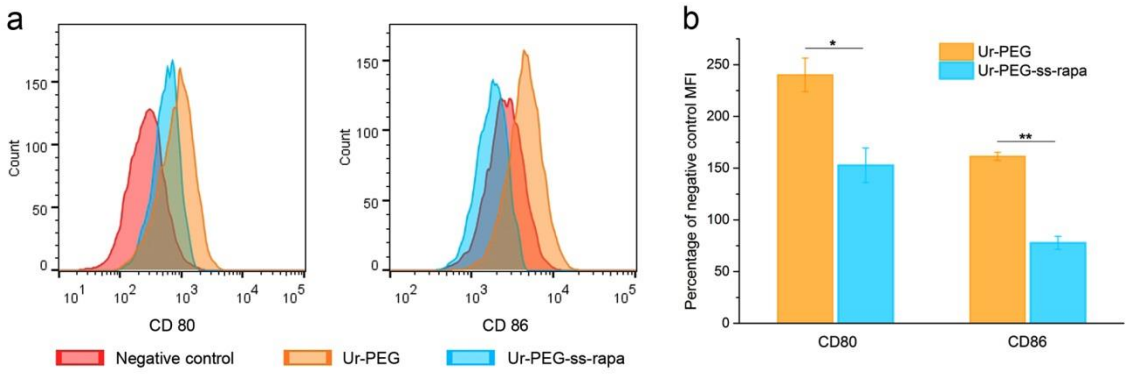

Figure 7.7 Ur-PEG-ss-rapa inhibited dendritic cell maturation. DC 2.4 cells were treated by the bioconjugates for 24 h and stimulated by LPS. The control cells were neither treated by bioconjugates nor the LPS. The upregulation of CD80 and CD 86 was analyzed by flowcytometry. a) Histograms and b) averaged mean fluorescence intensity (MFI) of the samples (n=3). Student's t test was chosen to compare two small sets of quantitative data, *p<0.05, **p<0.01..

Rapamycin is known to inhibit dendritic cell maturation, which is considered as the key mechanism for immune tolerance induction against specific antigens.[122] We incubated the Ur-PEG-ss-rapa bioconjugates with mouse dendritic cells (DC 2.4) to examine its influence on dendritic cell activation. The dendritic cells were firstly incubated with the bioconjugates for 24 h, followed by exposure to lipopolysaccharides (LPS) for another 24 h. The expression of two biomarkers, CD80 and CD86, was examined by flow cytometry. As shown in **Figure 7.7a**, the costimulatory molecules on DCs in the Ur-PEG group were all up-regulated compared with the untreated immature DC control, showing the sign of activation. The Ur-PEG-ss-rapa treated group exhibited lower surface expression of CD86 compared with immature control cells, which is consistent with previous reports regarding rapamycin treated DCs.[122] Similarly, the up-regulation of CD80 was also reduced compared with Ur-PEG treated cells. Normalization of independent experiments by the conversion of flow data to the

percentage of the MFI for the indicated group, relative to the MFI for immature control confirmed that the decreases in CD80 and CD86 on Ur-PEG-ss-rapa treated DCs were statistically significant (**Figure 7.7b**). Collectively, the low expression level of costimulatory molecules CD80 and CD86 in the Ur-PEG-ss-rapa group proved the biological activity of the conjugated rapamycin derivative.

7.3.3 Inhibition of ADA generation

The ADA generation against Ur-PEG-ss-rapa bioconjugate was revealed by measuring both protein and bioconjugate specific antibodies after three weekly intravenous (I.V.) injections in a rat model. An uricase-PEG-rapamycin (denoted as Ur-PEG-rapa) bioconjugate without cleavable disulfide bond was included for comparison. As shown in **Figure 7.8a**, the native uricase stimulated a robust antibody response due to its strong immunogenicity, while regular PEGylation reduced anti-uricase by about 6-fold. By contrast, Ur-PEG-ss-rapa bioconjugate only generated a negligible anti-uricase response, which was 35-fold lower than the regular PEGylated uricase. Simply mixing and co-injection of uricase with PEG-ss-rapa free polymers did not significantly reduce the anti-uricase response compared with the native uricase, suggesting that rapamycin needs to be co-delivered with the antigen. It should be noted that the Ur-PEG-rapa bioconjugate showed a similar anti-uricase response with regular PEGylated uricase, demonstrating that rapamycin needs to be released as the free form to function as an immunomodulator. The anti-bioconjugate antibody responses showed a similar trend as that of the anti-uricase antibody (**Figure 7.8b**). The non-releasing Ur-PEG-rapa bioconjugate showed a 3-fold less anti-bioconjugate titer compared with regular PEGylated uricase, while the cleavable Ur-PEG-ss-rapa reduced the titer by

34-fold to a negligible level. As a classic passive strategy, PEGylation reduced ADAs generation by the "stealth" effect; nonetheless, the effectiveness is limited by the achievable protein conjugation density. In addition, the immunogenic protein carrier amplified the immunogenicity of the haptenic PEG molecules, which results in the generation of anti-bioconjugate ADAs.[86] The combination of the proactive mechanism with traditional PEGylation breaks the limitation of the passive strategy, as the released drug actively modulates the immune activity.

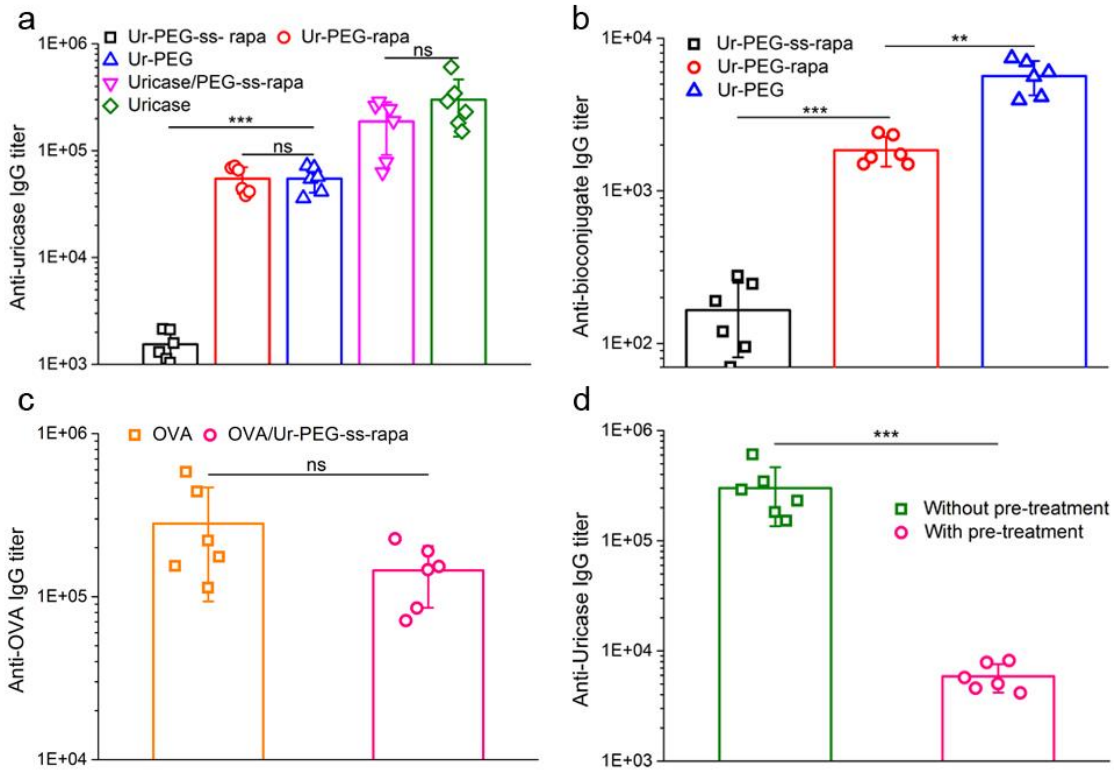

Figure 7.8 Antibody responses measured by enzyme-linked immunosorbent assay (ELISA). a) Anti-uricase and b) anti-bioconjugate antibodies after three weekly injections. c) Anti-OVA antibodies of the groups received OVA or OVA/Ur-PEG-ss-rapa co-injections. d) The pre-treatment group firstly received three weekly administrations of the immunomodulatory bioconjugates. After two weeks, three weekly administrations of native uricase were then given. The antibody responses were compared with the group received solely three injections of the native uricase. All statistical analyses were performed using a one-way ANOVA with a Bonferroni posttest, n=6, *p<0.05, **p<0.01, ***p<0.001.

The usage of immunosuppressive drug may cause non-selective immunosuppressive effect, which could result in increased susceptibility to infections.[129] To examine the selectivity of the antibody generation inhibition, we co-injected Ur-PEG-ss-rapa together with ovalbumin, and compared the anti-ovalbumin antibody titers with the group received ovalbumin alone. As shown in **Figure 7.8c**, both groups had strong responses against ovalbumin, with no significant differences in antibody titers. The similar antibody levels demonstrated that the conjugated rapamycin suppresses the immune responses in an antigen-specific manner. As showed in the above *in vitro* tests, the conjugated rapamycin inhibits DC maturation, and the immature DCs are known to induce immune tolerance.[130, 131] To further test whether the antibody inhibition is a result of antigen-specific tolerance, we conducted another study by measuring the antibody response of the native uricase administration post a pre-treatment regimen of the Ur-PEG-ss-rapa. In this test, the animals firstly received three dosages of Ur-PEG-ss-rapa as the pretreatment. Two weeks later, three weekly administrations of native uricase were given and the antibody titers were examined two weeks post the final injection. As shown in **Figure 7.8d**, the pretreatment resulted in a 51-fold lower anti-uricase IgG titer compared with the control group, demonstrating a persistent antigen-specific tolerance. As a benefit, the rapamycin-antigen conjugation strategy may also have the potential to be used as a treatment for autoimmune disease in addition to the reduction of ADAs.

7.4 Conclusions

In conclusion, we report a proactive strategy to reduce ADAs of the PEGylated biologic drugs by immunomodulatory bioconjugation chemistry. The rapamycin derivative was conjugated to PEGylated proteins via a cleavable disulfide linker. *In vitro*

tests showed that the conjugated rapamycin is capable to inhibit the maturation of dendritic cells. *In vivo* studies demonstrated that the rapamycin conjugation effectively mitigates ADAs against PEGylated proteins by induction of antigen-specific tolerance. All these results indicate that rapamycin conjugation offers a promising approach to minimize the issues of ADAs, which are associated with adverse hypersensitivity reactions and the loss of efficacy of otherwise effective drugs.

Chapter 8 Conclusions

This dissertation explored and investigated the modification strategies to improve the efficacy and safety of protein based therapeutics. We analyzed the limitations of the classical PEGylation technology and described the principles to improve the passive protein modification methods. By tailoring polymer structures and conjugation chemistries, new materials and methods are developed to overcome current challenges encountered by PEGylation.

The first part of the dissertation (Chapter 2-4) discussed the protein modification principles to reduce the unwanted immune responses. Two key factors need to be carefully considered when developing protein modification technologies – material immunogenicity and protein surface coverage density. We used the superhydrophilic PCB polymer as the non-immunogenic replacement to PEG. A crosslinked hydrogel network was used to overcome the coverage density limitation faced by traditional polymer conjugations. The zwitterionic gel encapsulation technology was developed based on these principles and applied to a highly immunogenic enzyme uricase, a protein drug used to treat chronic gout. *In vitro* and *in vivo* evaluations showed that the encapsulation significantly increased protein stability, prolonged circulation half-life and reduced immunogenicity. Pharmacokinetic study in a rat model showed that the circulation half-life of uricase nanocapsule was 3.6-fold longer than that of PEGylated uricase, without any accelerated blood clearance phenomenon. More importantly, neither anti-uricase nor anti-polymer antibodies were detected after three weekly injections of the nanocapsule. In contrast, significant amount of anti-uricase and anti-PEG antibodies were found in animals received PEGylated uricase.

In addition to therapeutic applications, we also applied this technology to construct bioscavengers to prophylactically countermeasure organophosphate threatening. Both stoichiometric (BChE) and catalytical (OPH) OP scavenging enzymes were used to fabricate the bioscavenging nanocapsules. Similar to uricase, the encapsulated BChE and OPH all outperformed their native precursors in terms of circulation half-life and immunogenicity. We further tested the protection efficacy of OPH nanocapsules against both paraoxon and sarin exposures. The results demonstrated that one single injection of the nanoscavenger can prevent lethality even if the victim was exposed to $2\times LD_{50}$ nerve agents one week after the prophylactic administration. The nanoscavenger prophylactic strategy provides a promising solution to fill the needs in both civilian and military applications.

The second part of the dissertation (Chapter 5-7) discussed new capabilities developed in the course of this work. First, a new SPR sensor was investigated for anti-PEG antibody detections. Three surface coating chemistries, including EG4 SAM, mPEG and PEGMA polymer brushes were compared as the sensor chip coating, and mPEG showed the highest signal/noise ratio. Using mPEG as the coating material, we built a simple, rapid, sensitive and reliable technique to directly detect anti-PEG antibodies in blood samples. Within 40 min, anti-PEG abs can be quantitatively detected from blood samples with 10 ng/mL limit of detection. By using secondary antibodies, different anti-PEG antibody isotypes can also be differentiated and measured. The potential clinical application of the SPR sensor was also demonstrated using blood samples from one leukemia patient.

Second, a zwitterionic polypeptide was designed and synthesized as a biodegradable protein modification material. The carboxybetaine group functionalized polypeptide was synthesized via the combination of NCA ring-opening polymerization and "click" type thiol-yne chemistry. The polypeptide did not induce any tissue histologic change in liver, kidney and spleen after three months of toxicity test in rats. No abnormal behavior, sickness or death was observed in the test period. With a sophisticatedly tailored backbone endgroup, the polymer was conjugated to uricase and compared with PEGylated uricase. The results demonstrated that PepCB conjugated uricase has longer circulation half-life than PEGylated uricase, with significantly less immune responses.

Third, we also described a strategy that proactively prevents anti-drug antibody generation by immunomodulatory bioconjugation. As a passive method, PEGylation faced two key limitations – insufficient epitope coverage and material immunogenicity. The previously described zwitterionic encapsulation is also a passive method that tried to directly overcome these limitations by increasing surface coverage density and changing material. In Chapter 7, we showed a proactive method that bypassed these limitations by incorporating immunomodulators. In this approach, rapamycin was conjugated to PEGylated proteins via a cleavable disulfide linker. The conjugated rapamycin can be released intracellularly, and inhibit dendritic cell maturation. Anti-drug antibodies were successfully suppressed when testing the immunomodulatory conjugated uricase in rats. Further studies proved that the inhibition of antibody was a result of the induced antigen-specific immune tolerance.

Biopharmaceutical drugs, including peptides, proteins, monoclonal antibodies, drug-antibody conjugates and aptamers, offer significant advantages over small molecule

therapeutics due to their specific bioactivity and high potency. Yet their widespread applications are still limited by stability, pharmacokinetics and immunogenicity problems. With the continuous developments in novel protein modification technologies, more immunogenic biologic therapeutics could enter into human therapeutic or protective applications. The improved drug circulation half-life and immunogenicity will benefit patients by reducing administration frequency and mitigating adverse reactions.

References

[1] Mitragotri S, Burke PA, Langer R. Overcoming the challenges in administering biopharmaceuticals: formulation and delivery strategies. Nature reviews Drug discovery. 2014;13:655-72.

[2] Chirino AJ, Ary ML, Marshall SA. Minimizing the immunogenicity of protein therapeutics. Drug discovery today. 2004;9:82-90.

[3] Veronese FM, Pasut G. PEGylation, successful approach to drug delivery. Drug discovery today. 2005;10:1451-8.

[4] Shankar G, Pendley C, Stein KE. A risk-based bioanalytical strategy for the assessment of antibody immune responses against biological drugs. Nature biotechnology. 2007;25:555-61.

[5] Harris JM, Chess RB. Effect of pegylation on pharmaceuticals. Nature reviews Drug discovery. 2003;2:214-21.

[6] Branca C, Magazu S, Maisano G, Migliardo F, Migliardo P, Romeo G. Hydration study of PEG/water mixtures by quasi elastic light scattering, acoustic and rheological measurements. J Phys Chem B. 2002;106:10272-6.

[7] Zheng J, Li L, Chen S, Jiang S. Molecular simulation study of water interactions with oligo (ethylene glycol)-terminated alkanethiol self-assembled monolayers. Langmuir : the ACS journal of surfaces and colloids. 2004;20:8931-8.

[8] Zheng J, Li L, Tsao HK, Sheng YJ, Chen S, Jiang S. Strong repulsive forces between protein and oligo (ethylene glycol) self-assembled monolayers: a molecular simulation study. Biophys J. 2005;89:158-66.

[9] Abuchowski A, van Es T, Palczuk NC, Davis FF. Alteration of immunological properties of bovine serum albumin by covalent attachment of polyethylene glycol. The Journal of biological chemistry. 1977;252:3578-81.

[10] Kolate A, Baradia D, Patil S, Vhora I, Kore G, Misra A. PEG - a versatile conjugating ligand for drugs and drug delivery systems. Journal of controlled release : official journal of the Controlled Release Society. 2014;192:67-81.

[11] Alconcel SNS, Baas AS, Maynard HD. FDA-approved poly(ethylene glycol)–protein conjugate drugs. Polym Chem. 2011;2:1442.

[12] Jevsevar S, Kunstelj M, Porekar VG. PEGylation of therapeutic proteins. Biotechnol J. 2010;5:113-28.

[13] Abuchowski A, McCoy JR, Palczuk NC, van Es T, Davis FF. Effect of covalent attachment of polyethylene glycol on immunogenicity and circulating life of bovine liver catalase. The Journal of biological chemistry. 1977;252:3582-6.

[14] Richter AW, Akerblom E. Antibodies against polyethylene glycol produced in animals by immunization with monomethoxy polyethylene glycol modified proteins. Int Arch Allergy Appl Immunol. 1983;70:124-31.

[15] Garay RP, El-Gewely R, Armstrong JK, Garratty G, Richette P. Antibodies against polyethylene glycol in healthy subjects and in patients treated with PEG-conjugated agents. Expert opinion on drug delivery. 2012;9:1319-23.

[16] Armstrong JK, Hempel G, Koling S, Chan LS, Fisher T, Meiselman HJ, et al. Antibody against poly(ethylene glycol) adversely affects PEG-asparaginase therapy in acute lymphoblastic leukemia patients. Cancer. 2007;110:103-11.

[17] Hershfield MS, Ganson NJ, Kelly SJ, Scarlett EL, Jaggers DA, Sundy JS. Induced and pre-existing anti-polyethylene glycol antibody in a trial of every 3-week dosing of pegloticase for refractory gout, including in organ transplant recipients. Arthritis Res Ther. 2014;16:R63.

[18] Longo N, Harding CO, Burton BK, Grange DK, Vockley J, Wasserstein M, et al. Single-dose, subcutaneous recombinant phenylalanine ammonia lyase conjugated with polyethylene glycol in adult patients with phenylketonuria: an open-label, multicentre, phase 1 dose-escalation trial. Lancet. 2014;384:37-44.

[19] Lipsky PE, Calabrese LH, Kavanaugh A, Sundy JS, Wright D, Wolfson M, et al. Pegloticase immunogenicity: the relationship between efficacy and antibody development in patients treated for refractory chronic gout. Arthritis Res Ther. 2014;16:R60.

[20] Ishida T, Ichihara M, Wang X, Yamamoto K, Kimura J, Majima E, et al. Injection of PEGylated liposomes in rats elicits PEG-specific IgM, which is responsible for rapid elimination of a second dose of PEGylated liposomes. Journal of controlled release : official journal of the Controlled Release Society. 2006;112:15-25.

[21] Ishida T, Maeda R, Ichihara M, Irimura K, Kiwada H. Accelerated clearance of PEGylated liposomes in rats after repeated injections. Journal of controlled release : official journal of the Controlled Release Society. 2003;88:35-42.

[22] Shiraishi K, Hamano M, Ma H, Kawano K, Maitani Y, Aoshi T, et al. Hydrophobic blocks of PEG-conjugates play a significant role in the accelerated blood clearance (ABC) phenomenon. Journal of controlled release : official journal of the Controlled Release Society. 2013;165:183-90.

[23] Ishida T, Kiwada H. Accelerated blood clearance (ABC) phenomenon upon repeated injection of PEGylated liposomes. International journal of pharmaceutics. 2008;354:56-62.

[24] Judge A, McClintock K, Phelps JR, Maclachlan I. Hypersensitivity and loss of disease site targeting caused by antibody responses to PEGylated liposomes. Mol Ther. 2006;13:328-37.

[25] Wang C, Cheng X, Su Y, Pei Y, Song Y, Jiao J, et al. Accelerated blood clearance phenomenon upon cross-administration of PEGylated nanocarriers in beagle dogs. Int J Nanomedicine. 2015;10:3533-45.

[26] Ishida T, Wang X, Shimizu T, Nawata K, Kiwada H. PEGylated liposomes elicit an anti-PEG IgM response in a T cell-independent manner. Journal of controlled release : official journal of the Controlled Release Society. 2007;122:349-55.

[27] Abu Lila AS, Kiwada H, Ishida T. The accelerated blood clearance (ABC) phenomenon: clinical challenge and approaches to manage. Journal of controlled release : official journal of the Controlled Release Society. 2013;172:38-47.

[28] Chen BM, Su YC, Chang CJ, Burnouf PA, Chuang KH, Chen CH, et al. Measurement of Pre-Existing IgG and IgM Antibodies against Polyethylene Glycol in Healthy Individuals. Anal Chem. 2016;88:10661-6.

[29] Yang Q, Jacobs TM, McCallen JD, Moore DT, Huckaby JT, Edelstein JN, et al. Analysis of Pre-existing IgG and IgM Antibodies against Polyethylene Glycol (PEG) in the General Population. Anal Chem. 2016;88:11804-12.

[30] van der Eijk AA, Vrolijk JM, Haagmans BL. Antibodies neutralizing peginterferon alfa during retreatment of hepatitis C. The New England journal of medicine. 2006;354:1323-4.

[31] Armstrong JK, Leger R, Wenby RB, Meiselman HJ, Garratty G, Fisher TC. Occurrence of an antibody to poly(ethylene glycol) in normal donors. Blood. 2003;102:556A-A.

[32] Saifer MG, Williams LD, Sobczyk MA, Michaels SJ, Sherman MR. Selectivity of binding of PEGs and PEG-like oligomers to anti-PEG antibodies induced by methoxyPEG-proteins. Molecular immunology. 2014;57:236-46.

[33] Schneck E, Berts I, Halperin A, Daillant J, Fragneto G. Neutron reflectometry from poly (ethylene-glycol) brushes binding anti-PEG antibodies: evidence of ternary adsorption. Biomaterials. 2015;46:95-104.

[34] Sherman MR, Williams LD, Sobczyk MA, Michaels SJ, Saifer MG. Role of the methoxy group in immune responses to mPEG-protein conjugates. Bioconjugate chemistry. 2012;23:485-99.

[35] Jiang S, Cao Z. Ultralow-fouling, functionalizable, and hydrolyzable zwitterionic materials and their derivatives for biological applications. Advanced materials. 2010;22:920-32.

[36] Smith RS, Zhang Z, Bouchard M, Li J, Lapp HS, Brotske GR, et al. Vascular catheters with a nonleaching poly-sulfobetaine surface modification reduce thrombus formation and microbial attachment. Sci Transl Med. 2012;4:153ra32.

[37] Moro T, Takatori Y, Ishihara K, Konno T, Takigawa Y, Matsushita T, et al. Surface grafting of artificial joints with a biocompatible polymer for preventing periprosthetic osteolysis. Nature materials. 2004;3:829-36.

[38] Ladd J, Zhang Z, Chen S, Hower JC, Jiang S. Zwitterionic polymers exhibiting high resistance to nonspecific protein adsorption from human serum and plasma. Biomacromolecules. 2008;9:1357-61.

[39] Zhang L, Cao Z, Bai T, Carr L, Ella-Menye JR, Irvin C, et al. Zwitterionic hydrogels implanted in mice resist the foreign-body reaction. Nature biotechnology. 2013;31:553-6.

[40] Yang W, Liu SJ, Bai T, Keefe AJ, Zhang L, Ella-Menye JR, et al. Poly(carboxybetaine) nanomaterials enable long circulation and prevent polymer-specific antibody production. Nano Today. 2014;9:10-6.

[41] Zhang Z, Vaisocherova H, Cheng G, Yang W, Xue H, Jiang S. Nonfouling behavior of polycarboxybetaine-grafted surfaces: structural and environmental effects. Biomacromolecules. 2008;9:2686-92.

[42] Bai T, Sun F, Zhang L, Sinclair A, Liu S, Ella-Menye JR, et al. Restraint of the differentiation of mesenchymal stem cells by a nonfouling zwitterionic hydrogel. Angewandte Chemie. 2014;53:12729-34.

[43] Nguyen TH, Kim SH, Decker CG, Wong DY, Loo JA, Maynard HD. A heparin-mimicking polymer conjugate stabilizes basic fibroblast growth factor. Nature chemistry. 2013;5:221-7.

[44] Keefe AJ, Jiang S. Poly(zwitterionic)protein conjugates offer increased stability without sacrificing binding affinity or bioactivity. Nature chemistry. 2012;4:59-63.

[45] Wei W, Du J, Li J, Yan M, Zhu Q, Jin X, et al. Construction of robust enzyme nanocapsules for effective organophosphate decontamination, detoxification, and protection. Advanced materials. 2013;25:2212-8.

[46] Yan M, Ge J, Liu Z, Ouyang P. Encapsulation of single enzyme in nanogel with enhanced biocatalytic activity and stability. J Am Chem Soc. 2006;128:11008-9.

[47] Elsabahy M, Wooley KL. Design of polymeric nanoparticles for biomedical delivery applications. Chem Soc Rev. 2012;41:2545-61.

[48] Caliceti P, Schiavon O, Veronese FM. Biopharmaceutical properties of uricase conjugated to neutral and amphiphilic polymers. Bioconjugate chemistry. 1999;10:638-46.

[49] Yasuda Y, Fujita T, Takakura Y, Hashida M, Sezaki H. Biochemical and biopharmaceutical properties of macromolecular conjugates of uricase with dextran and polyethylene glycol. Chemical & pharmaceutical bulletin. 1990;38:2053-6.

[50] Cao Z, Jiang S. Super-hydrophilic zwitterionic poly(carboxybetaine) and amphiphilic non-ionic poly(ethylene glycol) for stealth nanoparticles. Nano Today. 2012;7:404-13.

[51] Pombo Garcia K, Zarschler K, Barbaro L, Barreto JA, O'Malley W, Spiccia L, et al. Zwitterionic-coated "stealth" nanoparticles for biomedical applications: recent advances in countering biomolecular corona formation and uptake by the mononuclear phagocyte system. Small. 2014;10:2516-29.

[52] Zhang L, Cao Z, Li Y, Ella-Menye JR, Bai T, Jiang S. Softer zwitterionic nanogels for longer circulation and lower splenic accumulation. ACS nano. 2012;6:6681-6.

[53] Yang Q, Jones SW, Parker CL, Zamboni WC, Bear JE, Lai SK. Evading immune cell uptake and clearance requires PEG grafting at densities substantially exceeding the minimum for brush conformation. Mol Pharm. 2014;11:1250-8.

[54] Majorek KA, Porebski PJ, Dayal A, Zimmerman MD, Jablonska K, Stewart AJ, et al. Structural and immunologic characterization of bovine, horse, and rabbit serum albumins. Molecular immunology. 2012;52:174-82.

[55] Gupta RD, Goldsmith M, Ashani Y, Simo Y, Mullokandov G, Bar H, et al. Directed evolution of hydrolases for prevention of G-type nerve agent intoxication. Nat Chem Biol. 2011;7:120-5.

[56] Albuquerque EX, Pereira EF, Aracava Y, Fawcett WP, Oliveira M, Randall WR, et al. Effective countermeasure against poisoning by organophosphorus insecticides and nerve agents. Proc Natl Acad Sci U S A. 2006;103:13220-5.

[57] Pang ZQ, Hu CMJ, Fang RH, Luk BT, Gao WW, Wang F, et al. Detoxification of Organophosphate Poisoning Using Nanoparticle Bioscavengers. ACS nano. 2015;9:6450-8.

[58] Elsinghorst PW, Worek F, Thiermann H, Wille T. Drug development for the management of organophosphorus poisoning. Expert Opin Drug Discov. 2013;8:1467-77.

[59] Eddleston M, Buckley NA, Eyer P, Dawson AH. Management of acute organophosphorus pesticide poisoning. The Lancet. 2008;371:597-607.

[60] Saxena A, Sun W, Fedorko JM, Koplovitz I, Doctor BP. Prophylaxis with human serum butyrylcholinesterase protects guinea pigs exposed to multiple lethal doses of soman or VX. Biochem Pharmacol. 2011;81:164-9.

[61] Nachon F, Brazzolotto X, Trovaslet M, Masson P. Progress in the development of enzyme-based nerve agent bioscavengers. Chem Biol Interact. 2013;206:536-44.

[62] Doctor BP, Saxena A. Bioscavengers for the protection of humans against organophosphate toxicity. Chem Biol Interact. 2005;157-158:167-71.

[63] Ilyushin DG, Smirnov IV, Belogurov AA, Jr., Dyachenko IA, Zharmukhamedova T, Novozhilova TI, et al. Chemical polysialylation of human recombinant

butyrylcholinesterase delivers a long-acting bioscavenger for nerve agents in vivo. Proc Natl Acad Sci U S A. 2013;110:1243-8.

[64] Geyer BC, Kannan L, Garnaud PE, Broomfield CA, Cadieux CL, Cherni I, et al. Plant-derived human butyrylcholinesterase, but not an organophosphorous-compound hydrolyzing variant thereof, protects rodents against nerve agents. Proc Natl Acad Sci U S A. 2010;107:20251-6.

[65] Huang YJ, Huang Y, Baldassarre H, Wang B, Lazaris A, Leduc M, et al. Recombinant human butyrylcholinesterase from milk of transgenic animals to protect against organophosphate poisoning. Proc Natl Acad Sci U S A. 2007;104:13603-8.

[66] Koetzner L, Woods JH. Characterization of equine butyrylcholinesterase disposition in the mouse. Drug Metab Dispos. 2002;30:724-30.

[67] Cohen O, Kronman C, Raveh L, Mazor O, Ordentlich A, Shafferman A. Comparison of polyethylene glycol-conjugated recombinant human acetylcholinesterase and serum human butyrylcholinesterase as bioscavengers of organophosphate compounds. Mol Pharmacol. 2006;70:1121-31.

[68] Sun W, Luo C, Tipparaju P, Doctor BP, Saxena A. Effect of polyethylene glycol conjugation on the circulatory stability of plasma-derived human butyrylcholinesterase in mice. Chem Biol Interact. 2013;203:172-6.

[69] Zhang P, Sun F, Tsao C, Liu S, Jain P, Sinclair A, et al. Zwitterionic gel encapsulation promotes protein stability, enhances pharmacokinetics, and reduces immunogenicity. Proc Natl Acad Sci U S A. 2015;112:12046-51.

[70] Chilukuri N, Parikh K, Sun W, Naik R, Tipparaju P, Doctor BP, et al. Polyethylene glycosylation prolongs the circulatory stability of recombinant human butyrylcholinesterase. Chem Biol Interact. 2005;157-158:115-21.

[71] Stone R. How to defeat a nerve agent. Science. 2018;359:23.

[72] Benschop HP, Dejong LPA. Nerve Agent Stereoisomers - Analysis, Isolation, and Toxicology. Accounts Chem Res. 1988;21:368-74.

[73] Wales ME, Reeves TE. Organophosphorus hydrolase as an in vivo catalytic nerve agent bioscavenger. Drug Test Anal. 2012;4:271-81.

[74] Zhang P, Jain P, Tsao C, Sinclair A, Sun F, Hung HC, et al. Butyrylcholinesterase nanocapsule as a long circulating bioscavenger with reduced immune response. Journal of controlled release : official journal of the Controlled Release Society. 2016;230:73-8.

[75] Tsai PC, Bigley A, Li Y, Ghanem E, Cadieux CL, Kasten SA, et al. Stereoselective hydrolysis of organophosphate nerve agents by the bacterial phosphotriesterase. Biochemistry. 2010;49:7978-87.

[76] Tsai PC, Fox N, Bigley AN, Harvey SP, Barondeau DP, Raushel FM. Enzymes for the homeland defense: optimizing phosphotriesterase for the hydrolysis of organophosphate nerve agents. Biochemistry. 2012;51:6463-75.

[77] Bigley AN, Xu C, Henderson TJ, Harvey SP, Raushel FM. Enzymatic neutralization of the chemical warfare agent VX: evolution of phosphotriesterase for phosphorothiolate hydrolysis. J Am Chem Soc. 2013;135:10426-32.

[78] Novikov BN, Grimsley JK, Kern RJ, Wild JR, Wales ME. Improved pharmacokinetics and immunogenicity profile of organophosphorus hydrolase by chemical modification with polyethylene glycol. Journal of controlled release : official journal of the Controlled Release Society. 2010;146:318-25.

[79] Efremenko EN, Lyagin IV, Klyachko NL, Bronich T, Zavyalova NV, Jiang Y, et al. A simple and highly effective catalytic nanozyme scavenger for organophosphorus neurotoxins. Journal of controlled release : official journal of the Controlled Release Society. 2017;247:175-81.

[80] Liu S, Jiang S. Zwitterionic polymer-protein conjugates reduce polymer-specific antibody response. Nano Today. 2016;11:285-91.

[81] Zhang Y, Huo M, Zhou J, Xie S. PKSolver: An add-in program for pharmacokinetic and pharmacodynamic data analysis in Microsoft Excel. Comput Methods Programs Biomed. 2010;99:306-14.

[82] Worek F, Thiermann H, Wille T. Catalytic bioscavengers in nerve agent poisoning: A promising approach? Toxicology letters. 2016;244:143-8.

[83] Wetherell JR, Armstrong SJ, Read RW, Clough GF. VX Penetration Following Percutaneous Poisoning: A Dermal Microdialysis Study in the Guinea Pig. Toxicology mechanisms and methods. 2008;18:313-21.

[84] Schellenberger V, Wang CW, Geething NC, Spink BJ, Campbell A, To W, et al. A recombinant polypeptide extends the in vivo half-life of peptides and proteins in a tunable manner. Nature biotechnology. 2009;27:1186-90.

[85] Mima Y, Hashimoto Y, Shimizu T, Kiwada H, Ishida T. Anti-PEG IgM Is a Major Contributor to the Accelerated Blood Clearance of Polyethylene Glycol-Conjugated Protein. Mol Pharm. 2015;12:2429-35.

[86] Zhang P, Sun F, Liu S, Jiang S. Anti-PEG antibodies in the clinic: Current issues and beyond PEGylation. Journal of controlled release : official journal of the Controlled Release Society. 2016;244:184-93.

[87] Ganson NJ, Povsic TJ, Sullenger BA, Alexander JH, Zelenkofske SL, Sailstad JM, et al. Pre-existing anti-polyethylene glycol antibody linked to first-exposure allergic reactions to pegnivacogin, a PEGylated RNA aptamer. J Allergy Clin Immunol. 2016;137:1610-3 e7.

[88] Zhang P, Sun F, Hung HC, Jain P, Leger KJ, Jiang S. Sensitive and Quantitative Detection of Anti-Poly(ethylene glycol) (PEG) Antibodies by Methoxy-PEG-Coated Surface Plasmon Resonance Sensors. Anal Chem. 2017;89:8217-22.

[89] Villa AF, Houze P, Monier C, Risede P, Sarhan H, Borron SW, et al. Toxic doses of paraoxon alter the respiratory pattern without causing respiratory failure in rats. Toxicology. 2007;232:37-49.

[90] Stefanidou M, Athanaselis S, Spiliopoulou H. Butyrylcholinesterase: biomarker for exposure to organophosphorus insecticides. Internal medicine journal. 2009;39:57-60.

[91] Petrikovics I, Papahadjopoulos D, Hong K, Cheng TC, Baskin SI, Jiang J, et al. Comparing therapeutic and prophylactic protection against the lethal effect of paraoxon. Toxicological sciences : an official journal of the Society of Toxicology. 2004;77:258-62.

[92] Ashani Y, Rothschild N, Segall Y, Levanon D, Raveh L. Prophylaxis against organophosphate poisoning by an enzyme hydrolysing organophosphorus compounds in mice. Life sciences. 1991;49:367-74.

[93] Yang Q, Lai SK. Anti-PEG immunity: emergence, characteristics, and unaddressed questions. Wiley Interdiscip Rev Nanomed Nanobiotechnol. 2015;7:655-77.

[94] Povsic TJ, Lawrence MG, Lincoff AM, Mehran R, Rusconi CP, Zelenkofske SL, et al. Pre-existing anti-PEG antibodies are associated with severe immediate allergic reactions to pegnivacogin, a PEGylated aptamer. J Allergy Clin Immunol. 2016;138:1712-5.

[95] Wang X, Ishida T, Kiwada H. Anti-PEG IgM elicited by injection of liposomes is involved in the enhanced blood clearance of a subsequent dose of PEGylated liposomes. Journal of controlled release : official journal of the Controlled Release Society. 2007;119:236-44.

[96] Liu Y, Reidler H, Pan J, Milunic D, Qin D, Chen D, et al. A double antigen bridging immunogenicity ELISA for the detection of antibodies to polyethylene glycol polymers. J Pharmacol Toxicol Methods. 2011;64:238-45.

[97] Qi Y, Simakova A, Ganson NJ, Li X, Luginbuhl KM, Ozer I, et al. A brush-polymer/exendin-4 conjugate reduces blood glucose levels for up to five days and eliminates poly(ethylene glycol) antigenicity. Nature Biomedical Engineering. 2016;1:0002.

[98] Pelegri-O'Day EM, Lin EW, Maynard HD. Therapeutic protein-polymer conjugates: advancing beyond PEGylation. J Am Chem Soc. 2014;136:14323-32.

[99] Rudmann DG, Alston JT, Hanson JC, Heidel S. High molecular weight polyethylene glycol cellular distribution and PEG-associated cytoplasmic vacuolation is molecular weight dependent and does not require conjugation to proteins. Toxicologic pathology. 2013;41:970-83.

[100] Bendele A, Seely J, Richey C, Sennello G, Shopp G. Short communication: renal tubular vacuolation in animals treated with polyethylene-glycol-conjugated proteins. Toxicological sciences : an official journal of the Society of Toxicology. 1998;42:152-7.

[101] Xu J, Bussiere J, Yie J, Sickmier A, An P, Belouski E, et al. Polyethylene glycol modified FGF21 engineered to maximize potency and minimize vacuole formation. Bioconjugate chemistry. 2013;24:915-25.

[102] Ivens IA, Achanzar W, Baumann A, Brandli-Baiocco A, Cavagnaro J, Dempster M, et al. PEGylated Biopharmaceuticals: Current Experience and Considerations for Nonclinical Development. Toxicologic pathology. 2015;43:959-83.

[103] Turecek PL, Bossard MJ, Schoetens F, Ivens IA. PEGylation of Biopharmaceuticals: A Review of Chemistry and Nonclinical Safety Information of Approved Drugs. J Pharm Sci. 2016;105:460-75.

[104] Liu M, Johansen P, Zabel F, Leroux JC, Gauthier MA. Semi-permeable coatings fabricated from comb-polymers efficiently protect proteins in vivo. Nat Commun. 2014;5:5526.

[105] Knop K, Hoogenboom R, Fischer D, Schubert US. Poly(ethylene glycol) in drug delivery: pros and cons as well as potential alternatives. Angewandte Chemie. 2010;49:6288-308.

[106] Pelegri-O'Day EM, Paluck SJ, Maynard HD. Substituted Polyesters by Thiol-Ene Modification: Rapid Diversification for Therapeutic Protein Stabilization. J Am Chem Soc. 2017;139:1145-54.

[107] Engler AC, Bonner DK, Buss HG, Cheung EY, Hammond PT. The synthetic tuning of clickable pH responsive cationic polypeptides and block copolypeptides. Soft Matter. 2011;7:5627.

[108] Engler AC, Lee HI, Hammond PT. Highly efficient "grafting onto" a polypeptide backbone using click chemistry. Angewandte Chemie. 2009;48:9334-8.

[109] Zhang S, Zou J, Zhang F, Elsabahy M, Felder SE, Zhu J, et al. Rapid and versatile construction of diverse and functional nanostructures derived from a polyphosphoester-based biomimetic block copolymer system. J Am Chem Soc. 2012;134:18467-74.

[110] Dutheil D, Underhaug Gjerde A, Petit-Paris I, Mauco G, Holmsen H. Polyethylene glycols interact with membrane glycerophospholipids: is this part of their mechanism for hypothermic graft protection? J Chem Biol. 2009;2:39-49.

[111] Wu J, Zhao C, Lin W, Hu R, Wang Q, Chen H, et al. Binding characteristics between polyethylene glycol (PEG) and proteins in aqueous solution. Journal of Materials Chemistry B. 2014;2:2983.

[112] Shao Q, He Y, White AD, Jiang S. Different effects of zwitterion and ethylene glycol on proteins. J Chem Phys. 2012;136:225101.

[113] Shao Q, Jiang S. Molecular understanding and design of zwitterionic materials. Advanced materials. 2015;27:15-26.

[114] Casadevall N, Nataf J, Viron B, Kolta A, Kiladjian JJ, Martin-Dupont P, et al. Pure red-cell aplasia and antierythropoietin antibodies in patients treated with recombinant erythropoietin. The New England journal of medicine. 2002;346:469-75.

[115] Bartelds GM, Krieckaert CL, Nurmohamed MT, van Schouwenburg PA, Lems WF, Twisk JW, et al. Development of antidrug antibodies against adalimumab and association with disease activity and treatment failure during long-term follow-up. JAMA. 2011;305:1460-8.

[116] Chirmule N, Jawa V, Meibohm B. Immunogenicity to therapeutic proteins: impact on PK/PD and efficacy. AAPS J. 2012;14:296-302.

[117] Zhang P, Jain P, Tsao C, Yuan Z, Li W, Li B, et al. Polypeptides with High Zwitterion Density for Safe and Effective Therapeutics. Angewandte Chemie. 2018;57:7743-7.

[118] Rau RE, Dreyer Z, Choi MR, Liang W, Skowronski R, Allamneni KP, et al. Outcome of pediatric patients with acute lymphoblastic leukemia/lymphoblastic lymphoma with hypersensitivity to pegaspargase treated with PEGylated Erwinia asparaginase, pegcrisantaspase: A report from the Children's Oncology Group. Pediatr Blood Cancer. 2018;65.

[119] Parenky A, Myler H, Amaravadi L, Bechtold-Peters K, Rosenberg A, Kirshner S, et al. New FDA draft guidance on immunogenicity. AAPS J. 2014;16:499-503.

[120] Hackstein H, Taner T, Zahorchak AF, Morelli AE, Logar AJ, Gessner A, et al. Rapamycin inhibits IL-4--induced dendritic cell maturation in vitro and dendritic cell mobilization and function in vivo. Blood. 2003;101:4457-63.

[121] Taner T, Hackstein H, Wang Z, Morelli AE, Thomson AW. Rapamycin-treated, alloantigen-pulsed host dendritic cells induce ag-specific T cell regulation and prolong graft survival. Am J Transplant. 2005;5:228-36.

[122] Turnquist HR, Raimondi G, Zahorchak AF, Fischer RT, Wang Z, Thomson AW. Rapamycin-Conditioned Dendritic Cells Are Poor Stimulators of Allogeneic CD4+ T Cells, but Enrich for Antigen-Specific Foxp3+ T Regulatory Cells and Promote Organ Transplant Tolerance. The Journal of Immunology. 2007;178:7018-31.

[123] Maldonado RA, LaMothe RA, Ferrari JD, Zhang AH, Rossi RJ, Kolte PN, et al. Polymeric synthetic nanoparticles for the induction of antigen-specific immunological tolerance. Proc Natl Acad Sci U S A. 2015;112:E156-65.

[124] Kishimoto TK, Ferrari JD, LaMothe RA, Kolte PN, Griset AP, O'Neil C, et al. Improving the efficacy and safety of biologic drugs with tolerogenic nanoparticles. Nature nanotechnology. 2016;11:890-9.

[125] Gu J, Ruppen ME, Cai P. lipase-catalyzed regioselective esterification of rapamycin: synthesis of temsirolimus (CCI-779). Org Lett. 2005;7:3945-8.

[126] Shen ZH, Reznikoff G, Dranoff G, Rock KL. Cloned dendritic cells can present exogenous antigens on both MHC class I and class II molecules. Journal of Immunology. 1997;158:2723-30.

[127] Abraham RT. Mammalian target of rapamycin: immunosuppressive drugs uncover a novel pathway of cytokine receptor signaling. Current Opinion in Immunology. 1998;10:330-6.

[128] Graziani EI. Recent advances in the chemistry, biosynthesis and pharmacology of rapamycin analogs. Nat Prod Rep. 2009;26:602-9.

[129] Eiden AM, Zhang S, Gary JM, Simmons JK, Mock BA. Molecular Pathways: Increased Susceptibility to Infection Is a Complication of mTOR Inhibitor Use in Cancer Therapy. Clin Cancer Res. 2016;22:277-83.

[130] Mahnke K, Schmitt E, Bonifaz L, Enk AH, Jonuleit H. Immature, but not inactive: the tolerogenic function of immature dendritic cells. Immunol Cell Biol. 2002;80:477-83.

[131] Lutz MB, Schuler G. Immature, semi-mature and fully mature dendritic cells: which signals induce tolerance or immunity? Trends in Immunology. 2002;23:445-9.

Appendix A: Qualifications of the Author

Education

Ph.D in **Chemical Engineering**, expected Dec 2018

Department of Chemical Engineering, University of Washington

M.S. in **Material Science**, January 2012

School of Material Science and Engineering, Tianjin University, China

B.S. in **Material Science and Engineering**, July 2009

School of Material Science and Engineering, Tianjin University, China

Awards & Honors

- Chinese Government Award for Outstanding Self-Financed Students Abroad, 2017
- High Impact Publication Award, Department of Chemical Engineering, University of Washington, 2017
- GSFEI Graduate Student Travel Award, University of Washington, 2017
- Faculty Lecture Award, Department of Chemical Engineering, University of Washington, 2016
- Thomas G Thompson Endowed Fellowship, Department of Chemical Engineering, University of Washington, 2014
- Tianjin Excellent Master Degree Thesis Award, 2012
- E-TECH Award, Tianjin University, 2011
- WeiChai Power Award, Tianjin University, 2010
- Tianjin University Excellent Bachelor Degree Thesis Award, 2009
- Tianjin Government Award for Outstanding Undergraduate Students, 2007

Publications

First author publications:

1. **P. Zhang**, P. Jain, C. Tsao, K. Wu, S. Jiang*. Proactively Reducing Anti-Drug Antibodies via Immunomodulatory Bioconjugation. ***Angew. Chem. Int. Ed.*** Under revision.
2. **P. Zhang**, E. J. Liu, C. Tsao, S. A. Kasten, M. V. Boeri, T. L. Dao, S. J. DeBus, C. L. Cadieux, C. A. Baker, T. C. Otto, D. M. Cerasoli, Y. Chen, P. Jain, F. Sun, W. Li, H.-C. Hung, Z. Yuan, J. Ma, A. N. Bigley, F. M. Raushel, S. Jiang*. Nanoscavenger Provides Long-term Prophylactic Protection Against Nerve Agents. ***Sci. Transl. Med.***

Under revision.

3. **P. Zhang**, P. Jain, C. Tsao, Z. Yuan, W. Li, B. Li, K. Wu, H.-C. Hung, X. Lin, S. Jiang*. Polypeptide with High Zwitterion density for Safe and Effective Therapeutics. ***Angew. Chem. Int. Ed.*** 2018, 57 (26), 7743-7747.
4. **P. Zhang**,‡ F. Sun,‡ H.-C. Hung, P. Jain, K. J. Leger, S. Jiang*. Sensitive and Quantitative Detection of Anti-Poly(ethylene glycol)(PEG) Antibodies by Methoxy-PEG-Coated Surface Plasmon Resonance Sensors. ***Anal. Chem.*** 2017, 89, 8217-8222. (‡ **Equal contributions**)
5. **P. Zhang**, F. Sun, S. Liu, S. Jiang*. Anti-PEG Antibodies in the Clinic: Current Issues and beyond PEGylation. ***J. Control. Release*** 2016, 244, 184-193.
6. **P. Zhang**, P. Jain, C. Tsao, A. Sinclair, F. Sun, H.-C. Hung, T. Bai, K. Wu, S. Jiang*. Butyrylcholinesterase Nanocapsule as a Long Circulating Bioscavenger with Reduced Immune Response. ***J. Control. Release*** 2016, 230, 73-78.
7. **P. Zhang**, F. Sun, C. Tsao, S. Liu, P. Jain, A. Sinclair, H.-C. Hung, T. Bai, K. Wu, S. Jiang*. Zwitterionic Gel Encapsulation Promotes Protein Stability, Enhances Pharmacokinetics, and Reduces Immunogenicity. ***Proc. Natl. Acad. Sci. U S A*** 2015, 112 (39), 12046-12051.
8. **P. Zhang**, W. Li, X. Zhai, C. Liu, L. Dai and W. Liu*. A Facile and Versatile Approach to Biocompatible "Fluorescent Polymers" from Polymerizable Carbon Nanodots. ***Chem. Commun.*** 2012, 48, 10431-10433.
9. X. Zhai,‡ **P. Zhang**,‡ C. Liu, T. Bai, W. Li, L. Dai and W. Liu*. Highly Luminescent Carbon Nanodots by Microwave-assisted Pyrolysis. ***Chem. Commun.*** 2012, 48, 7955-7957. (‡ **Equal contributions**)
10. C. Liu,‡ **P. Zhang**,‡ F. Tian, W. Li, F. Li and W. Liu*. One-step Synthesis of Surface Passivated Carbon Nanodots by Microwave Assisted Pyrolysis for Enhanced Multicolor Photoluminescence and Bioimaging. ***J. Mater. Chem.*** 2011, 13163-13167. (‡ **Equal contributions**)
11. **P. Zhang**, J. Yang, W. Li, W. Wang, C. Liu, M. Griffith and W. Liu*. Cationic Polymer Brush Grafted-nanodiamond via Atom Transfer Radical Polymerization for Enhanced Gene Delivery and Bioimaging. ***J. Mater. Chem.*** 2011, 21, 7755-7764.
12. **P. Zhang**, W. Liu*. ZnO QD@PMAA-co-PDMAEMA Nonviral Vector for Plasmid DNA Delivery and Bioimaging. ***Biomaterials*** 2010, 31, 3087-3094.

Other publications

13. Y. Han, Z. Yuan, **P. Zhang**, S. Jiang*. Zwitterlation Mitigates Protein Bioactivity Loss *in vitro* over PEGylation. ***Chem. Sci.*** 2018, DOI: 10.1039/C8SC01777H.

14. X. Lin, P. Jain, K. Wu, D. Hong, H.-C. Hung, M. B. O'Kelly, B. Li, **P. Zhang**, Z. Yuan, S. Jiang*. Ultra-low Fouling and Functionalizable Surface Chemistry Based on Zwitterionic Carboxybetaine Random Copolymers. ***Langmuir*** 2018, DOI: 10.1021/acs.langmuir.8b02540.

15. B. Li, Z. Yuan, H.-C. Hung, J. Ma, P. Jain, C. Tsao, J. Xie, **P. Zhang**, X. Lin, K. Wu, S. Jiang*. Revealing the Immunogenic Risk of Polymers. ***Angew. Chem. Int. Ed.*** 2018, 130, 14069-14072.

16. P. Jain, H.-C. Hung, B. Li, J. Ma, D. Dong, X. Lin, A. Sinclair, **P. Zhang**, M. B. O'Kelly, L. Niu, S. Jiang*. Zwitterionic hydrogels based on a degradable disulfide carboxybetaine crosslinker. ***Langmuir*** 2018, DOI: 10.1021/acs.langmuir.8b02100

17. G. Zheng, S. Liu, J. Zha, **P. Zhang**, X. Xu, Y. Chen*, S. Jiang*. Protecting enzymatic activity via zwitterionic nanocapsulation for the removal of phenol compound from wastewater. ***Langmuir*** 2018, DOI: 10.1021/acs.langmuir.8b02001.

18. B. Li, Z. Yuan, **P. Zhang**, A. Sinclair, P. Jain, K. Wu, C. Tsao, J. Xie, H. - C. Hung, X. Lin, T. Bai, S. Jiang*. Zwitterionic Nanocages Overcome the Efficacy Loss of Biologic Drugs. ***Adv. Mater.*** 2018, 30, 1705728.

19. F. Sun, K. Wu, H.-C. Hung, **P. Zhang**, X. Che, J. Smith, X. Lin, B. Li, P. Jain, Q. Yu, S. Jiang*. Paper Sensor Coated with a Poly (carboxybetaine)-multiple DOPA Conjugate via Dip-coating for Biosensing in Complex Media. ***Anal. Chem.*** 2017, 89, 10999-11004.

20. P. Jain, H.-C. Hung, X. Lin, J. Ma, **P. Zhang**, F. Sun, K. Wu, S Jiang*. Poly(ectoine) Hydrogels Resist Nonspecific Protein Adsorption. ***Langmuir*** 2017, 33, 11264-11269.

21. H.-C. Hung, P. Jain, **P. Zhang**, F. Sun, A. Sinclair, T. Bai, B. Li, K. Wu, C. Tsao, E. J. Liu, H. S. Sundaram, X. Lin, P. Farahani, T. Fujihara, S. Jiang*. A Coating-Free Nonfouling Polymeric Elastomer. ***Adv. Mater.*** 2017, 29, 1700617.

22. D. Hong, H.-C. Hung, K. Wu, X. Lin, F. Sun, **P. Zhang**, S. Liu, K. E. Cook, S. Jiang*. Achieving Ultralow Fouling under Ambient Conditions via Surface-Initiated ARGET ATRP of Carboxybetaine. ***ACS Appl. Mater. Interfaces*** 2017, 9 (11), 9255-9259

23. F. Sun, H.-C. Hung, A. Sinclair, **P. Zhang**, T. Bai, D. D. Galvan, P. Jain, B. Li, S. Jiang*, Q. Yu*. Hierarchical Zwitterionic Modification of a SERS Substrate Enables

Real-time Drug Monitoring in Blood Plasma. ***Nat. Commun.*** 2016, 7, 13437.

24. X. Dai, Q. Guo, Y. Zhao, **P. Zhang**, T. Zhang, X. Zhang*, C. Li. Functional Silver Nanoparticle as a Benign Antimicrobial Agent That Eradicates Antibiotic-Resistant Bacteria and Promotes Wound Healing. ***ACS Appl. Mater. Interfaces*** 2016, 8 (39), 25798-25807.
25. Y.-N. Chou, F. Sun, H.-C. Hung, P. Jain, A. Sinclair, **P. Zhang**, T. Bai, Y. Chang, T.-C. Wen, Q. Yu, S. Jiang*. Ultra-Low Fouling and High Antibody Loading Zwitterionic Hydrogel Coatings for Sensing and Detection in Complex Media. ***Acta Biomater.*** 40, 31-37.
26. Y. Wei, H.-C. Hung, F. Sun, T. Bai, **P. Zhang**, A. K. Nowinski, S. Jiang*. Achieving Low-fouling Surfaces with Oppositely Charged Polysaccharides via LBL Assembly. ***Acta Biomater.*** 2016, 40, 16-22.
27. W. Li, Q. Liu, **P. Zhang**, L. Liu*. Zwitterionic Nanogels Crosslinked by Fluorescent Carbon Dots for Targeted Drug Delivery and Simultaneous Bioimaging. ***Acta Biomater.*** 2016, 40, 254-262.
28. J. An, Q. Guo, **P. Zhang**, A. Sinclair, Y. Zhao, X. Zhang*, K. Wu, F Sun, H.-C. Hung, C. Li, S. Jiang*. Hierarchical Design of A Polymeric Nanovehicle for Efficient Tumor Regression and Imaging, ***Nanoscale*** 2016, 8 (17), 9318-9327.
29. T. Bai, A. Sinclair, F. Sun, P. Jain, H.-C. Hung, **P. Zhang**, J.-R. Ella-Menye, W. Liu, S. Jiang*. Harnessing Isomerization-mediated Manipulation of Nonspecific Cell/Matrix Interactions to Reversibly Trigger and Suspend Stem Cell Differentiation. ***Chem. Sci.*** 2016, 7 (1), 333-338.
30. F. Sun, **P. Zhang**, T. Bai, D. D. Galvan, H.-C. Hung, N. Zhou, S. Jiang, Q. Yu*. Functionalized Plasmonic Nanostructure Arrays for Direct and Accurate Mapping Extracellular pH of Living Cells in Complex Media Using SERS. ***Biosens. Bioelectron.*** 2015, 73, 202-207.
31. F. Sun, J.-R. Ella-Menye, D. D. Galvan, T. Bai, H.-. Hung, Y.-N. Chou, **P. Zhang**, S. Jiang, Q. Yu*. Stealth Surface Modification of Surface-Enhanced Raman Scattering Substrates for Sensitive and Accurate Detection in Protein Solutions. ***ACS nano*** 2015, 9 (3), 2668-2676.
32. C. Liu, **P. Zhang**, X. Zhai, F. Tian, W. Li, J. Yang, Y. Liu, H. Wang, W. Wang, W. Liu*. Nano-carrier for Gene Delivery and Bioimaging Based on Carbon Dots with PEI-passivation Enhanced Fluorescence. ***Biomaterials*** 2012, 33, 3604-3613.

33. T. Bai, Y. Han, **P. Zhang**, W. Wang and W. Liu*. Zinc Ion-triggered Two-way Macro-/Microscopic Shape Changing and Memory Effects in High Strength Hydrogels with Pre-programmed Unilateral Patterned Surfaces. ***Soft Matter*** 2012, 8, 2846-2852.

34. Y. Liu, J. Yang, **P. Zhang**, C. Liu, W. Wang, W. Liu*. ZnO Quantum Dots-Embedded Collagen/Polyanion Composite Hydrogels with Integrated Functions of Degradation Tracking/Inhibition and Gene Delivery. ***J. Mater. Chem.*** 2012, 22, 512-519.

35. N. Wang, Y. Han, Y. Liu, T. Bai, H. Gao, **P. Zhang**, W. Wang*, W. Liu*. High-Strength Hydrogel as a Reusable Adsorbent of Copper Ions. ***J. Hazard. Mater.*** 2012, 258-264.

36. T. Bai, **P. Zhang**, Y. Han, Y. Liu, W. Liu,* X. Zhao and W. Lu. Construction of an Ultrahigh Strength Hydrogel with Excellent Fatigue Resistance Based on Strong Dipole–Dipole Interaction. ***Soft Matter*** 2011, 7, 2825-2831.

37. J. Yang, **P. Zhang**, L. Tang, P. Sun, W. Liu*, P. Sun, A. Zuo, D. Liang. Temperature-tuned DNA Condensation and Gene Transfection by PEI-g-(PMEO$_2$MA-b-PHEMA) Copolymer-based Nonviral Vectors. ***Biomaterials*** 2010, 31, 144-155.